

**ROLE OF NEURONAL CELL ADHESION MOLECULES
IN REGULATING FILOPODIAL DYNAMICS AND SYNAPSE
FORMATION IN THE *DROSOPHILA* VISUAL SYSTEM**

Inaugural Dissertation to Obtain the Academic Degree:
Doctor rerum naturalium (Dr. rer. nat.)

Submitted to:

The Department of Biology, Chemistry and Pharmacy
Freie Universität Berlin

Author:

Amr Hasan

March 2020

This thesis includes experiments that were performed between November 2015 and August 2019 in the lab of Prof. Hiesinger at the Freie Universität Berlin.

1st Reviewer: Prof. Dr. Peter Robin Hiesinger

Division of Neurobiology, Freie Universität Berlin

2nd Reviewer: Prof. Dr. Mathias F. Wernet

Division of Neurobiology, Freie Universität Berlin

Date of defense: 10 June 2020

Statement of Authorship

I hereby declare that the work presented in this thesis has been conducted and presented independently. Experimental contribution of others is specified and acknowledged in each respective section. All sources of information are referenced. I hereby declare that this thesis has not been submitted, either in the same or in a different form, to this or any other university for a degree.

For my Loving Family

SUMMARY

Brains in all biological systems consist of large numbers of interconnected neurons. The developmental processes to wire a functional brain are controlled by many protein families that govern neuronal targeting, synaptic partner specification, and synapse formation.

Using the fly visual system and the state-of-the-art live imaging of developing photoreceptors in intact *Drosophila* brains in *ex vivo* cultures, I studied the role of cell adhesion molecules (CAMs) in regulating R7 targeting and filopodial dynamics and their effect on synapse formation. The analyses presented here include the protein tyrosine phosphatases (PTPs), Lar and PTP69D, and the fly homologue of the amyloid precursor protein (APP), APP-like (APPL). I also report the novel function of Neurexin-1 (Nrx) in R7 targeting and synapse formation.

Lar interaction with Liprin- α during synapse formation is essential to stabilize R7 terminals in their target layer. Their loss of function causes filopodial dynamics changes and affects bulbous tip stability and synapse formation. Lar and Liprin- α regulate bulbous tip stability by stabilizing microtubules in the formed bulbous tips to provide mechanical support for pre-synaptic contacts to facilitate synapse formation. To test this hypothesis, I reduced actin depolymerization by knocking-down the cofilin phosphatase, Chronophin (dCIN), which increased filopodia stability and caused an increase in synapse count in R7s.

Loss of *ptp69d* caused very mild R7 retractions and a filopodia formation defect with no effect on bulbous tip dynamics and synapse formation, showing the distinct functions of PTP69D that are not redundant to Lar in R7s as was proposed previously.

nrx mutant R7s did not show a targeting defect but rather an elevated synaptic transmission. Mutant R7s fail to stabilize bulbous tips, yet they formed synapses with more and aberrant postsynaptic partners, suggesting that Nrx is a negative regulator of synapse formation in R7s.

Finally, the reported subtle retraction phenotype in *appl* mutant R7s was found to be independent of APPL. Additionally, studying the APPL proteolytic cleavage products showed that the extracellular and the intracellular fragments were differentially trafficked in different stages of developing neurons. The intracellular fragment localized to the axon terminals of R7s, while the extracellular fragment was secreted from photoreceptors and picked up by cortical glia where it eventually affects endolysosomal trafficking in a dose-dependent manner.

This study challenges the proposed function of the tested CAMs as guidance molecules. Live imaging revealed that none of the tested proteins instructed R7 targeting to their correct layer, but rather stabilize their terminals in the correct layer. Changes of filopodial dynamics associated with their loss of function and the corresponding synaptic changes imply that synapse formation relies on stabilizing pre-synaptic contacts and not on a molecular match-making mechanism.

ZUSAMENFASSUNG

Gehirne von höheren Tieren bestehen aus einem komplexen Netzwerk aus vielen verschalteten Neuronen. Die Entwicklungsprozesse, die an der Verschaltung eines funktionalen Gehirns beteiligt sind, werden durch eine Vielzahl von Proteinfamilien kontrolliert. Diese steuern neuronales Pathfinding und Targeting, die Spezifizierung synaptischer Partner, und Synapsenbildung.

Ich untersuchte die Rolle von Zelladhäsionsmolekülen (CAMs) im regulierenden R7-Photorezeptorterminal und die Dynamik von Filopodien und deren Effekt auf die Synapsenbildung. Dazu verwendete ich das visuelle System der Fruchtfliege, sowie Live Imaging von sich entwickelnden Photorezeptoren in intakten *Drosophila*-Gehirnen in *ex vivo* Kulturen. Ich untersuchte die zwei Tyrosinphosphatasen (PTPs), Lar und PTP69D, und das Fliegenhomolog des Amyloid-Precursor-Protein (APP) APP-like (APPL). Außerdem untersuchte ich die Funktion von Neurexin-1 (Nrx), wessen Rolle in Photorezeptor-Targeting und -Synapsenbildung bisher nicht bekannt war.

Lar und das damit interagierende Protein, Liprin- α , stabilisierten R7-Terminale in ihrer Zielschicht. Ihr Funktionsverlust in R7 führte zu Veränderungen in der Filopodiendynamik und beeinflusste die Stabilität der Bulbous Tips und Synapsenformation. Lar und Liprin- α steigerten die Stabilität der Bulbous Tips, indem sie die Mikrotubuli stabilisierten, und somit eine mechanische Stütze für prä-postsynaptische Kontakte bot, wodurch die Synapsenbildung erleichtert wurde. Um diese Hypothese zu testen reduzierte ich die Aktin Polymerisation durch Knock-Down von Chronophin (dCIN) was die Filopodienstabilität erhöhte und dadurch zu mehr Synapsen führte.

Der Verlust von *ptp69d* führte zu einer sehr milden R7-Rücknahme und einem Filopodiendefekt ohne Effekt auf die Bulbous Tip-Dynamik und Synapsenbildung. Das bestätigt die frühere Vermutung, dass die ausgeprägten Funktionen von PTP69D in R7 nicht zu Lar redundant sind.

In *nrx*-mutierten Photorezeptoren wurde kein R7 targeting Defekt bemerkt, dafür aber erhöhte synaptische Transmission. *nrx*-mutierte R7 bildeten keine stabilen Bulbous Tips aus, bildeten jedoch Synapsen mit mehr und abnormen postsynaptischen Partnern. Dies suggeriert, dass Nrx als ein negativer Regulator für Synapsenbildung in Photorezeptoren wirkt.

Schließlich konnte gezeigt werden, dass der subtile Retraktion-Phänotyp in *appl*-mutierten R7 unabhängig von APPL-Funktion in Photorezeptoren ist. Außerdem zeigten Experimente an den intra- und extrazellulären Fragmenten der proteolytischen Spaltungsprodukte von APPL, dass sie in unterschiedlichen Stadien der sich entwickelnden Neuronen verschieden transportiert werden. Das intrazelluläre Fragment lokalisierte sich in den Axonterminalien von R7, während das extrazelluläre Fragment aus den Photorezeptoren ausgeschieden und von

Gliazellen in Regionen der Hirnrinde aufgenommen wurde, wo es schließlich den endolysosomalen Transport spezifisch beeinflusste.

Diese Studie stellt die vorgeschlagene Funktion der getesteten CAMs als 'guidance' Moleküle in Frage. Live Imaging zeigte, dass keine der getesteten Proteine das Targeting zur richtigen Schicht von R7 kontrolliert, sondern stattdessen für eine Stabilisierung der Terminale in der richtigen Schicht sorgt. Veränderungen der Filopodiendynamik, die mit deren Funktionsverlust und daraus resultierenden Veränderungen in den Synapsen in Zusammenhang gebracht werden, implizieren, dass die Synapsenbildung auf eine Stabilisierung der prä-postsynaptischen Kontakte angewiesen ist, statt auf einen molekularen Match-Making-Mechanismus.

TABLE OF CONTENTS

SUMMARYIII

ZUSAMENFASSUNG IV

PART | 1 INTRODUCTION1

1.1. THE BRAIN WIRING PROBLEM2

1.1.1. THE CHEMOAFFINITY HYPOTHESIS 2

1.1.2. THE ‘UNIQUE MOLECULAR TAG’ PARADOX: HOW TO GENERATE MILLIONS OF UNIQUE IDENTITY TAGS USING A LIMITED GENOME?..... 3

1.1.3. CELL SURFACE MOLECULES SHAPE NEURONAL NETWORKS..... 4

1.1.4. FINDING SYNAPTIC PARTNERS IN SPACE AND TIME 5

1.1.5. AIM OF THE STUDY: WHAT FUNCTIONS DO CELL ADHESION MOLECULES PLAY IN BRAIN WIRING?.....6

1.2. THE *DROSOPHILA* VISUAL SYSTEM8

1.2.1. STRUCTURE OF THE FLY VISUAL SYSTEM 8

1.2.2. DEVELOPMENT OF THE FLY VISUAL SYSTEM..... 10

1.3. OBSERVING PHOTORECEPTOR DEVELOPMENT IN AN *IN VIVO* CONTEXT13

1.3.1. *EX VIVO* BRAIN CULTURE 13

1.3.2. LIVE IMAGING REVEALED THE ROLE OF GROWTH CONE STABILIZATION AND FILOPODIAL DYNAMICS IN R7 TARGETING..... 14

1.4. WHAT FUNCTIONS DO CELL ADHESION MOLECULES EXECUTE IN R7 DEVELOPMENT?15

1.4.1. LAR..... 16

1.4.1.1. Lar functions in developing neurons 16

1.4.1.2. Complex interactions of Lar to control its neuronal functions..... 16

1.4.2. PTP69D..... 17

1.4.2.1. Neuronal functions of PTP69D..... 17

1.4.2.2. Functional redundancy of PTP69D to other PTPs in neuronal development 17

1.4.3. NEUREXIN-1 18

1.4.3.1. The *Drosophila* Nrj..... 18

1.4.3.2. Synaptic functions of Nrj 18

1.4.4. AMYLOID PRECURSOR PROTEIN-LIKE..... 19

1.4.4.1. The *Drosophila* homologue of APP 19

1.4.4.2. Neuronal functions of APPL..... 19

PART | 2 MATERIALS AND METHODS21

TABLE OF CONTENTS

2.1. FLIES.....	22
2.2. GENERATING PHOTORECEPTOR CLONES.....	22
2.3. IMMUNOHISTOCHEMISTRY AND FIXED IMAGING	22
2.4. LIVE IMAGING	23
2.5. MOLECULAR BIOLOGY.....	23
2.5.1. GENETICS.....	23
2.5.2. CONFIRMING <i>NRX</i> RECOMBINANT LINES	23
2.5.3. <i>PTP69D</i> MUTANT ALLELE GENOTYPING.....	24
2.5.4. ANTEROGRADE TRANS-SYNAPTIC CIRCUIT TRACING.....	24
2.6. ELECTRORETINOGRAM (ERG) RECORDINGS.....	24
2.7. DATA PROCESSING AND ANALYSIS	24
2.8. RESOURCES TABLE.....	25
<u>PART 3 LAR.....</u>	<u>29</u>
3.1. CONTRIBUTION.....	30
3.2. RESULTS	30
3.2.1. ROLE OF LAR AND LIPRIN- α IN R7 LAYER TARGETING AND SYNAPSE FORMATION.....	30
3.2.1.1. LAR AND LIPRIN- α ARE REQUIRED TO STABILIZE R7S IN THEIR TARGET LAYER	30
3.2.1.2. TRIO OVEREXPRESSION PARTIALLY RESCUES THE RETRACTION OF <i>LAR</i> MUTANT R7S...	33
3.2.1.3. <i>LAR</i> R7S RETRACT TO THE LAYER WHERE R8S ARE.....	34
3.2.1.4. <i>LAR</i> AND <i>LIPRIN-α</i> R7S HAVE A SYNAPTIC FORMATION DEFECT IRRESPECTIVE OF THE TARGET LAYER	35
3.2.1.5. LAR AND LIPRIN- α ARE DISPENSABLE FOR SYNAPSE FORMATION IN DRA R7S AND FOR SYNAPTIC TRANSMISSION IN PHOTORECEPTORS	37
3.2.2. ROLE OF LAR AND LIPRIN- α IN REGULATING MICROTUBULE POLYMERIZATION IN R7S ...	37
3.2.2.1. STABLE MICROTUBULES CORRELATE WITH STABLE BULBOUS TIPS.....	38
3.2.2.2. LAR AND LIPRIN- α STABILIZE BULBOUS TIPS THROUGH STABILIZING MICROTUBULES	39
3.2.3. MANIPULATING THE ACTIN CYTOSKELETON TO CONTROL FILOPODIAL DYNAMICS AND SYNAPSE NUMBER.....	42
3.2.3.1. <i>DCIN</i> KNOCK-DOWN AFFECTS FILOPODIAL DYNAMICS IN R7S.....	46
3.2.3.2. <i>DCIN</i> KNOCK-DOWN IN PHOTORECEPTORS CAUSES THEM TO FORM MORE SYNAPSES....	46
3.3. DISCUSSION	48
3.3.1. R8S DICTATE THE LAYER TO WHICH <i>LAR</i> AND <i>LIPRIN-α</i> R7S RETRACT TO.....	48
3.3.2. LAR AND LIPRIN- α ARE DISPENSABLE FOR SYNAPSE FORMATION IN PHOTORECEPTORS	50
3.3.3. LAR AND LIPRIN- α STABILIZE MICROTUBULES IN BULBOUS TIPS.....	50

TABLE OF CONTENTS

3.3.4.	REDUCING ACTIN DEPOLYMERIZATION LEADS TO MORE STABLE FILOPODIA IN R7S	52
3.3.5.	DEPLETING <i>DCIN</i> IN PHOTORECEPTORS CAUSES THEM TO FORM MORE SYNAPSES.....	52
3.3.6.	PROPOSED ROLE OF LAR AND LIPRIN- α IN R7 TARGETING AND SYNAPSE FORMATION ..	53

PART | 4 PTP69D.....56

4.1.	CONTRIBUTION.....	57
4.2.	RESULTS	57
4.2.1.	PTP69D IS NOT REQUIRED FOR R7 LAYER TARGETING BUT IS REQUIRED FOR FILOPODIA FORMATION	57
4.2.2.	PTP69D IS NOT REQUIRED FOR SYNAPSE FORMATION IN PHOTORECEPTORS	60
4.3.	DISCUSSION.....	60
4.3.1.	PTP69D FUNCTION IN R7S IS NOT REDUNDANT TO LAR.....	60

PART | 5 NEUREXIN-1.....63

5.1.	CONTRIBUTION.....	64
5.2.	RESULTS	64
5.2.1.	NRX IS NOT REQUIRED FOR R7 CORRECT TARGETING	64
5.2.2.	LOSS OF <i>NRX</i> IN PHOTORECEPTORS CAUSES AN INCREASE IN NEUROTRANSMISSION....	64
5.2.3.	<i>NRX</i> R7S FORM CONTACTS WITH INCORRECT POSTSYNAPTIC NEURONS	64
5.2.4.	<i>NRX</i> R7S FAIL TO STABILIZE BULBOUS TIPS	66
5.3.	DISCUSSION.....	66
5.3.1.	LOSS OF <i>NRX</i> INCREASES R7S FILOPODIAL DYNAMICS.....	67
5.3.2.	NRX RESTRICTS SYNAPSE FORMATION IN PHOTORECEPTORS	68

PART | 6 AMYLOID PRECURSOR PROTEIN-LIKE.....71

6.1.	CONTRIBUTION.....	72
6.2.	RESULTS	72
6.2.1.	ROLE OF APPL IN R7 TARGETING AND SYNAPSE FORMATION.....	72
6.2.1.1.	<i>APPL^D</i> R7S INITIALLY TARGET CORRECTLY BEFORE RETRACTING TO M3.....	73
6.2.1.2.	<i>APPL^D</i> R7S FORM FEWER AND UNSTABLE BULBOUS TIPS TOGETHER WITH FEWER SYNAPSES	74
6.2.1.3.	SENSITIZING THE <i>APPL</i> MUTANT FLIES WITH GENETIC HETEROZYGOUS BACKGROUNDS CHANGES THE R7 RETRACTION PHENOTYPE	74

TABLE OF CONTENTS

6.2.1.4. OVEREXPRESSION OF APPL IN <i>APPL^D</i> FLIES DOES NOT RESCUE THE R7 RETRACTION PHENOTYPE.....	77
6.2.1.5. <i>APPL</i> MUTANT ALLELES, OTHER THAN <i>APPL^D</i> , DO NOT CAUSE R7 RETRACTIONS.....	79
6.2.2. <i>AN APPL SIDE-STORY: EXPRESSION PATTERN, DYNAMICS OF APPL'S PROTEOLYTIC CLEAVAGE PRODUCTS, AND THEIR EFFECT ON NEURONAL AND NON-NEURONAL TISSUES</i>	80
6.2.2.1. APPL IS A NEURON-SPECIFIC PROTEIN IN FLIES	80
6.2.2.2. APPL IS PROTEOLYTICALLY CLEAVED TO RELEASE THE SECRETED FRAGMENTS TO GLIA.....	84
6.2.2.3. APPL EXPRESSION IN NEURONS HAS CELL AUTONOMOUS AND NON-CELL AUTONOMOUS EFFECTS ON ENDOLYSOSOMAL TRAFFICKING	89
6.2.2.4. NEURONAL SAPPL ACCUMULATES IN THE NEPHROCYTES.....	94
6.3. DISCUSSION	94
6.3.1. APPL IS NOT REQUIRED FOR R7 TARGETING.....	94
6.3.2. NEURONAL AND NON-NEURONAL FUNCTIONS OF APPL.....	96
<u>PART 7 CONCLUDING REMARKS</u>	<u>99</u>
7.1. WHEN IS A PROTEIN CONSIDERED AS A GUIDANCE CUE?	100
7.2. THE DEVELOPMENTAL RULES THAT CONTROL R7 TARGETING	101
7.3. SYNAPSE FORMATION IN R7S IS A PROBABILISTIC PROCESS	101
7.4. DO GLIA HAVE A ROLE IN TARGETING AND SYNAPSE FORMATION IN R7S?.....	102
REFERENCES	104
ACKNOWLEDGEMENTS	121
<u>APPENDICES</u>	<u>122</u>
APPENDIX 1 LIST OF ABBREVIATIONS	123
APPENDIX 2 LIST OF FIGURES	126
APPENDIX 3 LIST OF GENOTYPES	128
APPENDIX 4 PUBLICATIONS	135
APPENDIX 5 CURRICULUM VITAE	136

PART | 1 INTRODUCTION

PART | 1 INTRODUCTION

Before the conception of modern neuroscience, the brain and its complexity were not held in high regard. Ancient Egyptians and Greeks believed it was not the brain, but rather the heart, that was responsible for thoughts and intelligence. Egyptians did not include the brains in the mummification process and were discarded altogether unlike the other internal organs that were well preserved. It was not until the early 19th century that we witnessed progress in our understanding of biological structures; Matthias Jakob Schleiden proposed that all plant structures are composed of cells which Theodor Schwann built upon to suggest that animal structures were also composed of cells in what is termed as the “Cell theory”. A key improvement to our view on the brain came with the development of Camillo Golgi’s silver staining of nerve cells from animals and humans, which he described as a continuous single network. Around the same time, Santiago Ramón y Cajal used Golgi’s silver staining to study the neurons in the brains of birds, based on which, he presented detailed and descriptive illustrations of different neuronal structures that, to date, remain scientifically as well as aesthetically significant (Fig. 1). More importantly, Cajal’s studies led him to identify that nerve cells are independent from each other yet connect to one another, which laid the foundation of the “Neuron doctrine” (Yuste 2015). Cajal also described dendritic spines and proposed that they contact and receive input from axons of other neurons in suggestion of the directionality of the information flow in neurons.

Due to neurons’ complex specialized structures, one of the major challenges for scientists is to explain how massively-extended axons and dendrites develop and identify their specific targets in order to form functional neuronal networks.

1.1. The Brain Wiring Problem

The neuronal network complexity does not just arise from the vast number of neurons and their synaptic partners they form contacts with, but it is also amplified as neuronal cell bodies are often located spatially distant from the synaptic regions of brains. Axons and dendrites need to travel long distances away from the cell bodies to contact their synaptic partners. The question here becomes how do neurons give rise to a complex network and form specific synaptic connections during brain development?

1.1.1. The chemoaffinity hypothesis

In the 1940s, Roger Sperry conducted a set of experiments on the visual system of amphibia, he found that the severed optic nerves regenerated and the fibers extended to their original loci in the brain. Interestingly, when he rotated the animals’ eyes by 180°, neurons regenerated and vision was restored but the animals perceived the visual field as if it were flipped upside-down (Sperry 1943). These observations led Sperry to formulate the chemoaffinity hypothesis postulating that each neuron carries unique identification tags that are distinguished from other

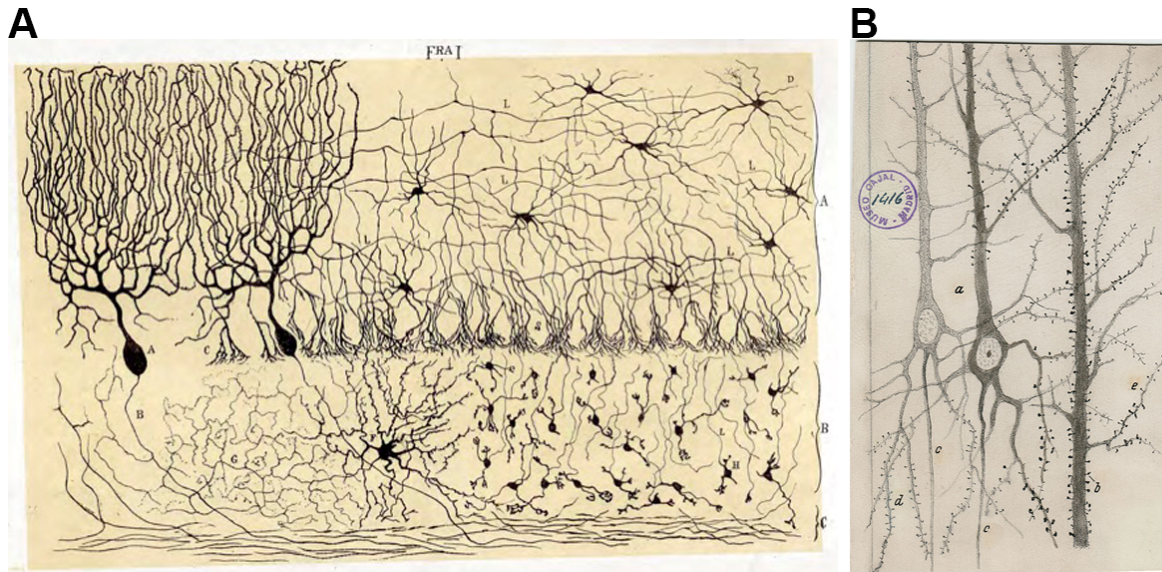


Fig. 1. Drawings of various neuronal structures by Ramón y Cajal.

Golgi impregnated preparations of neuronal tissues as illustrated and published by Cajal in the late 19th and the early 20th century. **(A)** Vertical section of the chicken cerebellar convolution. A represents the molecular zone, B represents the granular layer, C represents the white matter, and Purkinje cells to the left. Image from Cajal (1888). **(B)** Dendritic spines of pyramidal neurons in the cerebellar cortex of rabbit. Image from Instituto Cajal del Consejo Superior de Investigaciones Científicas, Madrid.

neurons almost to the level of single neuron. Sperry suggested that growing neurons carrying differential tags specifically attached to their targets that carried the corresponding tags by specific chemical affinities and that these markers were important to achieve specific synaptic connections (Sperry 1963; Meyer 1998).

Sperry, however, admitted that his postulations raised the concern that it was not possible to generate enough unique chemical tags to label millions of neurons that form a nervous system based on the information encoded in a genome (Sperry 1963). Another concern regarding Sperry's experiments is that the findings cannot be applied to explain how a nervous system is formed during development since the conclusions were made based on analyzing regenerating neurons in adults which eliminates normal developmental factors.

1.1.2. The 'unique molecular tag' paradox: How to generate millions of unique identity tags using a limited genome?

The postulations posed by Sperry's chemoaffinity hypothesis required unique identification tags for each of the millions of neurons forming a nervous system. This raised the question about which molecules were capable of executing such a function. In an attempt to answer this question, Sperry suggested that the differences among neurons might be quantitative rather than qualitative; neurons respond to a gradient of adhesive molecules and connections

PART | 1 INTRODUCTION

are formed between neurons bearing matching values (Sperry 1963). This postulation was supported by the later discovery of Eph kinases as 'gradient molecules' and their ligands, ephrins, that form complimentary gradients to establish the topographic organization of the chicken retinotectal map (Drescher et al. 1995). Molecular gradients, however, can only enable axons to distinguish spatially arrayed neuronal targets while intermingled neurons, as those in a ganglion, still require identification tags that are qualitatively distinct.

Neurons could, on the other hand, create qualitatively-distinct molecular tags by using three possible strategies; neurons could bear distinct identities by differentially expressing multigene families of guidance molecules among neurons within a population (Zipursky and Sanes 2010). Molecules belonging to plenty of conserved membrane protein families were identified to have roles in neuronal guidance such as semaphorins, slits, netrins, and several others (Dickson 2002; Kolodkin and Tessier-Lavigne 2011). Such an approach allows using the same molecules in different regions of the nervous system as long as they are physically separated. This significantly reduces the required number of necessary unique tags since a neuron should only have a tag that is distinct from those of other neurons within an intermingled population irrespective whether the same tag is used by other neurons in other regions. Another strategy is to generate unique molecular tags by expressing different isoforms of the same gene that differ in their binding affinities. The *Drosophila* Down syndrome cell adhesion molecule 1 (*Dscam1*) was found to undergo alternative splicing and generates over 38,000 isoforms that are non-deterministically generated in neurons as a form of random differentiating tags. Dscam1 proteins show isoform-specific homophilic interaction to mediate self- versus non-self-recognition in order to facilitate axonal and dendritic self-avoidance and outbranching (Schmucker et al. 2000; He et al. 2014; Dascenco et al. 2015). Neurons of vertebrate systems also employ self-avoidance as a means to branch out in their target areas using the clustered protocadherin (pcdh) family of cell surface proteins that gives rise to different isoforms via alternative splicing and functions in self- versus non-self-discrimination, analogous to the *Drosophila* Dscam1 (Lefebvre et al. 2012). Vertebrates also produce thousands of Neurexin (Nrx) isoforms by alternative splicing that vary in their binding specificity to their ligand Neuroligin (Nlg) that could, conceptually, be important to specify synaptic interactions (Südhof 2008). Finally, diverse tags could arise from expressing a multitude of molecules belonging to unrelated protein families, with different neurons expressing different combinations of such molecules whose combined action is what gives each neuron its unique identity.

1.1.3. Cell surface molecules shape neuronal networks

As neurons develop, they extend neurites that spatially navigate towards their receptive regions where they form synapses. The leading edges of extending neurons comprise of

highly-motile, actin- and microtubule-rich growth cones that extend filopodia and lamellipodia to sense cues from the environment and steer growth cones, and hence the neurite, towards their targets. Cell adhesion molecules (CAMs) act on growth cones through homophilic or heterophilic interactions with other cues on opposing cells, they signal through cytoskeleton regulators to control actin and tubulin rearrangement to direct neuronal growth in order to form stereotypical networks (Juliano 2002; Lowery and Vactor 2009). Such guidance cues execute two main functions; attraction or repulsion and in some cases they exhibit both functions depending on the spatio-temporal context (Huber et al. 2003).

Attractive interactions between recognition cues, as the name implies, can promote axons to extend along the surface of other axons, in a process called fasciculation, or facilitate the adhesive interactions of neurons to temporarily halt their growth, as the case with intermediary targets, or to form synapses with their terminal targets. Repulsive interactions, on the other hand, function as boundaries between distinct populations of growing neurites and cause them to diverge. Such cues prevent neurites from overlapping to form interactions in the same synaptic field, this function can be achieved among neurites of the same neuron to facilitate self-avoidance, or among neurons of the same neuronal class in what is called isoneural tiling (Fig. 1.1.3) (Hattori et al. 2008; Lawrence Zipursky and Grueber 2013).

Different combinations of attractive and repulsive guidance molecules are thought to provide instructive or permissive cues for neurons to, first, reach their correct synaptic targeting region, and, second, to interact and form synapses with their specific synaptic partners.

1.1.4. Finding synaptic partners in space and time

As compelling a notion that neurons reach and identify their targets using matching adhesion cues akin to a key-and-lock interaction, several examples that do not comply with this rule were also reported. Neurons were found to form synapses with wrong partners when redirected to wrong target regions of the brain and even with themselves as observed in living animals and in cultured neurons (Van Der Loos and Glaser 1972; Bekkers and Stevens 1991; Berger-Müller et al. 2013; Kulkarni et al. 2016). Such cases are indicative that targeting and synaptic specificity are not solely achieved by molecular codes but are rather combined with other spatial and temporal elements during the developmental wiring process (Agi et al. 2020). Neuronal progenitors were found to differentiate in a coordinated, temporally-controlled fashion (Holguera and Desplan 2018), the resultant neurons occupy different positions and further develop in a corresponding pattern. Developing neurons extend their neurites successively according to their birth order while maintaining their positions relative to their cell bodies (Sullivan et al. 2019). As such, growing neurites innervate their target areas in a temporal order which segregates and restricts interactions between synaptic partners. This is particularly evident in the visual systems of vertebrates and invertebrates as an axon of a

PART | 1 INTRODUCTION

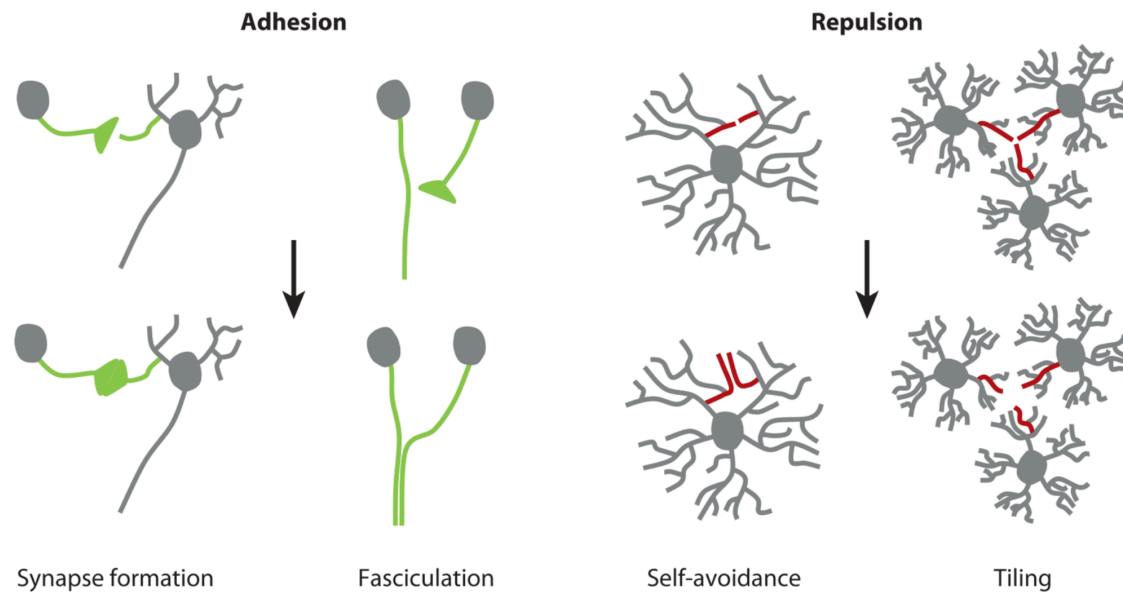


Fig. 1.1.3. Cell adhesion molecules induce attractive and repulsive neuronal interactions.

Homophilic or heterophilic binding of cell adhesion molecules on developing neurites (green and red in right and left, respectively) mediate attractive (left) or repulsive (right) responses. Attractive or adhesive interactions cause neurites of different neurons to either fasciculate and grow along the surface of other neurites or to bind and form synapses. Repulsive interactions between neurites causes them to avoid overlapping and extend away from one another to mediate self-avoidance in neurites of the same neurons or tiling between neurites of the same neuronal cell type. The figure was used with permission and was adapted from (Hattori et al. 2008).

retinal output neuron maintains its relative topographic position, in respect to the other output neurons, by establishing inter-axonal interactions and secondary intermediate structures before reaching their terminal targets (Kolodkin and Hiesinger 2017). Similarly, input from the facial whiskers of mice are transferred to the neocortex via thalamocortical axons that also maintain their topographic organization passing the basal ganglia primordium before terminating in the neocortex (Lokmane et al. 2013). These findings become interesting when viewed in line with the findings that axonal projections from the rat visual cortex formed synaptic contacts with every available postsynaptic target their terminals were in contact with and the number of the formed synapses correlated with dendritic and axonal overlap (Peters and Feldman 1976), a concept that was coined as 'Peters' rule' and was later extended to include all synapses in the rat cortices (Braitenberg and Schüz 1998).

1.1.5. Aim of the study: what functions do cell adhesion molecules play in brain wiring?

Brain wiring is, for most cases, a developmental process and its output is not altered by environmental factors. The developmental outcome of such a process is genetically encoded as several hundreds or thousands of genes encode proteins that undergo attractive or

repulsive interactions to orchestrate neuronal development. Since genes and their products are invariable, one would assume that they create a blueprint for the system which results in identical networks where every neuron identifies and interacts only with its pre-determined synaptic partners. This assumption, however, is not accurate, genetically identical Purkinje cells never form identical dendritic arbors, for example. Additionally, synapse formation as a process is surprisingly robust, and even non-specific, since neurons that innervate wrong target areas form synapses with wrong partners irrespective of their molecular tags. This raises the argument that brain wiring is rather a product of developmental rules in which cell surface molecules, through their molecular mechanisms, function as the executors of such rules (Hassan and Hiesinger 2015).

Dscam1 and its isoforms serve as an example of the previously-argued case. Different combinations of Dscam1 isoforms are produced in neurons giving them unique identities and, hence, thought to define their synaptic partners accordingly. In contrast to this assumption, the choice of isoforms in neurons was found to be stochastic and dynamic during different stages of development (Hattori et al. 2009; Sun et al. 2013; Miura et al. 2013; He et al. 2014). Therefore, the Dscam1 homophilic interaction that causes repulsion cannot be explained as a cue function but is rather important for neurons to distinguish self- vs non-self neurites in order to implement a pattern formation rule of self-avoidance and to branch-out in their respective target regions. Similarly, the rule of the cadherins N-Cadherin and Flamingo in the fly visual system was found to regulate photoreceptor growth cone polarization in respect to the adjacent photoreceptors within the cartridge (Schwabe et al. 2013, 2014). This also goes against their function as guidance cues but rather as executors of pattern formation rules.

Brain wiring can, thus, be explained through the implementation of pattern formation rules that are executed by different cell surface proteins as opposed to genetically-encoded processes. Self-avoidance, as a function, guarantees that arbors of a neuron branch-out and spread to cover a certain target area irrespective of the branching pattern, which can explain the variable branching pattern of the dendritic arbors of Purkinje cells. The seemingly-complex neural superposition of the fly visual system is another example for a neuronal structure whose wiring can be explained by pattern formation rules (Langen et al. 2015). On the other hand, synaptic-specificity, or the lack thereof, can be argued as an integral part of the developmental algorithm. The reported capability of neurons to form synapses with wrong synaptic partners or to form autapses indicates that the rule for neurons is to form synapses with every potential synaptic partner they encounter and that synapse formation is a non-specific process. The assumed synaptic-specificity, therefore, arises from the fact that pattern formation rules spatially or temporally sort synaptic partners together and, hence, allows synapses to form in less crowded spaces only between correct partners.

PART | 1 INTRODUCTION

The aforementioned findings and arguments motivated the study at hand which intended to understand the rules of cell adhesion molecules in brain wiring and whether they function as guidance cues or as executors of pattern formation rules. The main approach is to study the rule of cell adhesion molecules in a system that is amenable to molecular perturbation using techniques that reveal their functions in developing neurons. The aim is to understand the molecular mechanisms of the studied cell adhesion molecules by observing neuronal responses to perturbation experiments with the goal to understand their function and the developmental rules they execute.

1.2. The *Drosophila* Visual System

The use of *Drosophila melanogaster* in research started over a century ago as Thomas Morgan reported the identification of the *white* gene (Morgan 1910). Since then, the humble fruit fly has served as a genetic model organism to study the principles of inheritance. As the concepts and genetic tools matured towards the second half of the 20th century, *Drosophila* was also the subject to study many other biological topics including the nervous system that resulted in milestone discoveries in developmental and biomedical research (Bellen et al. 2010).

Drosophila offers a compact genome that encodes homologues to over 60% of the human genes in addition to a myriad of sophisticated genetic tools and manipulations. The relative ease by which experiments are performed and the short generation time made *Drosophila* an excellent research tool that is not surpassed by any other multicellular model organism. The available tools allow studying gene functions in flies either by generating mutant animals, creating mutant patches of cells in otherwise heterozygous animals using the yeast flippase (FLP)/flippase recognition target (FRT) system (Golic and Lindquist 1989; Golic 1991) as in the case of studying lethal mutations, or to ectopically express genes specifically in any tissue or cells using the yeast Gal4/upstream activating sequence (UAS) system (Brand and Perrimon 1993).

Similar to vertebrate and invertebrate neuronal structures, neurons of the fly visual system are arranged into regularly-spaced columns and terminate in defined layers with known developmental stages that occur at fixed developmental time points. Therefore, studying the organizational patterns of the fly visual system contributes to understanding the assembly of neurons into columns and layers (Clandinin and Zipursky 2002).

1.2.1. Structure of the fly visual system

An adult visual system is composed of around 60,000 neurons distributed among four neuropils in each of the optic lobes namely, the lamina, the medulla, the lobula, and the lobula plate (Morante and Desplan 2008). The optic lobes contain more than 60% of the neurons in an adult fly brain with the medulla being the largest neuropil in the optic lobes as they contain

about 40,000 neurons divided into over 70 neuronal subtypes (Fischbach and Dittrich 1989; Meinertzhagen and O'Neil 1991). The optic lobes contain two main types of neurons; interneurons, that have both their cell bodies and projections within the optic lobes, and projection neurons whose projections extend out of the optic lobes to connect with the central brain (Hofbauer and Campos-Ortega 1990).

The adult fly eye is a highly-organized structure that is made up of compound eyes, each contains 750-800 repetitive, independent units called ommatidia that have a crystalline arrangement (Campos-Ortega 1980). Each ommatidium contains eight photoreceptor cells (retinula cells, Rs) with their light-collecting rhabdomeres residing in the retina and their axons projecting into the optic lobe. Surrounding the photoreceptors within each ommatidium are four cone cells that secrete the lens and two primary pigment cells. Ommatidia, in turn, are surrounded and separated from one another by secondary and tertiary pigment cells and mechanosensory bristles (Cagan and Ready 1989).

The outer photoreceptor cells (R1-6) express Rhodopsin 1 (Rh1) and are responsible for motion detection (O'Tousa et al. 1985; Rister et al. 2007). The two inner photoreceptors, R7 and R8, may also contribute to motion detection but are primarily involved in color vision due to their expression of other Rhodopsins; R7s express the UV-sensitive Rh3 or Rh4, whereas R8s express either the blue-sensitive Rh5 or the green-sensitive Rh6 (Fortini and Rubin 1991; Salcedo et al. 1999; Yamaguchi et al. 2008; Gao et al. 2008). In addition to the different Rhodopsins they express, the inner and outer photoreceptors also differ in their connectivity. Axons of R1-6 terminate in the outer-most neuropil of the optic lobe, the lamina, while the axons of the inner photoreceptors extend beyond the lamina to terminate in the medulla with R8s targeting the layer M3 and R7s terminating in the layer M6 of the distal medulla (Fig. 1.2.1) (Fischbach and Dittrich 1989).

Rhabdomeres of the inner photoreceptors are organized in a circle that accommodate the rhabdomeres of R7 and R8 that are stacked on top of one another in the center. All rhabdomeres are located underneath a single lens which makes them detect light from seven different points in space with R7 and R8 detecting the same point. Each point in the fly visual field is detected by multiple photoreceptors originating in different ommatidia. In order to increase sensitivity without affecting the spatial resolution in the neural superposition fly eye, axons of the outer photoreceptors that detect the same point in space are pooled into a single bundle, named a cartridge, that represents one point in space in the form of a single synaptic unit in a retinotopic order (Braitenberg 1967; Meinertzhagen and Boycott 1976; Meinertzhagen and Sorra 2001; Langen et al. 2015). Cartridges, as single columnar units, contact monopolar lamina neurons that project into the medulla retinotopically as well. Inner photoreceptors also have similar retinotopic projections in the medulla, R7s and R8s of the same ommatidium are organized in repetitive columnar units each in their respective layer. They contact uni-columnar

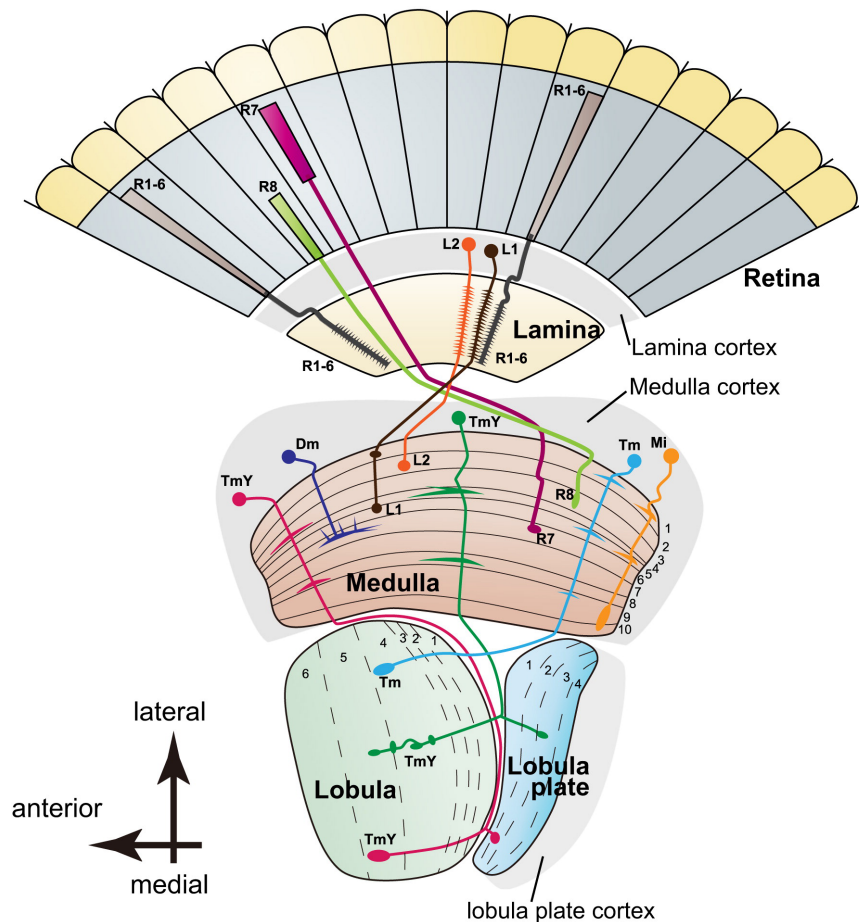


Fig. 1.2.1. Structure of the adult fly visual system.

A schematic drawing of the optic lobe of the adult fly. The optic lobe is composed of four neuropils; the lateral-most neuropil, the lamina, then the largest neuropil in the optic lobe, the medulla, followed by the lobula complex which is composed of the lobula and the lobula plate. The compound eyes contain ommatidia that are composed of six outer photoreceptors and two inner ones. Axons of the outer photoreceptors (R1-6) terminate in the lamina where they contact their postsynaptic lamina neurons that, in turn, project to the medulla in a retinotopic manner. R7s and R8s, on the other hand, have their rhabdomeres stacked on top of each other in the retina and project their axons to terminate in the medulla in the layers M6 and M3, respectively. The schematic shows examples of lamina and medulla neurons, together with their projections, that contact photoreceptors. The figure is used with permission and was adapted from (Sato et al. 2013).

and multi-columnar targets that project primarily to the lobula and the lobula plate (Fischbach and Dittrich 1989; Hofbauer and Campos-Ortega 1990).

1.2.2. Development of the fly visual system

Flies' development goes through three distinct phases; embryonic, larval, and pupal stages, the full process requires only ten days at 25° C. The embryonic stage is completed in 24 hours and then the egg hatches and goes through three larval instars in four days. Larvae are then

encapsulated and pupate as they lyse many larval structures and form the adult structures. The pupal stage lasts around 100 hours at 25° C with pupal stage marked as hour after pupal formation (APF) and ranges from 0-100 APF or, simply, P0-100, after which adult flies enclose. The optic lobe development commences in the embryonic stage from a 30-40 precursor cells located in the posterior part of the embryonic head (Green et al. 1993). Upon hatching, a small group of cells at the anterior-dorsal tip of the developing optic lobe of first and second instar larvae produce the inner and outer proliferation centers (IPC and OPC) neuroblasts that eventually develop to give rise to the lobula and the lobula plate, for the former, and the lamina and the medulla, for the latter (Hofbauer and Campos-Ortega 1990). During the third instar larval stage, the cells in the IPC and OPC divide and generate the neuroblasts that make up the neuropils of the optic lobe (Apitz and Salecker 2014). Neuroblasts of each neuropil differentiate in a temporal order, the medulla neurons and glia are the first to differentiate, followed by the lobula complex and, finally, the lamina which is separated from the medulla neuroblast by the formation of the deep lamina furrow. In each neuropil, cells differentiate in a sequential wave that moves from the posterior part to the anterior (Hofbauer and Campos-Ortega 1990; Egger et al. 2007).

The eye, on the other hand, develops from a bilayered epithelial tissue that originates from the embryonic epidermis, named the eye imaginal disc, during larval stages. Neuronal differentiation initiates, similar to the other neuropils of the optic lobe, at the posterior side of the eye imaginal disc as a transient invagination of the disc surface, known as the morphogenetic furrow, that gradually progresses and reaches the anterior side during the early pupal stage (Ready et al. 1976). Cells undergo disorganized divisions anterior to the morphogenetic furrow and become patterned into evenly-spaced arcs on the posterior side. These arcs transform into pre-clusters of five cells that differentiate to produce the photoreceptors. R8 is the first photoreceptor to differentiate in each ommatidium, followed by R2 and R5, and R3 and R4 in sequence. The remaining undifferentiated cells undergo another mitotic wave and differentiate to R1 and R6 followed by R7, cone cells and primary pigment cells (Fig. 1.2.2). During pupal stages, some of the remaining cells that surround ommatidial arcs either die or reorganize to form the hexagonal lattice that contain secondary pigment cells and mechanosensory bristles (Tomlinson and Ready 1987; Cagan and Ready 1989; Wolff and Ready 1991; Robertson et al. 2012).

By mid-third instar stage and shortly after differentiation, photoreceptors extend their axons towards the developing optic lobe through the optic stalk following the same order in which they differentiated (Tomlinson and Ready 1987). One important function of the extending photoreceptors is that they induce the differentiation of their target field, lamina precursor cells differentiate in response to a differentiation cue secreted by photoreceptors, via a signaling relay through glia, to generate lamina neurons (Selleck et al. 1992; Huang and Kunes 1996;

PART | 1 INTRODUCTION

Fernandes et al. 2017). Differentiated photoreceptors project their axons towards their targets, a process that concludes around the end of the first day of pupal development. R1-6 targeting follows two distinct steps; axons from the same ommatidium sequentially arrive in the lamina, in the order mentioned earlier, forming a bundle and position their axons between two layers formed of epithelial and marginal glia (Chotard et al. 2005). Afterwards, axons from different ommatidia that see the same point in space are sorted together to form a cartridge that extends and connects with lamina neurons as a single synaptic unit (Langen et al. 2015). R8s

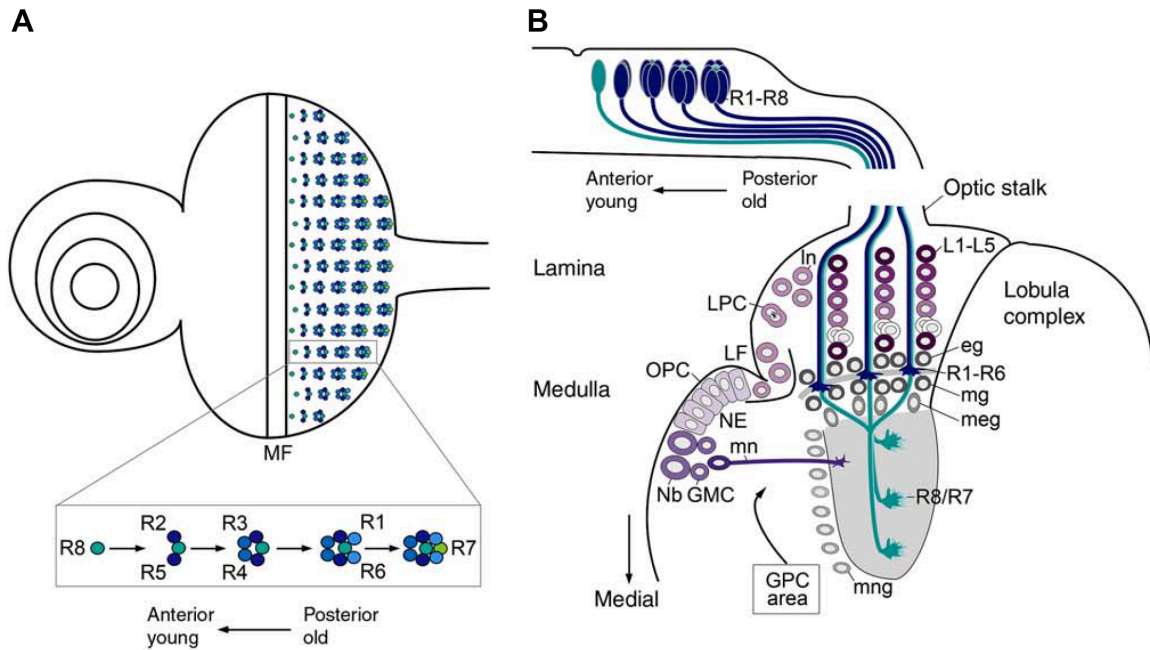


Fig. 1.2.2. Development of the fly visual system.

The precursors of the fly visual system originate in embryonic stages and develop starting larval stages. The development progresses in larval stages as cells differentiate and project to their targets that also synchronously develop to result in the final product of the adult structures by the end of pupal stages. **(A)** A schematic drawing of the eye imaginal disc in third instar larvae showing the morphogenetic furrow that originates at the posterior edge and sequentially sweeps towards the anterior edge driving the differentiation of photoreceptors in arrayed ommatidial clusters. R8 is the first cell to differentiate within a cluster followed by R2 and R5, R3 and R4, R1 and R6, and, finally, R7. MF: morphogenetic furrow. **(B)** Differentiated photoreceptors project their axons sequentially into the developing optic lobe right after they differentiate. As they pass through the optic stalk into their target regions, they signal the differentiation of their target cells in the lamina and the medulla. R1-6 axons terminate between two layers of glial cells while R8 and R7 axons terminate in the medulla. NE: lateral neuroepithelium, LF: lamina furrow, OPC: outer proliferation center, LPC: lamina precursor cells, LN: lamina neurons, NB: medulla neuroblasts, GMC: ganglion mother cells, EG: epithelial glia, MG: marginal glia, MN: medulla neurons, MEG: medulla glia, MNG: medulla neuropil glia, GPC: glial precursor cells. The figure was used with permission and was adapted from (Hadjieconomou et al. 2011).

sequentially project to the medulla, which is oriented at a right angle to the lamina during this developmental stage, and temporarily position their terminals at the distal-most layer, M0, before they synchronously extend to their final target layer, M3, by mid-pupal stage (Timofeev et al. 2012; Akin and Zipursky 2016; Kulkarni et al. 2016). R7 projections arrive in the medulla to terminate in the layer right proximal to R8s and establish contacts with their main targets, the Dm8 cells (Ting et al. 2014). As the medulla expands and more neurons intercalate between R8 and R7 terminals, R7 terminals passively-extend while remaining in the same layer, M6 (Ting et al. 2005; Özel et al. 2015). Around P25, the developing medulla gets pulled by the lamina and rotates to reach its eventual, adult position by P40 (White and Kankel 1978; Langen et al. 2015).

1.3. Observing photoreceptor development in an *in vivo* context

Live imaging, sometimes referred to as time-lapse imaging, of neurons has been used for decades to elucidate aspects of neuronal growth and chemotaxes as in the case with the pipette turning assay (Gundersen and Barrett 1979), the growth cone collapse assay (Raper and Kapfhammer 1990), and the Dunn turning assay (Yam et al. 2009). However, these tests were performed to test the responses of isolated neurons in primary 2D cultures which was shown to affect cellular morphology and behavior compared to 3D cultures (D'Aiuto et al. 2018).

Although observing cultured primary neurons is a simple, quick, and typically reproducible method to infer the molecular mechanisms of the tested proteins, the technique can lead to inaccurate conclusions since it isolates neurons from the crowded and complex native *in vivo* context. Therefore, live imaging of neurons in intact developing brains, when technically feasible, is superior to other *in vitro* methods. Live imaging of photoreceptors and their interactions over time revealed the rules that govern neuronal superposition in the fly visual system (Langen et al. 2015), and also revealed unexpected behavior and migration pattern of the displaced amacrine cells during retinal lamination in zebrafish (Chow et al. 2015).

1.3.1. *Ex vivo* brain culture

Cultured adult fly brains were used to investigate neuronal regeneration after injury. The versatile method was developed to enhance the accessibility to reproducible manipulations while keeping the brains alive for a period up to one week in culture (Ayaz et al. 2008). Based on this method, Özel and colleagues developed the technique to culture a developing fly brain which allowed observing neurons during various stages of development (Özel et al. 2015).

Eye-brain complexes were dissected and kept immobilized by embedding them in low-melting agarose positioned on a layer of a chemically-inert layer of Sylgard. Nutrients and oxygen were supplemented to the brain using oxygenated culture media and a coverslip was placed

PART | 1 INTRODUCTION

on spacers that prevented brains from being crushed under the weight of the coverslips before the chamber was sealed (Fig. 1.3.1.). *ex vivo* brains in chamber continued to develop for at least 24 hours while continuously being subjected to scanning laser without affecting development. This method allowed imaging of fluorescently-tagged photoreceptors for extended period of time at high spatial and temporal resolutions to observe the dynamics of individual growth cones and filopodia (Özel et al. 2015).

1.3.2. Live imaging revealed the role of growth cone stabilization and filopodial dynamics in R7 targeting

Özel and colleagues used the previously-described live imaging of *ex vivo* cultured brains to observe developing R7s and reported the morphological changes to R7 growth cones during key developmental stages. R7 growth cones exhibited an inverted cone-shape morphology at

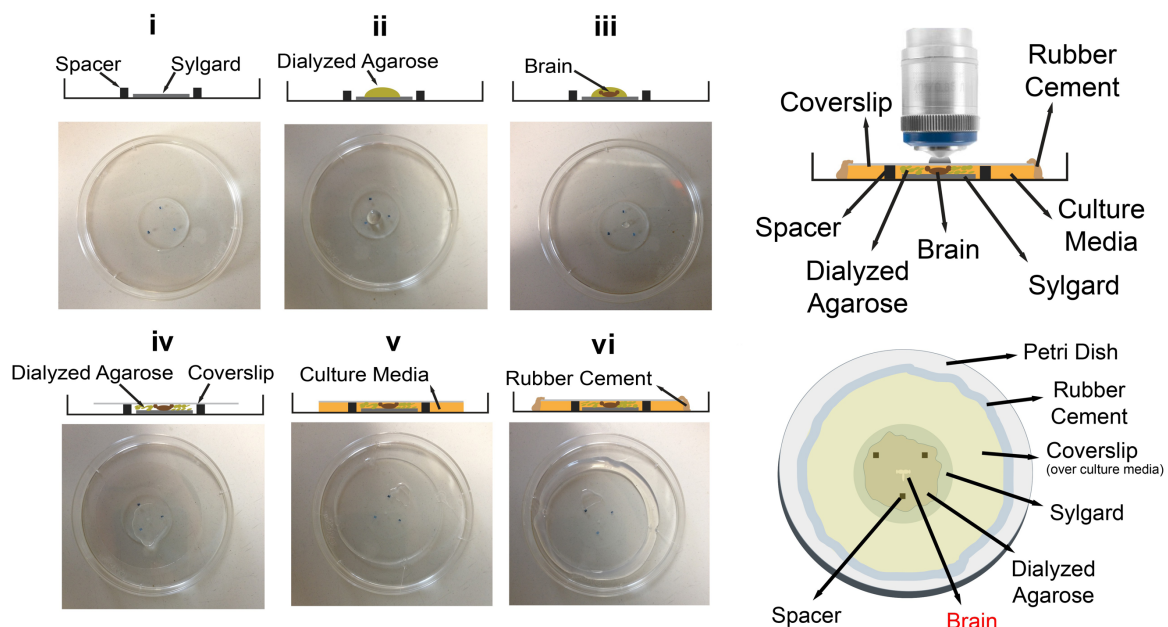


Fig. 1.3.1. The *ex vivo* brain culture imaging chamber.

To the left, step-by-step assembly of the imaging chamber. (i) spacers are positioned on a layer of Sylgard in the form of a triangle. (ii) a drop of low-melting agarose is pipetted onto the center of the Sylgard layer within the spacers triangle. (iii) The dissected eye-brain complex is carefully pipetted into the agarose drop and gently rotated to the correct orientation with the tissue of interest to the top. (iv) The coverslip was placed to cover the mix and gently adjusted to be completely horizontal resting on all the three spacers. (v) The agarose was allowed to polymerize before filling the space underneath the coverslip with the oxygenated culture media. (vi) Finally, the chamber was sealed and kept until all the components are fully immobilized before imaging. To the right, a schematic drawing of the imaging chamber viewed from the side (top) and the top (bottom), the objective of the scanning microscope is at the side of the coverslip. The figure was adapted from (Özel et al. 2015).

P30 with wider expansion at the proximal end, then new varicosities start to emerge at the distal end of the cone-shaped structure that passively-expands to turn the entire terminal into a bipartite structure. Interestingly, the observed varicosities at the distal edge of the cone-shaped growth cones were found to mark the layer that R8s actively extend to, suggesting that this layer (M3) is defined by other cell types (Özel et al. 2015). This finding confirmed the passive model that was proposed for R7 layer targeting (Ting et al. 2005), and opposes an earlier, commonly-accepted model which proposed that R7s initially target a temporary distal layer before they extend to a new proximal one (Mast et al. 2006; Melnattur and Lee 2011).

Live imaging of R7 filopodial dynamics captured the transition of growth cones before P50 that form numerous filopodia which invade adjacent columns into growth cones with fewer and shorter filopodia that are column-restricted. Filopodial dynamics were found to have distinct signatures depending on the developmental stage; growth cones at P28 formed numerous stable and transient filopodia and their kinetic characteristics were not changed until P50 that only showed a reduction in their number, then at the onset of synaptogenesis (P60) growth cones form much fewer transient filopodia while forming a new type of stable filopodia, termed bulbous tips, that are distinctly-different in both structure and dynamics. The two types of stable filopodia observed before and after P50 were correlated with two different developmental subprograms; before P50, stable filopodia stabilize and restrict growth cones within their columns, while the stable bulbous tips that emerge after P50 accompany interactions with presumptive synaptic partners after the layers are defined (Özel et al. 2015).

The analysis was expanded to include the changes in growth cone and filopodial dynamics in R7s upon loss of *n-cadherin* (*ncad*) which was previously-described to affect R7 targeting and causes them to retract to M3 (Lee et al. 2001; Ting et al. 2005). Live imaging of mutant R7s confirmed their initial correct targeting followed by probabilistic retractions and found that some R7s completely retract out of the medulla before they re-extended back to the medulla and even arborize in their correct layer or other incorrect layers. Mutant R7s also exhibited less dynamic filopodia that were also much shorter as they retract compared to wildtype R7s, suggesting that changes in filopodial dynamics can predict R7 stabilization in their correct layer and that NCad is required to stabilize R7s in their target layer rather than instruct such targeting (Özel et al. 2015).

These observations show the strength of live imaging as it revealed a phenotype that was not possible to recognize otherwise using fixed preparations. It also adds a new perspective and limitless capabilities to study neuronal development as a dynamic process.

1.4. What functions do cell adhesion molecules execute in R7 development?

Correct targeting of R7s required the function of several cell adhesion molecules. Such molecules were reported to execute their functions by interacting with several other proteins,

PART | 1 INTRODUCTION

primarily cytoskeleton regulators, or to execute functions redundant to that of other cell adhesion molecules. However, their precise rules in R7 targeting remain unclear. Therefore, I used live imaging of *ex vivo* cultured brains to observe the R7s responses to the loss of function of cell adhesion molecules (introduced below), how they affect filopodial dynamics and, consequently, synapse formation. In addition to live imaging, several molecular and genetic tools were used to reveal the functions of the studied cell adhesion molecules with the added hope that this will help us better understand what developmental rules they execute in brain wiring.

1.4.1. Lar

Leukocyte-antigen-related-like (Lar) is a broadly-expressed protein tyrosine phosphatase (PTP) that plays important developmental roles in neuronal and non-neuronal tissues. Lar belongs to the immunoglobulin (Ig) cell adhesion molecules superfamily and is a single-pass transmembrane protein with extracellular fibronectin and immunoglobulin domains and two phosphatase domains at the intracellular side that are conserved among all other PTPs (Streuli et al. 1989).

1.4.1.1. Lar functions in developing neurons

Lar is an active zone membrane protein that is implicated in axon guidance and synapse formation in vertebrate and invertebrate neurons (Stoker 2015). In *Drosophila*, loss of *lar* was reported to affect embryonic motor neuron guidance and synaptic growth (Krueger et al. 1996; Kaufmann et al. 2002) and the synaptic bouton size in larval neuromuscular synapses (Astigarraga et al. 2010). Lar was also found to be important for photoreceptor sorting (R1-6) and their correct layer targeting (R7s but not R8s) (Clandinin et al. 2001; Choe et al. 2006). R7s mutant of *lar* terminated in the distal medulla layer M3 instead of their correct layer M6, a phenotype that was found to be caused by R7 retraction rather than mistargeting (Maurel-Zaffran et al. 2001; Hakeda-Suzuki et al. 2017).

1.4.1.2. Complex interactions of Lar to control its neuronal functions

Neuronal functions of Lar require interaction with several other proteins. Most notably, its interaction with the active zone protein Liprin- α which is required for neuro-muscular junction (NMJ) synaptic growth and correct R7 targeting. Loss of function mutation for both proteins show overlapping but not identical phenotypes that are partially rescued by the overexpression of the RhoGEF Trio or the RhoGAP Syd-1 (Maurel-Zaffran et al. 2001; Hofmeyer et al. 2006; Astigarraga et al. 2010; Holbrook et al. 2012; Hakeda-Suzuki et al. 2017).

Furthermore, Lar functions upstream of the cytoskeleton regulators Abelson kinase (Abl) and Ena to control motor neuron guidance (Wills et al. 1999) and genetically interacts with the

formin Diaphanous (Dia) in the NMJ to promote synaptic growth as it controls microtubules stabilization and Actin polymerization (Pawson et al. 2008).

I aimed at investigating the role of Lar and its interacting proteins for R7 targeting, filopodial dynamics regulation and synapse formation. I also proposed Lar and Liprin- α interaction to regulate microtubule stabilization as a potential explanation for their functional requirement in R7 synapse formation.

1.4.2. PTP69D

Similar to Lar, PTP69D is another member of the protein tyrosine phosphatase family of transmembrane proteins. It shares the same structural domains as the other members of the PTP family with two intracellular phosphatase domains and extracellular fibronectin and immunoglobulin domains. The protein is widely-expressed and is enriched in the nervous system of both vertebrates and invertebrates.

1.4.2.1. Neuronal functions of PTP69D

The *Drosophila* PTP69D and its vertebrate homologue PTP σ are active zone proteins that regulate neuronal outgrowth and targeting (Desai and Purdy 2003; Sajnani et al. 2005). In the fly visual system, loss of *ptp69d* was reported to cause R1-6 overshoot and terminate in the medulla instead of the lamina, and also caused R7s to retract from their correct terminal layer to M3 (Garrity et al. 1999; Newsome et al. 2000a; Hakeda-Suzuki et al. 2017). PTP69D is also required for correct muscle targeting of embryonic motor neurons (Desai and Purdy 2003).

In the fly CNS, PTP69D promotes midline crossing of mechanosensory neuron collaterals by dephosphorylating Dscam1 (Dascenco et al. 2015) and of midline crossing neurons in the brain by regulating membrane presentation of Robo receptor (Oliva et al. 2016).

The vertebrate PTP σ , in addition to promoting neuronal outgrowth, also plays an essential role in glutamatergic synapse formation (Takahashi et al. 2011), a function that was not previously reported for the *Drosophila* PTP69D.

1.4.2.2. Functional redundancy of PTP69D to other PTPs in neuronal development

PTP69D interacts with other fly PTPs to control embryonic interneuron guidance. Its loss of function causes neuronal targeting defects, a phenotype that is enhanced when combined with loss of function of other PTPs (Sun et al. 2001). In the visual system, PTP69D was proposed to interact with Lar to regulate R7 targeting. Unlike Lar, the phosphatase activity of PTP69D is required for R7 targeting (Hofmeyer and Treisman 2009), and a chimeric PTP receptor with the extracellular Lar domains and the PTP69D intracellular phosphatase domains rescues the lar R7 mistargeting phenotype (Maurel-Zaffran et al. 2001). In addition, R7s mutant of both *lar*

PART | 1 INTRODUCTION

and *ptp69d* were found to retract to the lamina instead of terminating in M3 (Hakeda-Suzuki et al. 2017).

I intended to understand the previously-described interaction between PTP69D and Lar in regulating R7 targeting and their functional redundancy. For that, I characterized the effect of *ptp69d* loss of function on R7 filopodial dynamics and synapse formation and compared it to the phenotypes associated with *lar* loss of function.

1.4.3. Neurexin-1

Neurexins are presynaptic transmembrane proteins that are localized in presynaptic active zones. Vertebrates encode three neurexin genes controlled by two promoters which give rise to α - and β -neurexins. Their transcripts undergo alternative splicing to give rise to more than 1000 isoforms with varying binding specificity to the neurexin ligand, neuroligin (Ullrich et al. 1995). The interaction of neurexin and neuroligin is important to induce morphological and functional presynaptic differentiation in axons (Scheiffele et al. 2000). Mice mutant of the three neurexin genes showed that α -neurexin is not essential for synapse formation but rather for Ca^{2+} -triggered neurotransmitter release, as α -neurexin controls Ca^{2+} channel function but not their number (Missler et al. 2003).

1.4.3.1. The *Drosophila* NrX

The fly genome encodes two Neurexins (NrX); one is NrX-IV which is homologous to the vertebrate contactin and is primarily expressed in epithelial and glial cells to control the organization of the septate junctions (Faivre-Sarrailh et al. 2004). The other is NrX-1 which is homologous to α -neurexin, it is enriched in the synaptic neuropil regions of the fly central nervous system. Flies do not have a homologue to β -neurexins and NrX-1 is not alternatively spliced. Mutant flies are viable and fertile but have a reduced life span (Zeng et al. 2007).

1.4.3.2. Synaptic functions of NrX

In the larval NMJ, NrX mediates pre-postsynaptic apposition and it localizes at the presynaptic active zone. NrX function is required for the proliferation of synaptic boutons at the glutamatergic NMJs. Loss of *nrx* leads to the ectopic accumulation of the synaptic vesicle protein, Synaptotagmin, and the active zone protein Brp within motor neuron axons. Electron micrographs of *nrx* mutant synaptic boutons showed ultrastructural synaptic changes as active zones were abnormally long and the number of T-bars was increased as well. These structural changes in synaptic boutons caused electrophysiological changes in the NMJs as well; the amplitude and frequency of the miniature excitatory potentials (mEJPs) were increased while the evoked excitatory potentials (EJPs) was reduced suggesting a synaptic transmission defect (Li et al. 2007).

The function of Nr_x in photoreceptors was not described thus far. In this section, I asked if Nr_x's function in promoting pre-postsynaptic apposition is required for synapse formation and photoreceptor targeting. Furthermore, I aimed at finding whether Nr_x is essential for photoreceptors to specify their synaptic partners.

1.4.4. Amyloid Precursor Protein-Like

Amyloid precursor protein (APP) is a transmembrane protein known for its role in the pathogenesis of Alzheimer's disease. Amyloid- β (A β) is one of its proteolytic cleavage products that aggregate to form plaques as a hallmark of Alzheimer's disease. The APP protein family contains two other members; amyloid precursor-like protein (APLP)-1 and -2 that are assumed to be functionally redundant to APP (Shariati and De Strooper 2013). The APP isoform, APP₆₉₅ is enriched in neurons and its cleavage gives rise to A β .

Despite decades of research, the physiological functions of APP in neurons remains unclear. APP was reported to have broad functions in all aspects of neuronal biology, including neurite outgrowth, synapse formation, and neuronal survival. However, studies often report different, and sometimes contradicting, conclusions about the exact function of APP (Müller et al. 2017).

1.4.4.1. The *Drosophila* homologue of APP

The fly genome encodes only one homologue of APP, APP-like (APPL). It contains all the key domains and shares the same organization as APP₆₉₅ (Rosen et al. 1989). APPL is expressed in all post-mitotic neurons in the central and peripheral nervous systems, its transcripts localize to neurons, but not glia, in the cortical region of the central nervous system (Martin-Morris and White 1990).

APPL is proposed to be an excellent model to study the physiological functions of APP in neurons; both proteins share the same domains and are functionally homologous (Luo et al. 1992). At the same time, APPL is the only homologue in flies which eliminates any confounding effects of other APP family proteins or APPL that is produced in other non-neuronal tissues.

1.4.4.2. Neuronal functions of APPL

APPL abundantly localizes in growing axons and in terminals during synapse formation (Torroja et al. 1996). It is particularly enriched in the mushroom body where it is required for the formation of α and β lobes during development and for memory and learning in adult flies (Goguel et al. 2011; Soldano et al. 2013). APPL also regulates neuronal outgrowth and is upregulated after injury in adult brains to control neurite arborization (Li et al. 2004; Leyssen et al. 2005).

Similar to the vertebrate homologue, APPL is proteolytically cleaved by secretases to release the intracellular domain (AICD) and secrete the extracellular fragments (Luo et al. 1990), these

PART | 1 INTRODUCTION

cleavage products are processed and trafficked differentially within neurons in different developmental stages (Ramaker et al. 2016). APPL is cleaved by α - and β -secretases to release the α - and β -secreted fragments (sAPPL), respectively, that functioned as neuroprotective in adult flies (Wentzell et al. 2012; Bolkan et al. 2012).

APPL functions as a co-receptor for a variety of membrane proteins that interact with APPL through its conserved endocytic YENPTY motif in the AICD which regulates their endocytosis, trafficking, and signaling (King et al. 2003; Gunawardena et al. 2013; Müller et al. 2017; Penserga et al. 2019). APPL interacts with FasII in the NMJ and promotes synapse formation in a dose-dependent manner (Torroja et al. 1999; Ashley et al. 2005).

In the fly visual system, APPL is expressed in all photoreceptors and enriched in the UV sensitive R7. Its loss of function reduced flies UV light preference and caused a subtle R7 mistargeting defect to terminate in M3 (Mora et al. 2013).

I characterized the role of APPL in R7 targeting and synapse formation and if its interaction with other membrane proteins is required for such functions. I also studied the dynamics of the APPL proteolytic cleavage products and their localization in photoreceptors during development.

PART | 2 MATERIALS AND METHODS

PART | 2 MATERIALS AND METHODS

2.1. Flies

Flies were raised on standard *Drosophila* food in dark, 25°C incubators. Crosses were constantly maintaining in a healthy state with around 15 flies in each vial. Flies were transferred to fresh vials every other day and new males and females were added regularly to the crosses. To study different developmental stages, white pupa (P0) were selected and kept in humid chambers at 25°C until the desired stage. Unless otherwise mentioned, pupae were not selected for gender in any of the experiments. The detailed information regarding the used fly lines and alleles will be specified in each respective section.

2.2. Generating photoreceptor clones

Three strategies were used to generate photoreceptor clones:

- Generating whole-mutant eyes in otherwise heterozygous animals: The FRT/flip system was used to generate homozygous mutant clones and *ey3.5flip* was used to restrict the recombination to photoreceptors (Newsome et al. 2000a). This system flips the desired mutant gene over *minute* mutation (referred to as *cl*), which results in homozygous clones of either gene. The *minute* mutation prevents photoreceptor survival in homozygosity, and the only remaining populations were the homozygous photoreceptors mutant of the desired gene that proliferated and formed full-mutant eyes together with a small population of heterozygous photoreceptors.
- Generating R7 mutant clones in otherwise heterozygous animals: Using Mosaic analysis with a repressible cell marker (MARCM) (Lee and Luo 1999) and driving the mitotic recombination with *GMRflip*. This generated R1 and R6 clones in the lamina, and R7s clones in the medulla.
- Generating sparse photoreceptor clones: To express a certain marker or RNAi sparsely in photoreceptors, *hsflip* was used to flip out a stop cassette terminating the expression of Gal4 in the construct *GMR-FRT-stop-FRT-Gal4* (Chen et al. 2014), the size of the clones could be controlled by the duration of the applied heat-shock. Experimental crosses were set at room temperature and flies were allowed to lay eggs for two days before they were flipped to another fresh vial. After a further two days, vials with developing eggs and larvae were heat-shocked in a water bath at 37°C for 12 minutes and then kept at room temperature until further experimental steps.

2.3. Immunohistochemistry and Fixed Imaging

Eye-brain complexes were dissected in cold Schneider's *Drosophila* medium. Brains were then transferred to 3.7% formaldehyde (FA) in PBS and fixed for an hour before washing in PBST (PBS+0.4% Triton-X). Brains were then either directly mounted in antifade mounting medium

(Vectashield) or further processed for antibody staining. The antibodies used will be specified in each section later on.

Imaging was performed at 18°C in a temperature-controlled room using a Leica TCS SP8-X white laser confocal microscope with 20x/0.95 and 63x/1.3 glycerol objectives.

2.4. Live Imaging

Ex vivo eye-brain complexes were prepared as described in (Özel et al. 2015). For filopodial imaging, scanning was performed using a Leica SP8 MP microscope with a 40x/1.1 IRAPO water objective with a Chameleon Ti:Sapphire laser and Optical Parametric Oscillator (Coherent). A single excitation laser was set to 900 nm for single-fluorophore GFP scans, and to 950 nm for two-fluorophore GFP/Tom scans. For two-fluorophore GFP/mCherry scans, lasers were set to 890 nm (pump) and 1110 (OPO).

For sAPPL migration (in section 6.2.2.2), scanning was performed using a Leica TCS SP8-X white laser confocal microscope with a resonant scanner with the 20x/0.95 water objective.

2.5. Molecular Biology

2.5.1. Genetics

To recombine the *nrx*²⁴¹ allele on FRT82B, virgin females with the two components in heterozygosity were crossed to 3rd chromosome balancer lines. Flies were allowed two days on regular food until they started laying eggs, then they were transferred to fly food vials containing 500 µg neomycin/ 1ml fly food. Flies were kept at 25°C and regularly transferred to fresh neomycin vials. Males from the off-spring were individually tested to have both the components and eventually used to establish stocks.

2.5.2. Confirming *nrx* recombinant lines

To test the candidate recombinant lines, A PCR strategy was designed to test for the *nrx*²⁴¹. Three primers were designed; one common forward and two different complementary reverse primers. The forward primer with the sequence: 5'- CGCGCTAAAATCCAGCCC-3' binds upstream of the reported excised genomic region. The reverse primers were: 5'- GCCGGTGCCGATGTCTATG-3' (which was named the long reverse primer) and 5'- CGACTGTTAACGGCACTGC-3' (which was named the short reverse primer). The forward and the long reverse primers were designed as reported in (Li et al. 2007).

Genomic DNA was extracted as explained before from heterozygous flies and two PCRs were set for each candidate line. The PCR program was set to have a short annealing time that will only allow amplification of fragments shorter than 6 kb which will amplify the short fragment (which acts as a control) and the long fragment only in the case of *nrx*²⁴¹ where 18 kb were

PART | 2 MATERIALS AND METHODS

excised leaving a shorter, amplifiable fragment. The exact excised fragment was not defined in the original paper; hence, it was not possible to predict the size of the 'long' PCR product.

2.5.3. *ptp69d* mutant allele genotyping

Primers were designed to amplify a fragment of around 1.5 kb of the genomic region of *ptp69d* that includes the second exon carrying the reported point mutation. Primer sequences were: 5'- TACCGACGCATGTCGATGC-3' and 5'- GCCTCCTGCAGAGTGATGAAG-3'. Primers were designed to have an annealing temperature of 60°C.

Genomic DNA was extracted from heterozygous flies bearing the homozygous lethal *ptp69d*^{D1689} allele. Flies were digested in fly squishing buffer with Proteinase-K and then 2 µl of the solution were used as a template to amplify the genomic fragment. The polymerase chain reaction (PCR) was done using Phusion® High-Fidelity DNA Polymerase following the manufacturer's instructions. The PCR products were then separated on 1% agarose gel and the desired band was then purified from the gel and sequenced using the sequencing primers: 5'- GGCTAAACAAAAGTAGTCGCGC-3' and 5'- GGAATTCAAACACTGGCTGCCG-3'.

2.5.4. Anterograde trans-synaptic circuit tracing

Crosses were set and maintained at room temperature. As soon as the off-spring encloses, flies bearing the correct genotype were kept at 18°C in the dark for 7 days. Eye-brain complexes were then dissected, fixed, and stained for NCad as a neuropil marker and for HA-tag to enhance the labeling of the post-synaptic cells.

2.6. Electroretinogram (ERG) Recordings

For this experiment, flies with whole-mutant eyes, and their respective controls, were generated in otherwise heterozygous animals. In other cases, genes were knocked-down in photoreceptors using GMR-Gal4 driving the expression of the corresponding RNAi lines and scRNAi as a control.

Newly-hatched flies were glued on glass slides using non-toxic school glue. Flies were exposed to cycles of 1 second pulses of light stimulus followed by 2 seconds of dark provided by computer-controlled white-light-emitting diode system (MC1500; Schott). ERGs were recorded using Clampex (Axon Instruments) and quantified using Clampfit (Axon Instruments).

2.7. Data processing and Analysis

3D-fixed and 4D-live imaging data were deconvolved using Microvolution Fiji extension (10 iterations with the theoretical PSF). Data were analyzed and presented using Imaris 9.1 (Bitplane). Quantifications were done manually unless otherwise mentioned. Statistical analysis was done using Prism 8 (GraphPad) by unpaired, parametric student's t-test. Graphs

were also prepared using Prism 8 with data represented as the mean \pm SEM. Figures were eventually assembled using Adobe Photoshop and Illustrator.

2.8. Resources Table

Reagent or Resource	Source	Identifier
Fly lines and alleles		
<i>Drosophila</i> , <i>cs</i>	BDSC	6365
<i>Drosophila</i> , <i>ey3.5flp</i> (X)	Bloomington <i>Drosophila</i> Stock Center (BDSC)	35542
<i>Drosophila</i> , <i>GMRflp</i> (X)	BDSC	42735
<i>Drosophila</i> , <i>hsflp</i> (X)	BDSC	8862
<i>Drosophila</i> , <i>FRT40A</i> , <i>ry</i>	BDSC	8212
<i>Drosophila</i> , <i>FRT80B</i> , <i>ry</i>	BDSC	1988
<i>Drosophila</i> , <i>FRT82B</i> , <i>ry</i>	BDSC	2035
<i>Drosophila</i> , <i>FRT40A</i> , <i>Tub-Gal80</i>	BDSC	5192
<i>Drosophila</i> , <i>FRT42D</i> , <i>GMR-Gal80</i>	(Özel et al. 2019)	
<i>Drosophila</i> , <i>FRT80B</i> , <i>Tub-Gal80</i>	BDSC	5191
<i>Drosophila</i> , <i>FRT82B</i> , <i>Tub-Gal80</i>	BDSC	5135
<i>Drosophila</i> , <i>FRT40A</i> , <i>cl</i> , <i>w⁺</i>	BDSC	5622
<i>Drosophila</i> , <i>FRT80B</i> , <i>RpS17⁴</i> , <i>w⁺</i>	BDSC	5621
<i>Drosophila</i> , <i>FRT82B</i> , <i>cl</i> , <i>w⁺</i>	BDSC	5620
<i>Drosophila</i> , <i>GMR-Gal4</i> (II)	BDSC	1104
<i>Drosophila</i> , <i>GMR-Gal4</i> (III)	BDSC	29967
<i>Drosophila</i> , <i>GMR>Stop>Gal4</i>	(Chen et al. 2014)	
<i>Drosophila</i> , <i>Rh4-Gal4</i> (II)	Gift from M. Wernet	
<i>Drosophila</i> , <i>Elav-Gal4</i> (II)	BDSC	8765
<i>Drosophila</i> , <i>Elav-Gal4</i> (III)	BDSC	8760
<i>Drosophila</i> , <i>9B08-Gal4</i>	BDSC	41369
<i>Drosophila</i> , <i>GMR-Gal80</i>	(Özel et al. 2019)	
<i>Drosophila</i> , <i>Repo-Gal4</i>	BDSC	7415
<i>Drosophila</i> , <i>APPL-TG4</i>	BDSC	66900
<i>Drosophila</i> , <i>Repo-lexA</i>	Gift from T. Lee	
<i>Drosophila</i> , <i>GMRmyrtdTom</i> (II)	Gift from S. Lawrence Zipursky	
<i>Drosophila</i> , <i>GMRmyrtdTom</i> (III)	Gift from S. Lawrence Zipursky	
<i>Drosophila</i> , <i>UAS-CD4tdGFP</i> (II)	BDSC	35839

PART | 2 MATERIALS AND METHODS

<i>Drosophila</i> , UAS-CD4tdGFP (III)	BDSC	35836
<i>Drosophila</i> , UAS-CD4tdTom (III)	BDSC	35837
<i>Drosophila</i> , lexAop-CD4tdGFP (II)	BDSC	77136
<i>Drosophila</i> , lexAop-CD4tdTom (III)	BDSC	77139
<i>Drosophila</i> , UAS-BrpD3-GFP	(Schmid et al. 2008)	
<i>Drosophila</i> , UAS-BrpD3-mKate2	(Özel et al. 2019)	
<i>Drosophila</i> , UAS-myrGFP, QUAS-mtdTomato (3xHA); trans-Tango	(Talay et al. 2017)	
<i>Drosophila</i> , UAS-APPL	Gift from B. Hassan	
<i>Drosophila</i> , UAS-mCherry-APPL-GFP	Gift from B. Hassan	
<i>Drosophila</i> , UAS-Liprin- α -GFP	(Fouquet et al. 2009)	
<i>Drosophila</i> , UAS-Eb1-mCherry	(Alves-Silva et al. 2012)	
<i>Drosophila</i> , UAS-GFP-Tub (III)	BDSC	7373
<i>Drosophila</i> , UAS-Trio	(Newsome et al. 2000b)	
<i>Drosophila</i> , IGMR-GFP-Hth	Gift from M. Wernet	
<i>Drosophila</i> , FRT40A, <i>lar</i> ²¹²⁷	BDSC	63796
<i>Drosophila</i> , FRT40A, <i>liprin-α^E</i>	(Choe et al. 2006)	
<i>Drosophila</i> , FRT40A, <i>dia</i> ⁵	BDSC	9138
<i>Drosophila</i> , FRT80B, <i>ptp69d</i> ^{D1689}	Gift from D. Schmucker	
<i>Drosophila</i> , FRT82B, <i>syd-1</i> ^{w46}	(Holbrook et al. 2012)	
<i>Drosophila</i> , <i>nrx</i> ²⁴¹	Gift from S. Sigrist	
<i>Drosophila</i> , <i>app</i> ^d	Gift from B. Hassan	
<i>Drosophila</i> , <i>app</i> ^d , <i>hsflp</i>	Gift from B. Hassan	
<i>Drosophila</i> , <i>app</i> ^{dc21}	Gift from B. Hassan	
<i>Drosophila</i> , <i>cadn</i> ⁴⁰⁵	(Lee et al. 2001)	
<i>Drosophila</i> , <i>gogo</i> ^{H1675}	Gift from I. Kadow	
<i>Drosophila</i> , <i>caps</i> ^{c28fs}	Gift from T. Hummel	
<i>Drosophila</i> , <i>fm</i> ^{te59}	Gift from T. Suzuki	
<i>Drosophila</i> , <i>brp</i> ^{c04298}	Gift from S. Sigrist	
<i>Drosophila</i> , <i>trio</i> ³	BDSC	9130
<i>Drosophila</i> , <i>rab5</i> ²	BDSC	42702
<i>Drosophila</i> , <i>rab7</i> ^{KO}	(Cherry et al. 2013)	
<i>Drosophila</i> , <i>fra</i> ³	BDSC	8813
<i>Drosophila</i> , <i>vang</i> ¹	Gift from B. Hassan	

PART | 2 MATERIALS AND METHODS

<i>Drosophila</i> , <i>psn</i> ⁹	BDSC	8295
<i>Drosophila</i> , <i>ref</i> ^{E20}	BDSC	9457
<i>Drosophila</i> , <i>abl</i> ²	BDSC	8565
<i>Drosophila</i> , <i>dab</i> ¹	BDSC	32653
<i>Drosophila</i> , <i>nrt</i> ²	BDSC	25033
<i>Drosophila</i> , Df(3R)5Ca	Gift from S. Sigrist	
<i>Drosophila</i> , UAS-scRNAi	Vienna Drosophila Resource Center (VDRC)	60200
<i>Drosophila</i> , UAS- <i>dcin</i> RNAi	VDRC	22163
<i>Drosophila</i> , UAS- <i>ptp69d</i> RNAi (II)	VDRC	27090
<i>Drosophila</i> , UAS- <i>ptp69d</i> RNAi (III)	VDRC	27091
<i>Drosophila</i> , UAS- <i>kuz</i> RNAi	VDRC	107036
<i>Drosophila</i> , UAS- <i>bace</i> RNAi	VDRC	15541
<i>Drosophila</i> , Hand-GFP	Gift from Z. Han	

Antibodies

Mouse anti-Chaoptin	Developmental Studies Hybridoma Bank (DSHB)	24B10
Rat anti-nCad	DSHB	DN-Ex #8
Mouse anti-DNrx	Gift from J. Han	
Mouse anti-Elav	DSHB	9F8A9
Rabbit anti-APPL	Cell Signaling	2452S
Rabbit anti-Rab5	Abcam	ab3126
Rabbit anti-Rab7	Gift from Patrick Dolph	
Guinea pig anti-V100	(Hiesinger et al. 2005)	
HA-Tag (C29F4) Rabbit mAb	Cell Signaling Technology	3724
Cy3™ AffiniPure Goat Anti-Rabbit IgG (H+L)	Jackson laboratories	111-165-003
Cy3™ AffiniPure Goat Anti-Mouse IgG (H+L)	Jackson Laboratories	115-165-166
Cy5™ AffiniPure Goat Anti-Mouse IgG (H+L)	Jackson laboratories	115-175-166
Cy5™ AffiniPure Goat Anti-Rat IgG (H+L)	Jackson laboratories	112-175-143
DyLight™ 405 AffiniPure Donkey Anti-Mouse IgG (H+L)	Jackson Laboratories	715-475-150
Alexa Fluor® 488 AffiniPure Goat Anti-Rabbit IgG (H+L)	Jackson Laboratories	111-545-003
Alexa Fluor® 647 AffiniPure Goat Anti-Guinea Pig IgG (H+L)	Jackson Laboratories	106-605-003

Reagents and Recombinant proteins

Vectashield	Vector Laboratories	H-1000
-------------	---------------------	--------

PART | 2 MATERIALS AND METHODS

Formaldehyde	Merck KgaA	1.03999.1000
PBS	Gibco	70011-36
Triton X-100	Sigma-Aldrich	T8787
Schneider's <i>Drosophila</i> Medium [+] L-Glutamine	Gibco	21720-024
Agarose, low gelling temperature	Sigma-Aldrich	A9045-10G
Insulin, human recombinant, zinc solution	Gibco	12585014
Penicillin/Streptomycin	Gibco	15140122
ES Cell FBS	Gibco	16141-061
20-Hydroxyecdysone	Sigma-Aldrich	5289-74-7
SilGard and Silicone Elastomer Kit	Dow Corning	184
Proteinase-K	New England BioLabs (NEB)	P8107S
SapphireAmp fast PCR—hot-start master mix	Takara	RR350A
Phusion® High-Fidelity DNA Polymerase	NEB	M0530S
Agarose	Sigma-Aldrich	A6361
G 418 disulfate salt	Sigma-Aldrich	A1720

Software

Imaris 9.1	Bitplane, Switzerland
ImageJ	National Institute of Health (NIH)
Microvolution Plug-in	Microvolution
GraphPad Prism 8	GraphPad Software, La Jolla, USA
SnapGene 3.2.1	GSL Biotech LLC
Clampfit	Axon Instruments
Clampex	Axon Instruments
Photoshop CC 2019	Adobe Inc.
Illustrator CC 2019	Adobe Inc.

PART | 3 LAR

Complex Interactions of Lar to Regulate
Photoreceptor Targeting and Synapse Formation

3.1. Contribution

I designed and generated all the fly lines in this section. I also performed all the experiments and analyzed the results myself, with the exception of the live imaging of both wildtype and *liprin- α* mutant R7s in Fig. 3.2.1.1-1 which were performed by M. Neşet Özel.

3.2. Results

3.2.1. Role of Lar and Liprin- α in R7 layer targeting and synapse formation

Lar and its cytoplasmic interacting protein Liprin- α were shown to affect synapse formation and maturation in the NMJ. In the fly visual system, both proteins were reported to control R7 target layer selection. Their loss of function caused R7s to terminate in the distal M3 medulla layer instead of the correct M6 layer. However, their role in synapse formation in R7 was not known. Part of this work was published in (Özel et al. 2019).

3.2.1.1. Lar and Liprin- α are required to stabilize R7s in their target layer

To understand the requirement of Lar and Liprin- α for R7 layer targeting, I generated R7 clones mutant for either gene in otherwise heterozygous animals. I then performed long term live imaging of photoreceptors in *ex vivo* brain cultures to follow their developmental dynamics. Özel et al. (Özel et al. 2015) reported that after correct layer targeting wildtype R7s passively elongate as the medulla expands during development and eventually terminate in their final target medulla layer M6 (Fig. 3.2.1.1-1, top panel). On the other hand, *lar* and *liprin- α* mutant R7s (referred to as *lar* or *liprin- α* R7s from here onwards) initially target the correct layer but fail to maintain their contact and probabilistically retract to terminate in the medulla layer M3 (Fig. 3.2.1.1-1, middle and bottom panels). As observed in live imaging, *lar* R7s initiated retractions around 5 hours earlier compared to the *liprin- α* R7s. Interestingly, *lar* mutant R7s that retracted before P55 initially retracted all the way to the distal most medulla layer M0 and then actively extended to M3 by P55 (Fig. 3.2.1.1-1, middle panel) in a similar fashion to R8s dynamics in developing brains (Akin and Zipursky 2016). While R7s that retracted after P55, in both the mutants, all retracted directly to M3. Retracted *lar* and *liprin- α* R7s retained the capability to re-extend to M6 (Fig. 3.2.1.1-1, middle and bottom panels). They, however, never managed to stabilize in layers proximal to M3 which they eventually retracted back to.

To better understand the *lar* and *liprin- α* R7s retractions, I analyzed the phenotype progression in different developmental stages. Fixed analysis of newly hatched adult flies with whole-eyes mutant of either gene showed that around 80% of *lar* R7s and almost 60% of *liprin- α* R7s

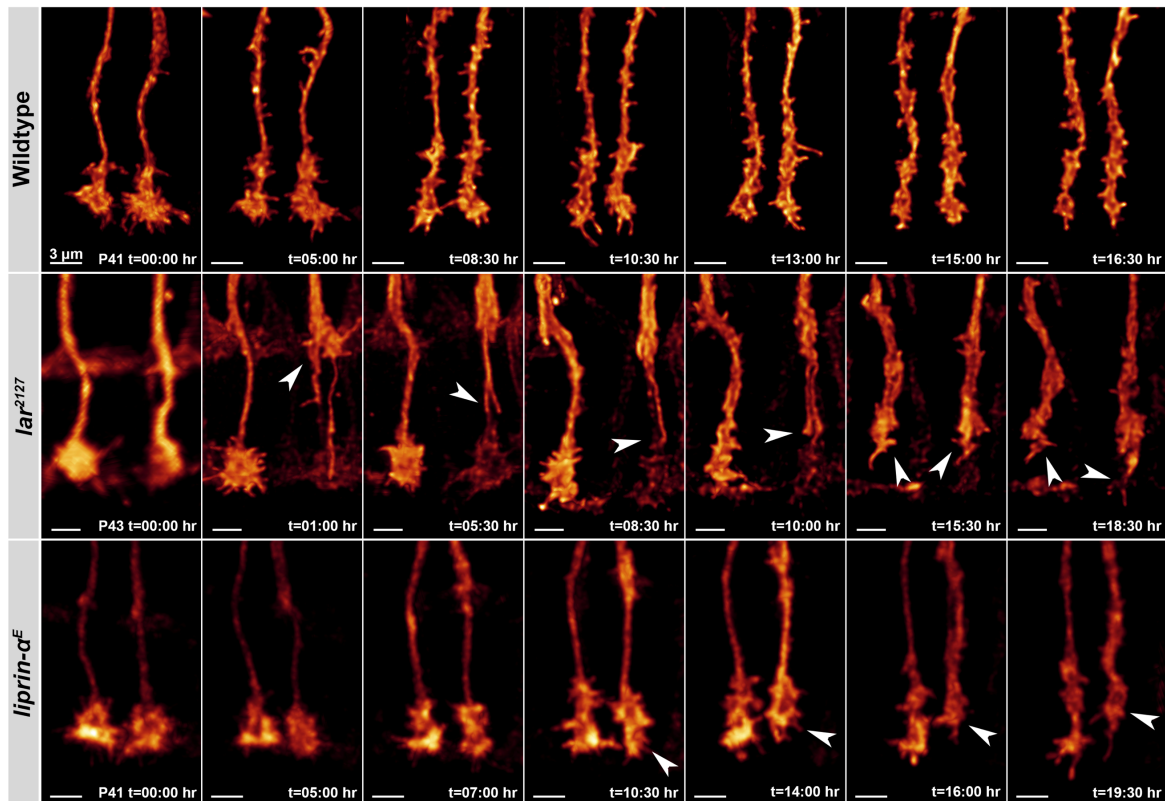


Fig. 3.2.1.1-1. Lar and Liprin- α are not required for R7 targeting.

Snapshots of key developmental stages observed during live imaging of *ex vivo* cultured brains with R7 clones that are either wildtype (top panel), *lar* mutant (middle panel), or *liprin- α* mutant (bottom panel). Wildtype R7s reach their target layer and their terminals expand as the medulla layers expand. The number of filopodia in R7s growth cones gradually reduces as they become more column-restricted before they become slender with few filopodia closer to the adult R7 terminal morphology. *lar* and *liprin- α* R7s, however, correctly reach their target layer before they destabilize and retract with *lar* R7s showing first retractions around 5 hours before *liprin- α* R7s. *lar* R7s that destabilize early (before P50) retract to M0 before they re-extend back to M3 as opposed to the *lar* and *liprin- α* R7s that destabilize later and retract directly to M3. Retracted *lar* and *liprin- α* R7s kept extending filopodia to M6 but never fully stabilized there.

Imaging was performed with a time resolution of 30 minutes and the stage (P) in which imaging started is indicated in the first frame of each panel. Scale bar = 3 μ m. Arrow heads show retracted R7 terminals.

retracted to M3 (Fig. 3.2.1.1-2, A and B) comparable to previously reported levels (Hofmeyer et al. 2006).

During early pupal stages, mutant R7s initially targeted the correct layer and were morphologically similar to wildtype R7s. They, then, probabilistically initiated to retract by P40 in the case of *lar* and by P45 in the case of *liprin- α* R7s (Fig. 3.2.1.1-2, C and D). For mutants of both genes, more R7s kept gradually retracting until P65, after which, minimal retraction

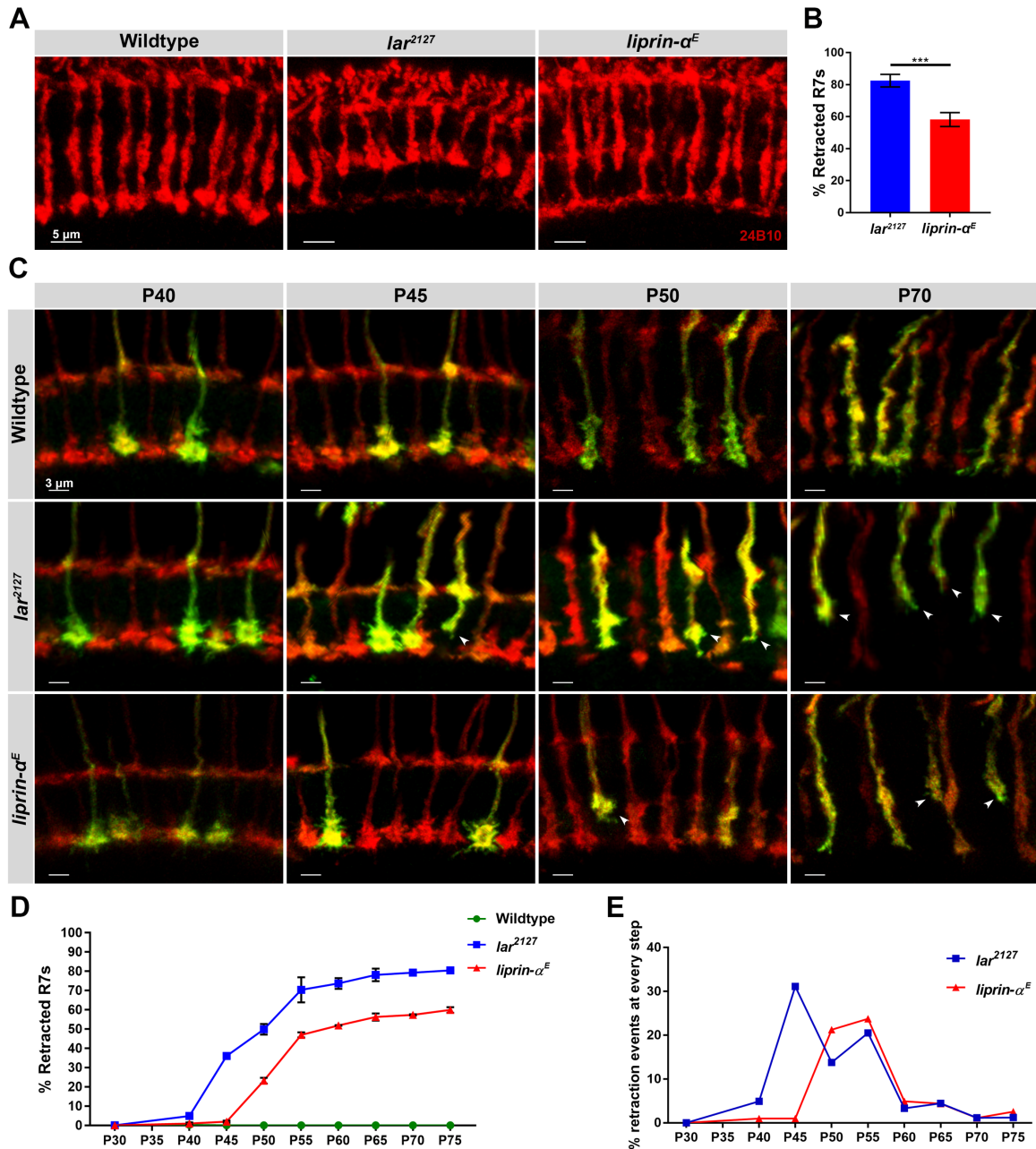


Fig. 3.2.1.1-2. *lar* R7s retraction pattern is overlapping with but not identical to *liprin-α* R7s.

Lar and Liprin- α interact to control R7 targeting to M6. Loss of either of them causes R7s to retract to M3 with quantitative differences. **(A)** Fixed preparations of whole-eyes mutant of *lar* and *liprin- α* and their respective control showing photoreceptor columns in the medulla lacking R7s in M6 as they retract to M3 in both the mutants but not in wildtype photoreceptors. Photoreceptors are labelled with 24B10 staining (red), scale bar = 5 μ m. **(B)** Quantification of the retracted R7s in *lar* and *liprin- α* eyes shown in (A) with their respective penetrance. Graph bars represent mean \pm SEM, *lar*: 82.5 \pm 2.25%, n=692 columns from 3 brains, *liprin- α* : 58.2 \pm 2.18%, n=635 columns from 4 brains (P=0.0006). **(C)** Different developmental stages showing the phenotype progression in R7 clones (figure legend continues in the next page)

that are wildtype, *lar*, or *liprin-α* in otherwise heterozygous animals, clones are labelled with CD4tdGFP (green) while all photoreceptors are labelled with GMRmyrtdTom (red). Wildtype R7s arrive at their target layer and their terminals expand as the medulla expands. *lar* and *liprin-α* R7s also target correctly but fail to stabilize and retract, with *lar* R7s initiating retractions 5 hours earlier than *liprin-α* R7s. Arrow heads mark retracted/retracting R7s. Scale bar = 3 μm. **(D)** Quantification of the *lar* and *liprin-α* R7s retraction progression, data points represent the mean±SEM. *lar*: P30: 0±0%, n=352 R7s from 3 brains, P40: 4,91±0,70%, n=324 R7s, P45: 36,04±1,2%, n=370 R7s, P50: 49,84±2,75%, n=293 R7s, P55: 70,36±6,52%, n=262 R7s, P60: 73,67±2,78%, n=258 R7s, P65: 78,12± 3,27%, n=305 R7s, P70: 79,25±0,94%, n=321 R7s, P75: 80,45±0,25%, n=220 R7s. *liprin-α*: P30: 0±0%, n=365 R7s, P40: 0,97±0,58%, n=323 R7s, P45: 1,94±0,50%, n=352 R7s, P50: 23,19±1,52%, n= 260 R7s, P55: 46,93±1,33%, n=362 R7s, P60: 51,86±0,15%, n=301 R7s, P65: 56,25±1,89%, n=359 R7s, P70: 57,37± 0,33%, n=340 R7s, P75: 59,93±1,46%, n=378 R7s. Each point was quantified from 3 different brains. **(E)** The contribution of each developmental stage to the total retractions in *lar* and *liprin-α* R7s assuming they reach the adult level by P75. *lar* R7s show two large peaks between P40-45 and P50-55 while *liprin-α* R7s show one peak between P45-55. The figure shows the overlap of the retraction phenotypes starting at P50 while highlighting the difference in the early peak of *lar* R7s retractions.

events took place until P75 as they reached the adult retraction levels (Fig. 3.2.1.1-2, D and E). Interestingly, most of the R7 retraction events happened around the time of synapse formation which suggested a role of both proteins in this process (Fig. 3.2.1.1-2, E). However, *lar* mutant R7s showed an early peak of retraction events between P40 and P45 before the phenotype followed a pattern similar to *liprin-α* R7s (Fig. 3.2.1.1-2, E). Indicating an early, Liprin-α-independent function of Lar.

3.2.1.2. Trio overexpression partially rescues the retraction of *lar* mutant R7s

The retraction phenotype seen in *lar* R7s was reported to be partially-rescued by the overexpression (OE) of the RhoGEF Trio (Astigarraga et al. 2010). For that, I generated *lar* mutant R7s that also OE Trio (referred to as *lar*-Trio OE from now on) and followed them in different developmental stages. Mutant R7s, again, targeted correctly before they probabilistically destabilized and retracted (Fig. 3.2.1.2, A). Surprisingly, the retraction phenotype progression changed to be similar to the pattern seen with loss of *liprin-α* (Fig. 3.2.1.2, B), which suggested that Trio OE only rescued the Liprin-α-independent function of Lar.

I then performed live imaging of *lar*-Trio OE in *ex vivo* culture as explained before. As with *lar* or *liprin-α* mutants, *lar*-Trio OE R7s showed initial correct targeting followed by gradual, probabilistic retraction to M3 (data not shown). Fast imaging (time resolution of one minute for an hour) of R7s that remained in their correct target layer during the peak of synapse formation

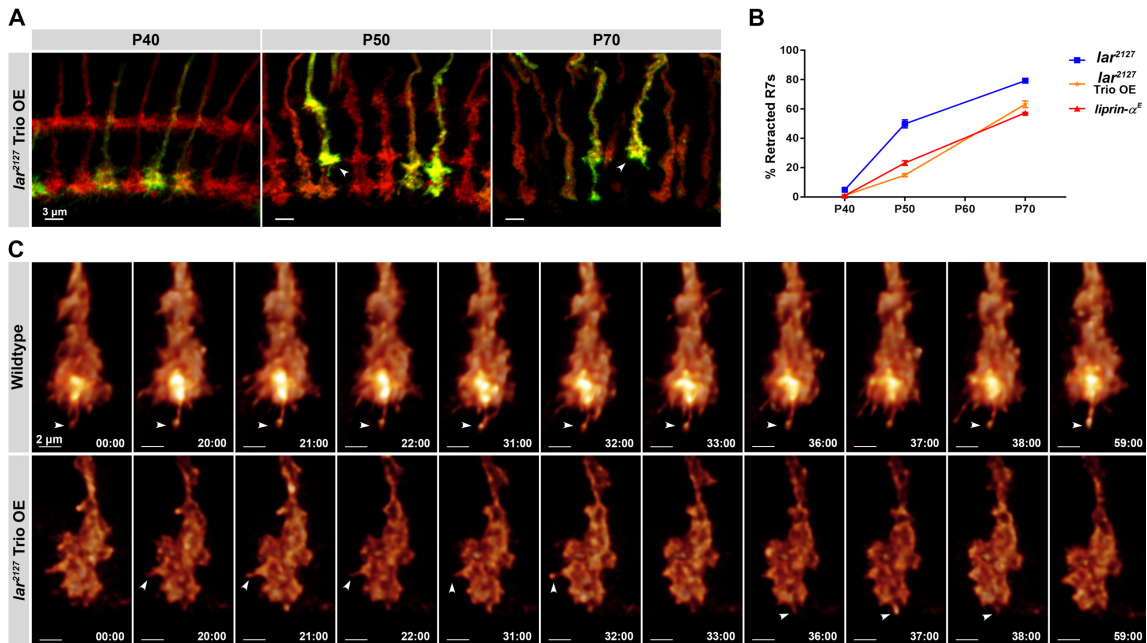


Fig. 3.2.1.2. Trio overexpression rescues the early retractions of *lar* R7.

Overexpressing Trio in *lar* R7s partially rescues the retraction phenotype. **(A)** Fixed images showing different developmental stages of *lar* R7 clones that overexpress Trio labelled with CD4tdGFP (green) and all photoreceptors are labelled with GMRmyrtdTom (red). Arrow heads point at the retracted R7s. Scale bar = 3 μ m. **(B)** Quantification of the *lar* R7 retraction progression upon Trio overexpression with the respective stages of *lar* and *liprin- α* replotted from the previous figure. Overexpressing Trio in *lar* R7s transforms the retraction pattern to resemble that of *liprin- α* R7s by rescuing the early *lar* R7 retraction. Data points show the mean \pm SEM; *lar* Trio OE; P40: 1.02 \pm 0.31%, n=290 R7s from 2 brains, P50: 14.84 \pm 1.06%, n=773 R7s from 5 brains, P70: 63.18 \pm 2.25%, n=264 R7s from 2 brains. **(C)** Live imaging of wildtype and *lar* Trio OE R7 terminals fast dynamics at P60. Wildtype R7s form a bulbous tip that is stable for the whole duration of the 1-hour imaging window (arrow heads), while *lar* Trio OE R7s form a few transient bulbous tips with lifetimes not exceeding 10 minutes (arrow heads

(P60) showed that R7s can form bulbous tips with a lifetime of only a few minutes as opposed to wildtype R7s that can form at least one bulbous tip that is stable for longer than 40 minutes (Fig. 3.2.1.2, C) (Özel et al. 2019). These findings were only qualitative as they were based on visual observation and not 4D filopodia tracking, which makes it difficult to discriminate between bulbous tip formation or stabilization defect (as reported for *lar* and *liprin- α* R7s, respectively, in Özel et al 2019).

3.2.1.3. *lar* R7s retract to the layer where R8s are

Analysis of fixed adult brains showed a retraction penetrance of almost 80% for *lar* and 60% for *liprin- α* R7s (section 3.2.1.1). Interestingly, the distribution of retracted and unretracted *lar*

R7s across the medulla at P70 showed that the R7s in the center of the medulla were all retracted to M3. Whereas those remaining in M6 were situated in the posterior, dorsal, and anterior edges of the medulla (Fig. 3.2.1.3-A), a region in which R7s and R8s of the dorsal rim area (DRA) terminate. DRA ommatidia occupy a crescent-shaped region in the dorsal-most part of the fly eye and span parts of the anterior and posterior regions of the eyes as well. The DRA photoreceptors require the expression of the transcription factor Homothorax (Hth) (Wernet and Desplan 2014) and, importantly, both the inner photoreceptors terminate in M6 (Sancer et al. 2019).

To test whether R7 layer choice depends on R8s when they retract from M6, I generated *lar* mutant R7 clones while transforming the whole eye into DRA by overexpressing Hth under the control of the photoreceptor driver GMR (Wernet and Desplan 2014). Mutant R7s initially targeted their specific layer normally before starting to probabilistically retract to the edge of the medulla as seen at P50. Surprisingly, the majority of the mutant R7s terminated in M6 at P70 (Fig. 3.2.1.3-B) during which time the DRA R8s would have extended from the edge of the medulla to M6 (Sancer et al. 2019).

These results support the earlier-presented live imaging recordings in which dynamic behavior of *lar* mutant R7s followed R8s and not retracted to M3 as suggested in earlier reports.

3.2.1.4. *lar* and *liprin-α* R7s have a synaptic formation defect irrespective of the target layer

Lar and Liprin- α were previously shown to be required for synapse formation in the *Drosophila* NMJs. To test if they play a similar role in R7s, I generated R7 mutant clones of either gene in otherwise heterozygous animals while expressing fluorescently-tagged Brp-D3 as a presynaptic active zone marker (Schmid et al. 2008). I manually quantified Brp-D3-positive active zones (referred to as synapses from now on) at P70 along R7 axons within the medulla (between M0 and M6). The choice of P70 was motivated by two reasons; R7s were found to have formed the majority of their synapses by this stage (Özel et al. 2019), and the fact that it was the latest developmental stage where I could reliably identify mutant clones, which is caused by leaky Gal80 suppression in later pupal stages.

lar and *liprin-α* R7s both showed a decreased number of synapses. *lar* R7s managed to form only around 40% while *liprin-α* R7s formed around 30% of the synapses found in wildtype R7s (Fig. 3.2.1.4). Quantification of synapses found between M0 and M6 in *liprin-α* R7s showed that despite similar synaptic defects, almost half of them were not retracted by P70. In contrast, all *lar* R7s were already retracted to M3 by P70 (this will be discussed later in more detail).

To uncouple the role of Lar in layer targeting and synapse formation, I quantified synapses in the unretracted *lar*-Trio OE R7s where the penetrance was comparable to *liprin-α* R7s. Even

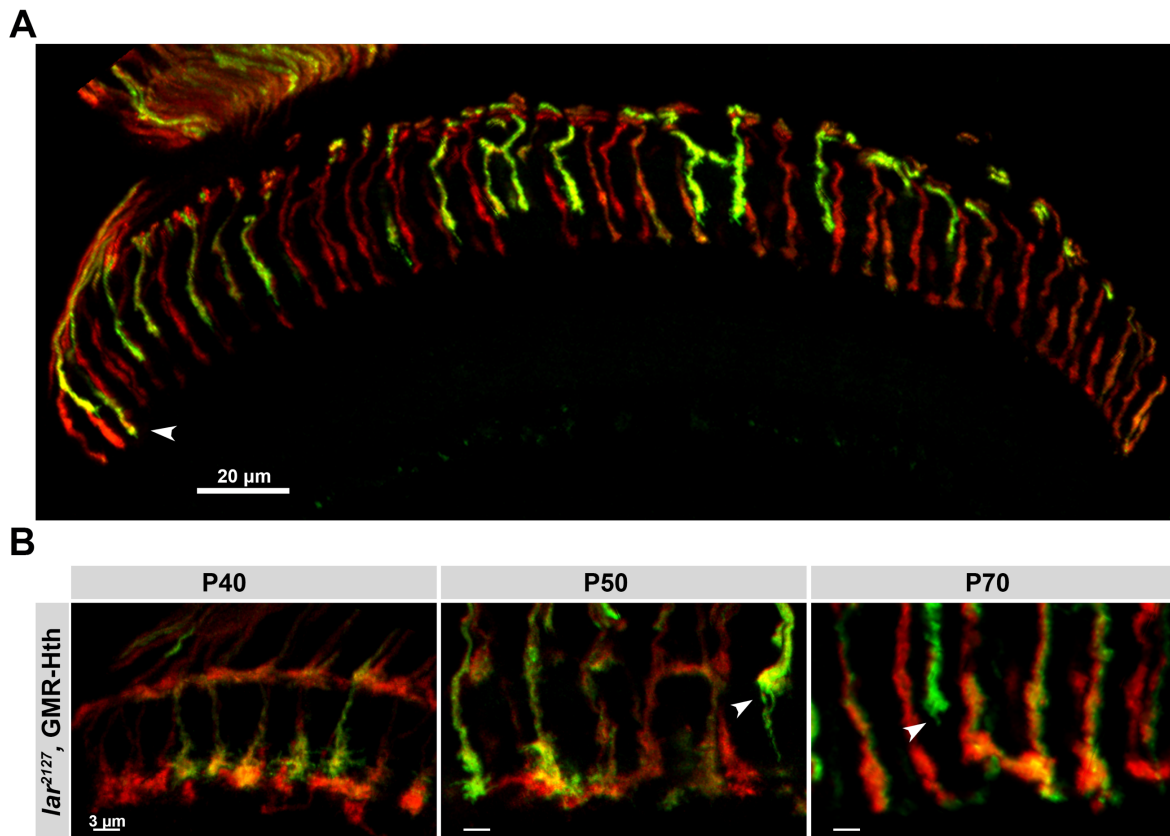


Fig. 3.2.1.3. *lar* R7s retract to the layer where R8 terminals are.

Most of the *lar* R7s retract and terminate in layer M3, as R8s do. **(A)** Section through the medulla at P70 showing *lar* R7 clones (green) and all photoreceptors (red) with the dorsal side to the left and the ventral side to the right. All *lar* R7s terminate in M3 except for the mutant R7 in the dorsal rim area that terminate in M6 (arrow head). In that area, R8s also terminate in M6. Scale bar = 20 μm. **(B)** fixed preparations at different developmental points showing *lar* R7s while transforming all photoreceptors into dorsal rim photoreceptors by Hth overexpression. *lar* R7s target correctly until P40 and then retract to M0 by P50, later in development the majority of R7s terminate in M6 together with the R8s that are directed to the deeper layer. Arrow heads mark retracted *lar* R7s, scale bar = 3 μm.

though *lar*-Trio OE R7s formed slightly more synapses compared to both *lar* or *liprin-α* R7s, they still formed half the number of synapses wildtype R7s formed (Fig. 3.2.1.4). Retracted *lar*-Trio OE R7s in M3 also formed a similar number of synapses as the unretracted ones (data not shown). This is still consistent with the findings of (Özel et al. 2019) as failure of *lar*-Trio OE R7s to stabilize bulbous tips resulted in a reduction in the synapses they formed (as seen in section 3.2.1.2).

Taken together, both Lar and Liprin-α are required in R7s to form and stabilize bulbous tips which is reflected in the number of synapses they eventually form regardless the layer they terminate in.

3.2.1.5. Lar and Liprin- α are dispensable for synapse formation in DRA R7s and for synaptic transmission in photoreceptors

As shown earlier, *lar* and *liprin- α* R7s formed fewer synapses in the medulla whether they terminate in M3 or M6. My follow-up question then was, if they both are also required for synapse formation in other photoreceptor subtypes.

To test this, I generated R7 mutant clones of either gene which also generated mutant R7 clones in the DRA region. I quantified synapses in *lar* and *liprin- α* DRA R7s where they terminated in M6 as their layer targeting was dependent on R8. Wildtype R7s formed a similar number of synapses compared to wildtype DRA R7s (Fig. 3.2.1.5, A-B), consistent with DRA active zone numbers and non-DRA R7s quantified from EM reconstruction (Emil Kind; personal communication). Interestingly, *lar* and *liprin- α* DRA R7s formed more synapses compared to their non-DRA counterparts which were comparable to the synapse numbers wildtype DRA R7s formed (Fig. 3.2.1.5, A-B).

To assess the role of Lar and Liprin- α in synapse formation in photoreceptors terminating in the lamina, I exploited the GMRflp MARCM system which generates, in addition to R7, R1 and R6 mutant clones. Loss of either gene was previously reported to affect sorting of photoreceptors within cartridges, but not their targeting to the lamina. Unfortunately, this approach was not successful because of low signal to noise fluorescence ratios prohibiting the identification of mutant clones (data not shown). Instead, I used synaptic transmission as a readout of synaptic activity and, subsequently, the number of synapses. Therefore, I generated animals with whole-eyes mutant of *lar* and *liprin- α* plus their respective control and then recorded electroretinograms (ERG) which primarily captures the activity of R1-6. Photoreceptors mutant of *lar* and *liprin- α* did not have synaptic transmission defect as measured by the On-transient. In fact, *lar* mutant photoreceptors showed a slight increase in synaptic transmission. These results stand in contrast to ERG recordings from *syd-1* mutant photoreceptors that completely lost synaptic transmission (Fig. 3.2.1.5, C-D). Photoreceptors in either case were significantly less healthy as shown by the sharp decrease in depolarization (Fig. 3.2.1.5, C-E).

These results suggested that Lar and Liprin- α were not required in R1-6 and in DRA R7s for synapse formation unlike their role in non-DRA R7s.

3.2.2. Role of Lar and Liprin- α in regulating microtubule polymerization in R7s

Lar was reported to function upstream of the formin Dia which phenocopied its effect on guidance and synapse formation in the NMJ by controlling microtubule polymerization (Pawson et al. 2008). On the other hand, the mouse homologues of Liprin- α (Liprin- α 1 and 3) were reported to bind to mDia and this interaction was found important for mDia localization

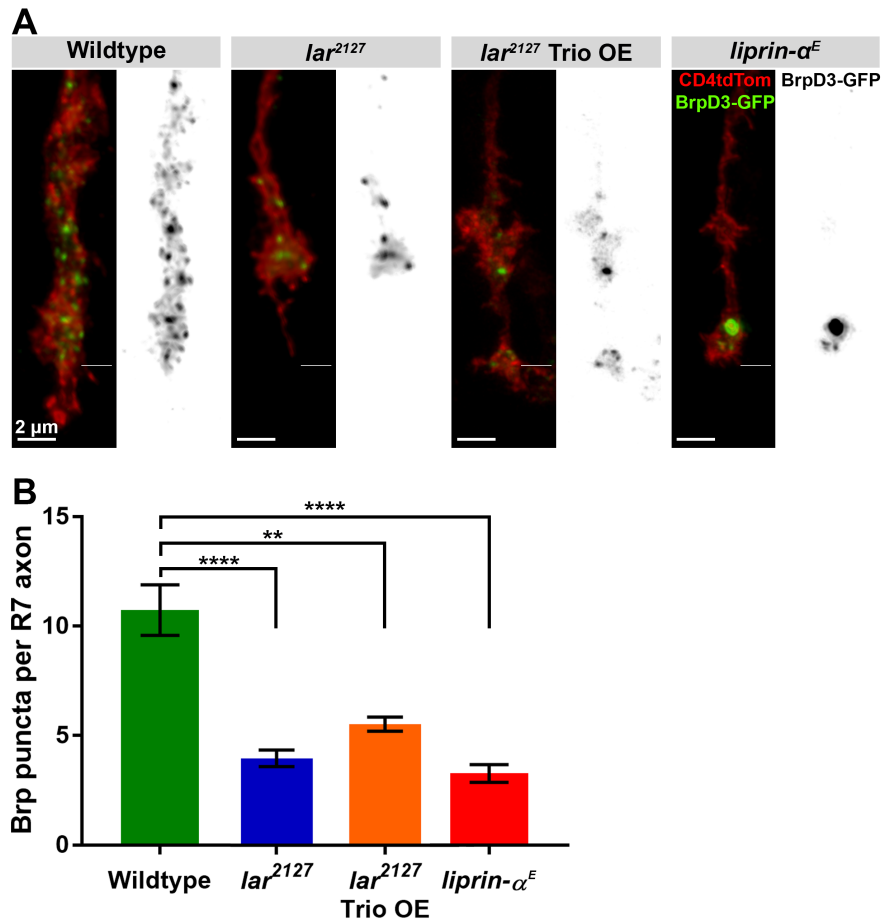


Fig. 3.2.1.4. Loss of *lar* and *liprin-α* in R7s cause synaptic defect.

lar and *liprin-α* R7s that are in the middle of the medulla form fewer synapses compared to wildtype R7s at P70. This analysis included the *liprin-α* R7s that remained in M6 and retracted *lar* R7s in M3. Trio overexpression in *lar* R7s rescues the targeting defect but not the synapse formation defect. **(A)** Representative single R7 terminals at P70 of wildtype, *lar*, *lar* rescued with Trio overexpression, and *liprin-α* R7s, the membranes are labelled with CD4tdTom (red) and active zone are marked with Brp-D3 (green). Brp-D3 is shown in a separate panel in black for better contrast, and depicts fewer number of Brp-D3 dots in the three conditions compared to wildtype R7s. Line marks M6, scale bar = 2 μm. **(B)** Quantification of Brp-D3 dots in the three mentioned conditions compared to wildtype R7s showing a significant reduction in the number of synapses in the three conditions. Bars represent mean±SEM synapses per R7 axon. Wildtype; 10.74±1.15 synapses, n=38 R7s. *lar*; 3.95±0.37 synapses, n=47 R7s, (P<0.0001). *lar* Trio OE; 5.5±0.31, n=16 R7s, (P=0.0053). *liprin-α*; 3.15±0.23 synapses, n=38 R7s, (P<0.0001).

(Sakamoto et al. 2012). Taken together, these studies led me to hypothesize that Lar and Liprin-α interaction recruits Dia which in turn promotes and directs microtubule polymerization to stabilize contacts initiated by Lar.

3.2.2.1. Stable microtubules correlate with stable bulbous tips

To test whether loss of *dia* shows a similar phenotype to loss of *lar* in R7s as it does in the NMJ, I generated animals with whole-eyes mutant of *dia*. Unlike the eyes of control flies, *dia* mutant eyes were morphologically deformed; they were smaller in size and lacked the smooth mosaic pattern seen in control animals (Fig. 3.2.2.1-1). This was not surprising since Dia might have affected photoreceptor division or axon extension which caused mutant photoreceptors to die. Thus, it was not possible to test a potential role of Dia in R7 targeting and synapse formation in detail.

Subsequently, I tried to understand how microtubules were organized in developing R7s. Therefore, I generated R7 clones expressing GFP-tagged α -tubulin (referred to as GFP-Tub) while marking the membrane with CD4tdTomato. During synapse formation, R7s go through morphological and dynamic changes during which axon terminals elongate, showing fewer column-restricted filopodia and they form bulbous tips (Özel et al. 2015, 2019). Interestingly, analysis of fixed R7s showed that GFP-Tub was not only localized in the axon and the central domain but was also seen in the peripheral domain of R7 growth cones (Fig. 3.2.2.1-2, A), an area that was thought to be actin-rich and devoid of microtubules (Biswas and Kalil 2018). Another interesting finding was that GFP-Tub was never detected in filopodia but only seen in some bulbous tips which when quantified, GFP-Tub was only in one bulbous tip per growth cone at P60 and P70 (Fig. 3.2.2.1-2, B). This is especially important in light of our recent findings that R7s can only stabilize one synaptogenic bulbous tip at a time (Özel et al. 2019). To understand the relationship between microtubules and bulbous tips' stability, I performed live imaging to observe the fast dynamics of microtubules at P60 (time resolution of one minute for an hour). Since the fluorophore tdTomato that labels the R7 membranes bleaches quickly during imaging when exposed to scanning laser, I decided to dissect the pupal eye-brain complexes at P40 and kept them in culture for 20 hours at 25°C before imaging. As in fixed preparations, GFP-Tub occupied the axons, central and peripheral domains of the growth cones. Following bulbous tips over a one-hour imaging window showed that R7s formed one bulbous tip remaining stable longer than 40 minutes and a few transient bulbous tips with a lifetime of less than 10 minutes. A bulbous tip formed as the membrane pushes a protrusion through the growth cone followed by GFP-Tub migrating to fill the formed bulbous tip, a process that took around 2 minutes to be completed. GFP-Tub remained in the bulbous tip when becoming stable, or retracted back to the growth cone when the bulbous tip was destabilized shortly after (Fig. 3.2.2.1-2, C).

These results suggested a relation between microtubules and bulbous tip stability, where microtubules provide the structural and mechanical support needed for bulbous tip stabilization and, hence, promote the synaptogenic nature of such bulbous tips.

3.2.2.2. Lar and Liprin- α stabilize bulbous tips through stabilizing microtubules

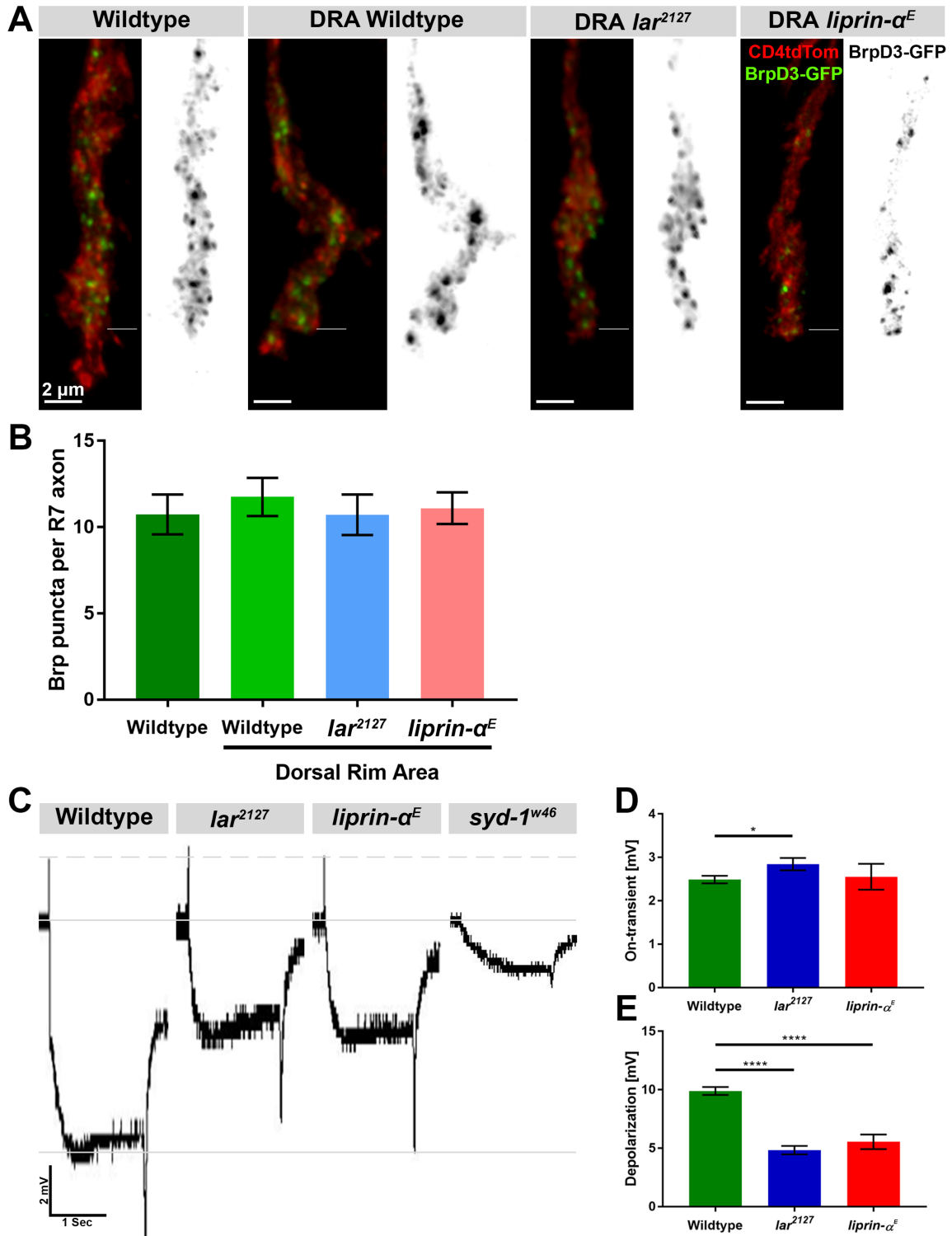


Fig. 3.2.1.5. Lar and Liprin-α do not affect synapse formation in dorsal rim R7s and synaptic transmission in photoreceptors.

As opposed to non-DRA R7s, *lar* and *liprin-α* DRA R7s do not have a synaptic defect. ERG recording of *lar* and *liprin-α* mutant eyes does not show synaptic transmission defect as well. **(A)** Representative single DRA R7 terminals at P70 that are wildtype, *lar*, or *liprin-α* mutant, compared to the non-DRA wildtype R7 from the previous figure. R7s are labelled with CD4tdTom (red) and the *(Figure legend continues in the next page)*

active zones are marked with Brp-D3 (green) that is also shown in black in a separate panel. Line marks M6, scale bar = 2 μm . **(B)** Quantification of Brp-D3 puncta per R7 axon in *lar* and *liprin- α* DRA R7s compared with DRA and non-DRA wildtype R7s. Both the mutants formed the same number of synapses as wildtype DRA R7s that was also not significantly different from wildtype non-DRA R7s. Graph bars represent mean \pm SEM synapses/R7. Non-DRA wildtype; 10.74 \pm 1.15 synapses, n=38 R7s. DRA wildtype; 11.75 \pm 1.1 synapses, n=4 R7s (P=0.7803 from non-DRA wildtype R7s). DRA *lar*; 10.71 \pm 1.17 synapses, n=14 R7s (P=0.6599 from DRA wildtype R7s). DRA *liprin- α* ; 11.1 \pm 0.92 synapses, n=10 R7s (P=0.6979 from DRA wildtype R7s). **(C)** Representative ERG traces recorded from wildtype, *lar*, *liprin- α* , and *syd-1* eyes. The solid lines mark the baseline (middle line) and the wildtype depolarization (bottom line), the dashed line marks the wildtype On-transient level. *liprin- α* eyes do not show synaptic transmission defect, while it is slightly increased in *lar* eyes. Both mutant eyes show a decreased depolarization as a sign of reduced health. Traces from *syd-1* eyes are shown as an example of a mutant that reduces synaptic transmission, ERG traces for its respective control is shown in Fig. 6.4.2. **(D, E)** Quantification of ERG On-transient and depolarization amplitudes, respectively, of wildtype, *lar*, and *liprin- α* eyes. Graph bars represent mean \pm SEM mV. Wildtype; On-transient: 2.48 \pm 0.08 mV, depolarization: 9.89 \pm 0.33 mV, n=27 flies. *lar*; On-transient: 2.84 \pm 0.14 mV (P= 0.0345), depolarization: 4.83 \pm 0.35 mV (P <0.0001), n=11 flies. *liprin- α* ; On-transient: 2.55 \pm 0.29 mV (P= 0.7732), depolarization: 5.54 \pm 0.62 (P <0.0001), n=7 flies.

Live imaging of *lar* and *liprin- α* R7s revealed profound changes in the dynamics of bulbous tips; *lar* R7s showed a bulbous tip formation and stabilization defect, while *liprin- α* R7s only showed bulbous tip stabilization defect (Özel et al. 2019). Since the formin Dia was reported to function downstream of Lar in *Drosophila* and Liprin- α in *Mouse*, it was fair to assume a link between Lar and Liprin- α and microtubules migrating into bulbous tips.

To find out if and how Lar and Liprin- α regulate microtubule dynamics, I sought to perform fast live imaging to study the respective dynamics of both the proteins in wildtype R7s. It was not possible to follow Lar behavior in a live brain since a fluorescently-tagged construct was not available. However, Liprin- α -GFP is available and it localized to bulbous tips without affecting their dynamics (Özel et al. 2019). To combine with Liprin- α -GFP, only a microtubule marker with a fluorescent tag in the far-red region could be used. This restricted the choice to the mCherry-tagged EB1 which binds the plus end of polymerizing microtubules. Unfortunately, the 2-photon microscope used for imaging only allows scanning of two channels simultaneously and it was not possible to use a third channel for a membrane marker.

Remarkably, Liprin- α puncta were in constant motion aligned around the peripheral domain of the growth cone. EB1 puncta, on the other hand, filled the axon and the central and peripheral domains of the growth cone, resembling GFP-Tub. Liprin- α puncta would push outwards from the growth cone (Fig. 3.2.2.2-1, yellow arrow heads), in what seemed to be invading filopodia

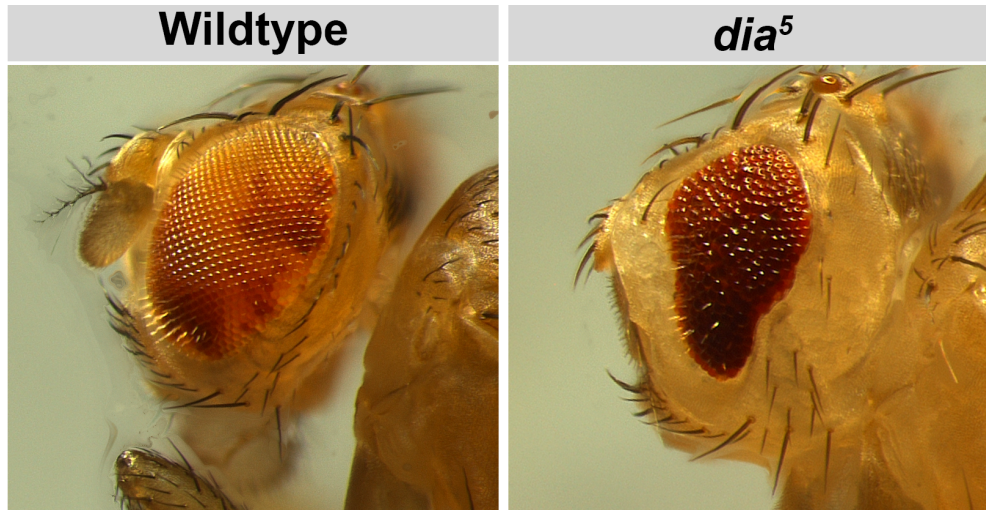


Fig. 3.2.2.1-1. Loss of *dia* causes eye deformation.

Wildtype mosaic eyes show a smooth regular pattern (left) unlike whole eyes mutant of the formin *dia* (right) that are deformed and smaller in size with a rough disorganized surface.

or bulbous tips, immediately followed by EB1 puncta (Fig. 3.2.2.2-1, white arrow heads) but never in the opposite order. Together, Liprin- α and EB1 stabilized the formed structure, presumably a bulbous tip, for a period longer than 40 minutes. Such colocalization of both the proteins was also seen in fixed brains (Fig. 3.2.2.2-1, right panel). This result suggested that Liprin- α recruited microtubules to bulbous tips which, subsequently, led to stabilizing them.

Based on this result, I continued with testing how the microtubules behave in *lar* or *liprin- α* R7s. I performed fast live imaging of R7s mutant of either gene, labelling mutant R7s with CD4tdTomato while expressing GFP-Tub. In *lar* R7s, GFP-Tub was more condensed in the central growth cone domain compared to the control clones. They were dynamic and invaded the formed bulbous tips. However, after a short time period, they retracted again to the growth cone followed by the retraction of the bulbous tip altogether. In rare occasions, R7s would form a bulbous tip that never received GFP-Tub, such a bulbous tip would retract promptly (Fig. 3.2.2.2-2, A). In the case of *liprin- α* R7s, the GFP-Tub was more expanded than *lar* R7s, and more comparable to wildtype R7s. Mutant R7s formed bulbous tips that received transient GFP-Tub invasion before they retracted similar to *lar* R7s (Fig. 3.2.2.2-2, B).

Taking these results together, *lar* and *liprin- α* R7s fail to stabilize microtubules in the formed bulbous tips which always led to their retraction. This defect, however, doesn't explain the reported bulbous tip formation defect in *lar* mutant R7s.

3.2.3. Manipulating the actin cytoskeleton to control filopodial dynamics and synapse number

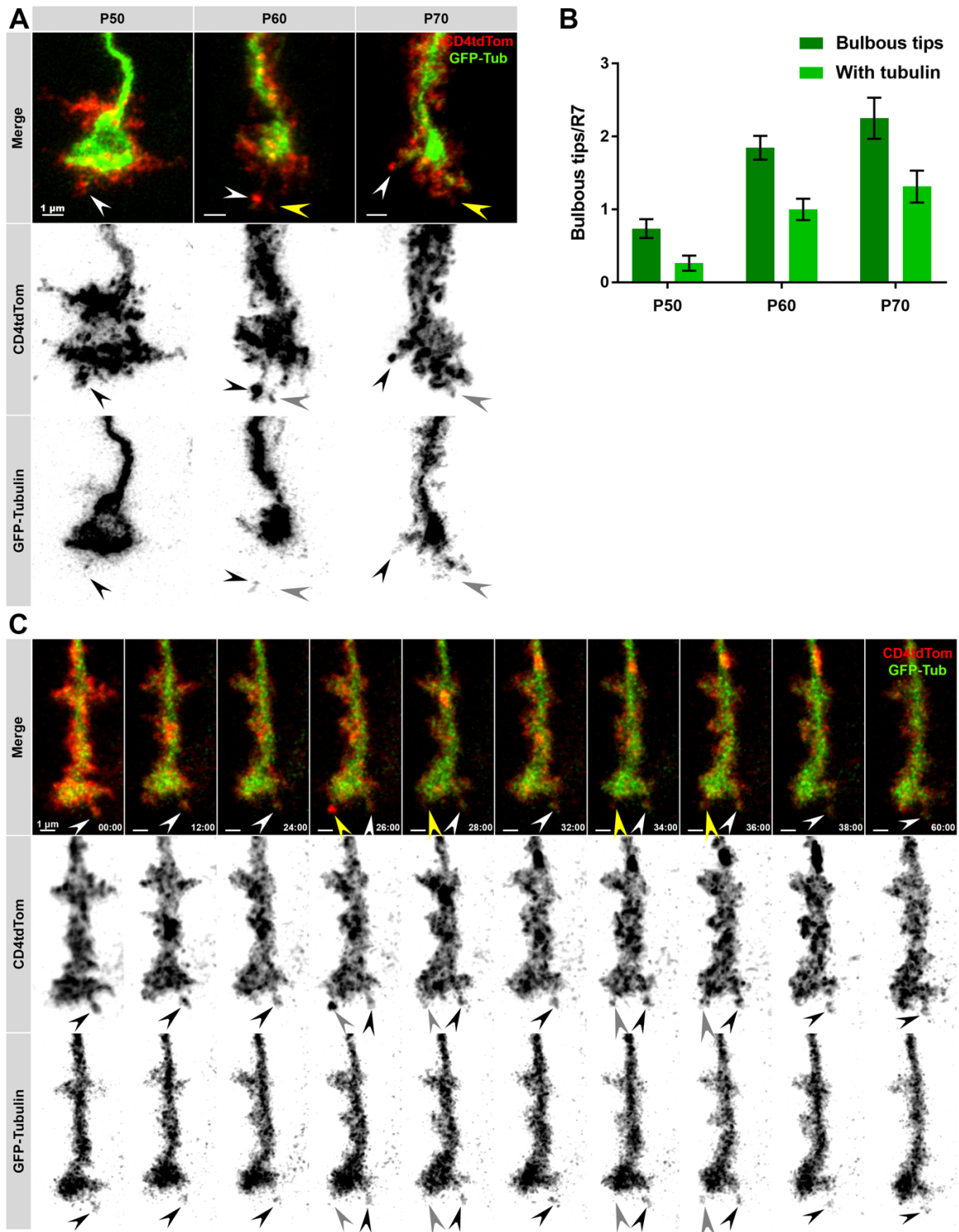


Fig. 3.2.2.1-2. Microtubules are recruited to bulbous tips.

Microtubules in wildtype R7s occupy the central and peripheral domains of the growth cones, they are also found in bulbous tips but not in filopodia. R7 terminals are labelled with CD4tdTom (red) and microtubules are labelled with GFP-Tub (green) and both channels are shown separately. **(A)** Fixed preparations in different developmental stages showing microtubule organization in R7 growth cones. Microtubules are only in a subset of bulbous tips (white arrow heads) and others do not show any microtubule signal (yellow arrow heads). Scale bar = 1 μ m. *(Figure legend continues in the next page)*

PART 3 | LAR

(B) Quantification of the total number of bulbous tips in each stage (dark green bars) and the subset of those that have GFP-Tub signal in them (light green). At P60, microtubules are found in one bulbous tip per R7 growth cone which has more bulbous tips with no GFP-Tub signal. Graph bars represent mean \pm SEM bulbous tip per R7 terminal. Total number of bulbous tips; P50: 0.73 \pm 0.12, P60: 1.84 \pm 0.16, P70: 2.25 \pm 0.28 bulbous tips. Number of bulbous tips with GFP-Tub signal; P50: 0.26 \pm 0.1, P60: 1 \pm 0.14, P70: 1.31 \pm 0.21 bulbous tips. **(C)** Live imaging of GFP-Tub in R7 terminals at P60 shows a bulbous tip with GFP-Tub signal that is stable for the whole imaging duration (white arrow head). Other transient bulbous tips form that sometimes recruit GFP-Tub before they retract to the growth cone followed by the bulbous tip (yellow arrow head). Time resolution = 2 minutes, scale bar = 1 μ m.

To challenge the postulated function of Lar and Liprin- α in R7s that they are required to stabilize bulbous tips and, thus, enable synapses to form. I aimed at manipulating the cytoskeleton and find if and how this affects filopodial dynamics and synapse formation in photoreceptors.

The cytoskeleton is an integral part of all cellular processes, it primarily provides mechanical support for cellular structures and due to its dynamic behavior regulates cell migration, cell division, and intracellular transport. It is an adaptive dynamic structure formed by interlinking actin and tubulin filaments that are kept in constant flux under the tight control of numerous regulatory proteins (Pollard and Cooper 2009).

Neurons are polarized cells whose axons and dendrites travel relatively long distances to arrive at their target area where they form synapses. Neuronal progenitor cell division, pathfinding, and synaptogenesis all rely on the constant cytoskeleton rearrangement (Menon and Gupton 2016). Growth cones reside at the leading edge of axons and extend dynamic, actin-rich filopodia to survey and respond to external stimuli to steer axons to their target cells. Pharmacologically depleting actin filaments in developing neurons halted filopodia formation and led to disoriented growth cone steering (Bentley and Toroian-Raymond 1986). In a later independent study, actin filament depletion caused a reduction in size and number of synapses of young primary neurons in culture (Zhang and Benson 2001).

The cytoskeleton applies push and pull forces on membranes through constant coordinated polymerization and depolymerization of actin and microtubule filaments. This process is controlled through the action of a large number of regulatory elements classified into actin monomer-binding, filamentous actin severing, capping, branching, cross-linking, and formin families of proteins (Pollard 2016).

In developing neurons, the actin-depolymerizing factor, cofilin promotes growth cone dynamics and filopodial extension. Cofilin binds and severs filamentous actin. Its activity is controlled by its phosphorylation state at Ser-3, it is repressed by LIM- and TES- kinases and it is activated by slingshot (SSH) and Chronophin (CIN) phosphatases (Wiggin et al. 2005). The effect of

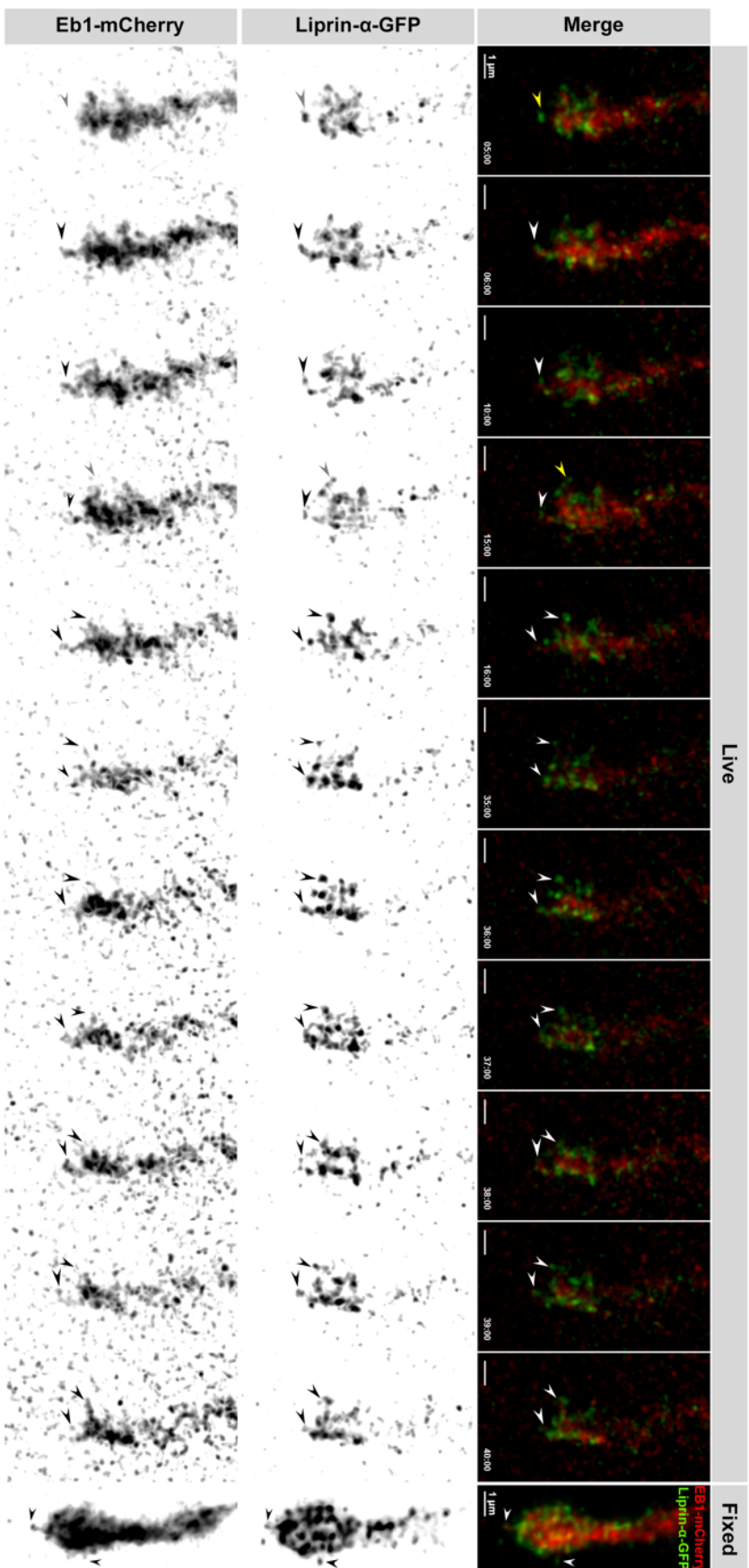


Fig. 3.2.2-1. Liprin- α precedes microtubules to bulbous tips.

Live imaging of R7 terminals at P60 expressing Liprin- α -GFP (green) and Eb1-mCherry (red) to mark the plus end of microtubules and both the channels are shown separately, membrane labelling was not possible in this experiment. Liprin- α and microtubules are in constant motion within the growth cones marking its edge. Liprin- α extends out of the growth cone into filipodia (yellow arrow heads) and then followed by microtubules (white arrow heads). Filipodia remained stable longer than 40 minutes suggesting that they are bulbous tips. The same is also seen in fixed preparations at P60 (right panel), Liprin- α localized with microtubules in extensions from the growth cone. n=13 growth cones from 3 repeats. Time resolution = 1 minute, scale bar = 1 μ m.

PART 3 | LAR

SSH and LIMK overexpression on cofilin was reported to affect growth cone motility and neurite extension in developing chick dorsal root ganglion neurons (Endo et al. 2003).

CIN localizes with cofilin in motile and dividing cells, its loss of function stabilizes filamentous actin and causes cell division defects (Gohla et al. 2005; Delorme-Walker et al. 2015). In neurons, CIN modulates synaptic plasticity in mice and its loss of function causes the dentate granule cells to have gigantic dendritic spine heads (Kim et al. 2016).

In an unbiased RNAi screen for phosphatases and kinases that affect synapse formation in *Drosophila* mechanosensory neurons, knock-down of *cg5577* during development caused ectopic synapse formation in the posterior projecting branch of the anterior dorsocentral (aDC) neuron (O. Urwyler and D. Schmucker; personal communication, unpublished data). The protein sequence of CG5577 shares the same functional domains as CIN and was shown to cause a similar cell division defect *in vitro*, suggesting it is the fly homologue of human CIN, and, hence, referred to as dCIN (A. Hasan, O. Urwyler, D. Schmucker; unpublished data).

3.2.3.1. *dcin* knock-down affects filopodial dynamics in R7s

To test the effect of *dcin* knock-down (KD) in photoreceptors, I drove the expression of *dcin* RNAi using the photoreceptor driver GMR-Gal4. This did not cause any eye deformation and the photoreceptors in the medulla all terminated in their respective layers with no signs of pattern disruption (data not shown).

Then, I generated sparse photoreceptor clones expressing *dcin* RNAi while labelling them with CD4tdGFP. *dcin* KD in R7s showed a small reduction in the total number of filopodia formed at P70 while it had no effect on the number of bulbous tips they formed which remained around 1.8 bulbous tip per R7 terminal (see Fig. 3.2.3.1, A-B). Live imaging of *dcin* KD R7s at P60 showed that filopodia and bulbous tips dynamics were altered compared to wildtype R7s that formed transient filopodia together with one or two stable bulbous tips and a few transient ones. *dcin* KD led to the formation of morphologically-thicker filopodia that remained stable much longer than wildtype filopodia, such filopodia then transitioned into stable bulbous tips. *dcin* KD R7 filopodia and bulbous tips were generally slower to retract and even the transient bulbous tips had a longer life-time compared to wildtype ones (Fig. 3.2.3.1, C). Having such stable filopodia and bulbous tips is consistent with stabilizing actin filaments as the cofilin-severing activity is reduced by *dcin* KD.

3.2.3.2. *dcin* knock-down in photoreceptors causes them to form more synapses

To test *dcin* KD effect on synapse formation in R7s, I generated sparse clones expressing *dcin* RNAi while expressing Brp-D3 as an active zone marker and labelling these photoreceptors with CD4tdTom at the same time. For this experiment, my quantification was restricted to the synapses between M3 and M6 of R7s since the labelled clones might also include R8s of the

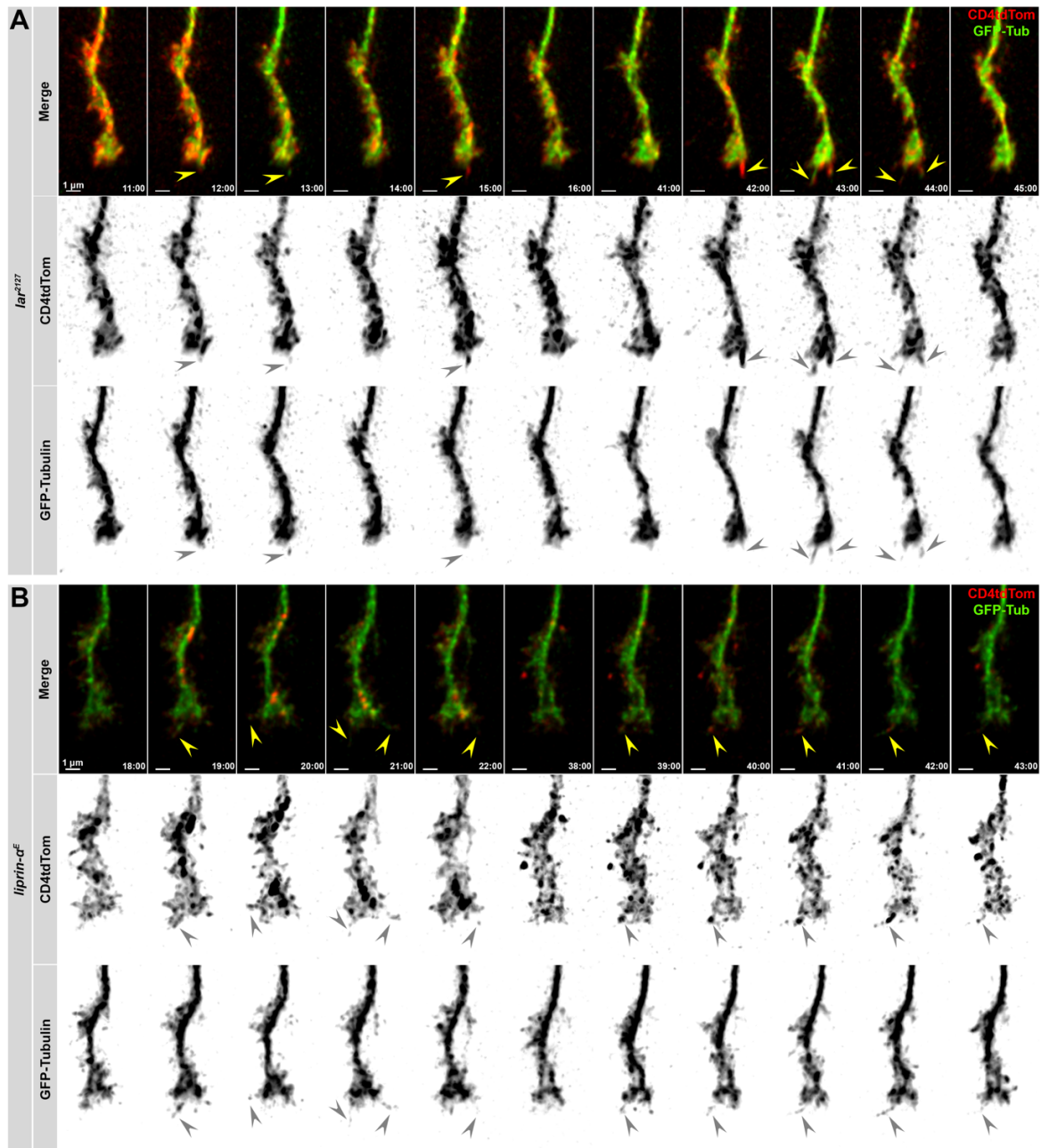


Fig. 3.2.2.2-2. Microtubules are not stabilized in bulbous tips of *lar* and *liprin-α* R7s.

Live imaging of *lar* (A) and *liprin-α* (B) R7 terminals at P60 with the membrane labelled with CD4tdTom (red) and expressing GFP-Tub to mark the microtubules (green), the channels are shown separately as well. Both mutants form transient bulbous tips that have a lifetime of a few minutes (yellow arrow heads). Bulbous tips form when the membrane extends out of the growth cone and then GFP-Tub follow to fill the bulbous tip. GFP-Tub then retracts to the growth cone and the membrane retracts immediately after. In rare cases, a bulbous tip forms without recruiting GFP-Tub and promptly retracts (in A, min. 15). *lar*: n=9 growth cones from 2 repeats, *liprin*: 14 growth cones from 3 repeats. Time resolution = 1 minutes, scale bar = 1 μm.

PART 3 | LAR

same column (red boxes in Fig. 3.2.2, A). *dcin* KD led to a highly-significant, 1.7-fold increase in the number of synapses R7s formed compared to wildtype R7s (Fig. 3.2.3.2, A-B). Such an increase in synapse number is in line with the slower filopodial and bulbous tip dynamics shown by *dcin* KD where slower dynamics, presumably, led to a more stable pre-post synaptic contact and eventually form a higher number of synapses.

To assess whether *dcin* KD affects synaptic transmission in photoreceptors, I expressed *dcin* RNAi in all photoreceptors using GMR-Gal4 and recorded ERG upon light stimulation. As expected, the On-transient was slightly increased in *dcin* KD eyes as compared to wildtype ones which suggested an increase of synapses in R1-6. *dcin* KD didn't show any effect on photoreceptors' health as the depolarization levels remained unchanged compared to wildtype photoreceptors (Fig. 3.2.3.2, C-D).

3.3. Discussion

In this study, I described the function of Lar and Liprin- α in R7s for targeting and synapse formation. Lar and Liprin- α are proposed to promote synapse formation by stabilizing microtubules in bulbous tips which is supported by the observed increase in synapse count with increasing filopodial stability upon manipulating the actin cytoskeleton dynamics.

3.3.1. R8s dictate the layer to which *lar* and *liprin- α* R7s retract to

Previous reports showed that *lar* and *liprin- α* R7s target, or retract to, the layer M3 in fixed adult preparations. Live imaging of *lar* R7s however showed a different result. When *lar* R7s destabilize from their correct layer and retract before P50, they retracted to the M0 and then extended again to M3. This coincides with the dynamics of R8s that initially remain in the M0 and then actively extend to M3 by P55 (Akin and Zipursky 2016). This explains why DRA *lar* and *liprin- α* R7s always terminate in M6 as the DRA R8s terminate in the same layer as well (Sancer et al. 2019). This was not seen with *liprin- α* R7s as they started retractions after P50 and they always retracted to M3 directly.

To support this finding, when all R8s were forced to terminate in M6 by expressing Hth and transforming them into DRA R8s, *lar* R7s terminated in M6 as well. One caveat of this experiment was that all the photoreceptors were transformed into DRA photoreceptors since Hth was expressed under the control of GMR, so it is possible that R7s termination in M6 was caused by their transformation instead of them following R8s. Consistently, forcing R8s to terminate in M0 by Gogo overexpression in all photoreceptors caused *liprin- α* R7s to retract to M0. (Dr. Abhishek Kulkarni; personal communication). Gogo overexpression in all photoreceptors was reported to only affect R8s and caused them to terminate in M0 by prevented their extension to M3 (Tomasi et al. 2008).

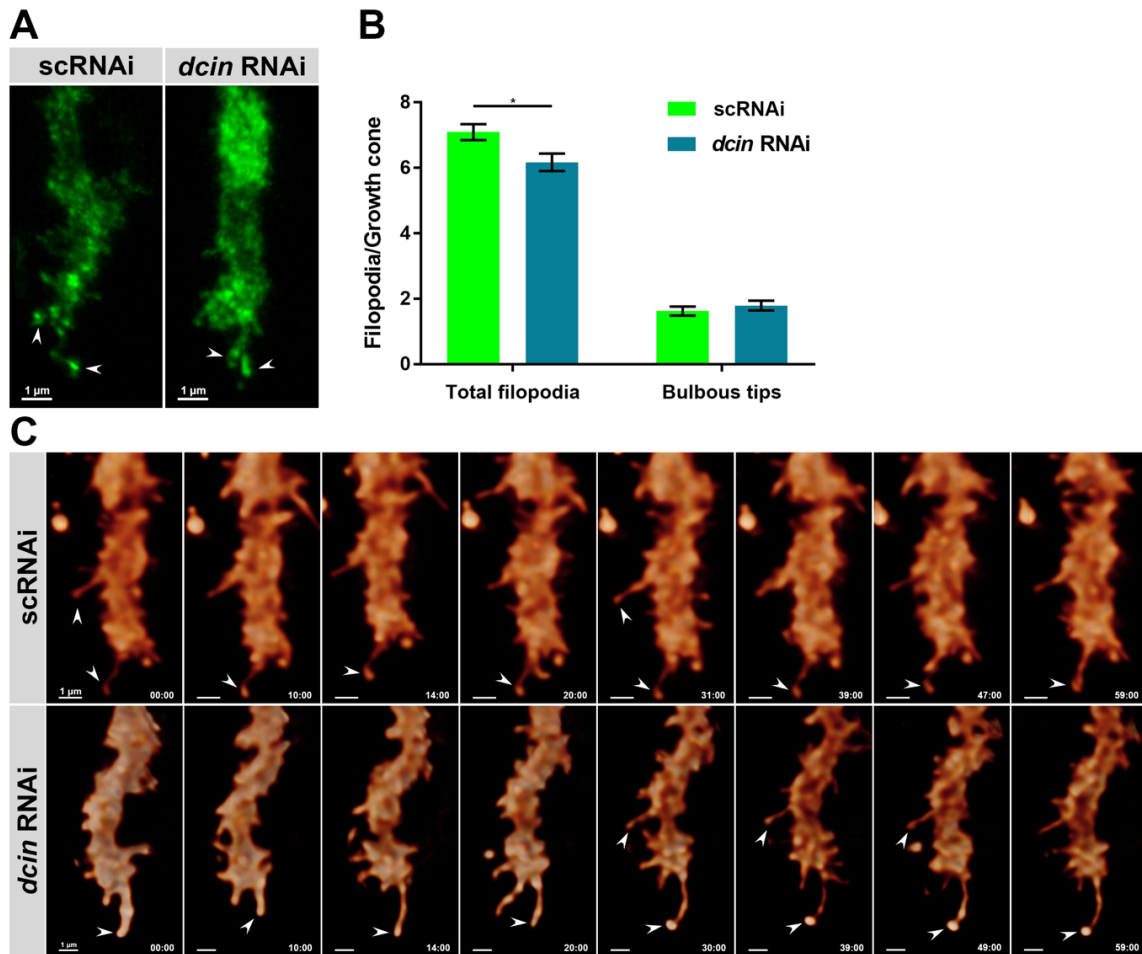


Fig. 3.2.3.1. dCIN affects R7 filopodial dynamics.

dCIN affects actin polymerization through its effect on cofilin. Expressing *dcin* RNAi in R7s has a minimal effect on filopodia formation but affects filopodia dynamics and stability. **(A)** At P70, R7 terminals expressing *dcin* RNAi form filopodia and bulbous tips (arrow heads), they are not morphologically different to the respective control R7s. Scale bar = 1 μm. **(B)** Quantification of the total number of filopodia and bulbous tips formed by R7s expressing *dcin* RNAi and the control R7s. The total filopodia count is slightly reduced upon *dcin* RNAi expression but the number of bulbous tips is not altered. Figure bars represent the mean±SEM filopodia per R7 terminal. Total filopodia counts; scRNAi: 7.09±0.24 filopodia, n=32 R7s. *dcin* RNAi: 6.17±0.26 filopodia, n=29 R7s (P=0.0133). Bulbous tip counts; scRNAi: 1.62±0.14 bulbous tips, n=32 R7s. *dcin* RNAi: 1.79±0.15 bulbous tips, n=29 R7s (P=0.4188). **(C)** Live imaging of R7s that express *dcin* RNAi or scRNAi as a control. Control R7s form a bulbous tip that is stable during the whole imaging duration, they also form other bulbous tips that are transient (arrow heads). R7s expressing *dcin* RNAi have thicker and longer filopodia that were more stable and slower to retract, they formed stable and transient bulbous tips as well (arrow heads). Time resolution = 1 minute, scale bar = 1 μm.

PART 3 | LAR

3.3.2. Lar and Liprin- α are dispensable for synapse formation in photoreceptors

Loss of *lar* and *liprin- α* in non-DRA R7s caused a synaptic defect similar to their loss in the NMJ. The synaptic defect did not depend on the layer in which R7s terminated and Trio OE in *lar* R7s failed to rescue the synaptic defect. This is proposed to be due to the affected filopodial dynamics as R7s mutant of *lar* and *liprin- α* failed to stabilize synaptogenic bulbous tips, with *lar* R7s showing a bulbous tip formation defect as well.

Contrary to the earlier findings, *lar* and *liprin- α* DRA R7s did not have the synaptic defect seen with the non-DRA R7s. Furthermore, synaptic transmission in R1-6 was not affected in both the mutants, indicating they are capable of forming normal number of functional synapses as wildtype R7s. This finding is consistent with the EM reconstruction data that showed a normal average number of synapses per R1-6 terminal for both *lar* (Hiesinger et al. 2006) and *liprin- α* (Prof. Ian Meinertzhagen; personal communication). Additionally, loss of both the genes did not affect active zone assembly but were rather required for synaptic vesicle clustering in mechanosensory neurons (Urwylar et al. 2015).

In brief, both proteins are required for synapse formation only in the non-DRA R7s but not in other photoreceptor subtypes, their requirement for synapse formation in R8s was never tested to be accurate, and other neurons. Suggesting that their effect on synapse formation is not a primary defect, but rather a consequence of another function that is important solely for non-DRA R7s to form synapses.

3.3.3. Lar and Liprin- α stabilize microtubules in bulbous tips

Lar and Liprin- α were reported to function upstream of the formin Dia to regulate microtubule polymerization (Pawson et al. 2008; Sakamoto et al. 2012). This interaction was not possible to prove in photoreceptors as homozygosity of *dia* was lethal to photoreceptors and formed deformed rough eyes. As an indirect way to test the interaction, the effect of Lar and Liprin- α on microtubules was investigated.

The current view of neuronal growth cones is that they are divided into three domains; the central domain which is composed primarily of microtubules, the actin-rich peripheral domain which contains the highly dynamic filopodia, and the transitional domain which separated the two other domains (Biswas and Kalil 2018). As a response to external stimuli, microtubules transiently invade the actin-rich filopodia to support the growth cone stabilization or steering (Craig 2018). Microtubule dynamics, labelled with either GFP-Tub or EB1-mCherry, in developing R7s in intact brains showed different results than what was expected. Microtubules were found occupying the entire growth cone instead of being concentrated in the central domain, they never invaded filopodia but rather invaded bulbous tips only. The difference might

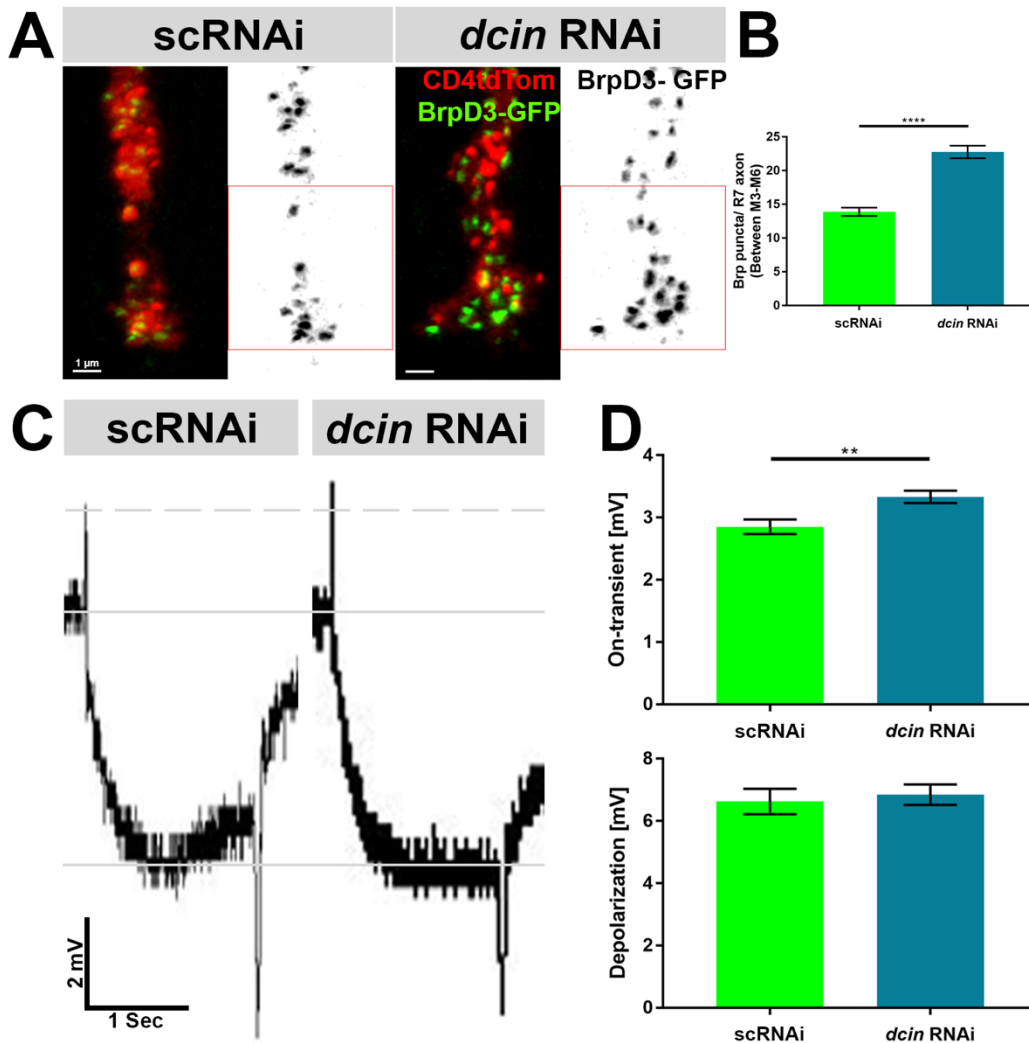


Fig. 3.2.3.2. *dcin* knock-down enhances synapse formation in photoreceptors.

Reducing filopodial dynamics by *dcin* knock-down increases the number of synapses in R7s and increases the synaptic transmission from R1-6 as recorded by ERG. **(A)** Sparse R7 clones at P70 expressing scRNAi as a control or *dcin* RNAi, the membranes are labelled with CD4tdTom (red) and Brp-D3 is used as an active zone marker (green) which is also shown in a separate panel. Synapses were only quantified between M3 and M6 (red box). Scale bar =1 μ m. **(B)** Quantification of the synapses in R7s expressing *dcin* RNAi and the respective control. Bars represent mean \pm SEM synapses per R7. scRNAi: 13.9 \pm 0.61 synapses, n=29 R7s. *dcin* RNAi: 22.77 \pm 0.92 synapses, n=43 R7s (P<0.0001). **(C)** Representative ERG traces recorded from eyes expressing scRNAi or *dcin* RNAi using GMR-Gal4. The solid lines mark the baseline (middle line) and the control depolarization level (bottom line), the dashed line marks the control On-transient level. Photoreceptors expressing *dcin* RNAi are healthy with a normal depolarization level and their synaptic transmission is increased shown by a higher On-transient. **(D)** Quantification of ERG On-transient and depolarization amplitudes shown in (C). Graph bars represent mean \pm SEM mV. scRNAi; On-transient: 2.85 \pm 0.11 mV, depolarization: 6.62 \pm 0.41 mV, n=22 flies. *dcin* RNAi; On-transient: 3.33 \pm 0.09 mV (P=0.0031), depolarization: 6.84 \pm 0.32 mV (P=0,6772), n=33 flies.

PART 3 | LAR

arise because the previous reports studied the cytoskeleton dynamics in 2D neuronal cell lines or primary cultures while I studied microtubule dynamics in intact brains.

Microtubules were found to stabilize one bulbous tip per R7 growth cone at P60, further supporting our recent report that R7s can stabilize one synaptogenic bulbous tip at a given time point (Özel et al. 2019). *lar* and *liprin-α* R7s however failed to stabilize microtubules that invaded the formed bulbous tips. This result showed that R7s can form bulbous tips whether they recruit microtubules or not, and that stable bulbous tips always correlate with stable microtubules. It is not clear, however, whether microtubule stabilization is the cause or a result of bulbous tip stabilization. On a side note, one needs to be careful when overexpressing GFP-Tub as it might affect microtubule polymerization, these results should be confirmed with fluorescently-tagged EB1 (Pawson et al. 2008).

We recently reported that Liprin-α localizes in filopodia and bulbous tips and that this localization was reduced in *lar* R7s (Özel et al. 2019). Liprin-α preceded the leading edge of microtubules to invade and stabilize in bulbous tips. This can provide an explanation to the destabilization of microtubules in either mutant. In both cases, less or no Liprin-α is recruited to the formed bulbous tips to stabilize microtubules that eventually retract back to the growth cones followed by the bulbous tip destabilization.

3.3.4. Reducing actin depolymerization leads to more stable filopodia in R7s

Cofilin is reported to densely-localize to the leading tips of growth cones and its activity is regulated locally to control the stability of actin filaments and filopodia dynamics (Bamburg and Bray 1987; Aizawa et al. 2001). CIN colocalizes with cofilin in tips of migrating cells, it activates cofilin and promotes actin filament severing. In *Drosophila* R7s, RNAi depletion of *dcin* caused a minor decrease in the number of formed filopodia which were much larger than wildtype R7 filopodia, these changes are similar to the observed increase in spine head size in *cin* mutant neurons in mice (Kim et al. 2016). Live imaging of the *dcin* KD R7s fast dynamics showed that filopodia and bulbous tip formation was not affected but, as expected, they were slower to retract.

3.3.5. Depleting *dcin* in photoreceptors causes them to form more synapses

Filopodia are dynamic protrusions formed at the leading edges of axons to sense the environment for cues that are important for growth cone steering and pathfinding. They also function as the pre-postsynaptic contact points that mature and give rise to synapses. Stabilizing filopodial contacts is central to synapse formation, this explains the synaptic defect upon blocking filopodia formation. By virtue, increasing filopodial stability should promote synapse formation. Indeed, the increased filopodial stability upon *dcin* KD in photoreceptors is reflected in an increased number of synapses in R7s and an increased synaptic transmission

as recorded from photoreceptors. It is not known, however, whether *dcin* KD changes photoreceptors wiring and leads them to form synapses with incorrect synaptic partners.

It was surprising that CIN is not required in *Drosophila* photoreceptors and mechanosensory neurons or *Mouse* neurons for cell division and pathfinding as opposed to the severe cell division defects seen *in vitro*. This could be attributed to other cofilin phosphatases (e.g. SSH) that are redundant for CIN's role in other earlier functions than regulating cofilin in filopodia. Another explanation could be the differences in cellular localization of different cofilin phosphatases in developing neurons with CIN being only present in filopodial tips. Further characterization of CIN and cofilin localization will be the goal of future investigation.

The shown effect of dCIN on synapse formation should, however, be taken with caution as its knock-down might also affect axonal transport or other functions of the cytoskeleton that lead to an increased synapse number. These findings should be verified by manipulating other regulators of the cytoskeleton and by excluding any possible effect on axon transport.

3.3.6. Proposed role of Lar and Liprin- α in R7 targeting and synapse formation

Here, I suggest that Lar and Liprin- α are not required for R7 correct layer targeting and the synaptic defect in R7s mutant of both genes is not a primary defect. Based on the findings at hand, the function of Lar and Liprin- α in R7s is to stabilize pre-postsynaptic contacts, which, when increased, was found sufficient to increase synapse formation presumably by increasing synaptic contact time.

Moreover, I propose a molecular model that explains how Lar and Liprin- α achieve their function in R7s. Both the proteins are independently probabilistically recruited to the bulbous tips and their interaction stabilizes it in two different ways; Lar stabilizes the pre-post synaptic interaction by binding to its postsynaptic ligand, and Liprin- α by recruiting Dia which promotes microtubule polymerization to support and maintain the bulbous tip structure. Lar consolidates the contact point by clustering presynaptic NCad with which it physically interacts (Prakash et al. 2009). As a result, the trans-homophilic binding of NCad strengthens the bulbous tip adhesion to the postsynaptic side. These interactions are all probabilistic and follow a stochastic order, this is evident as Liprin- α is still recruited to filopodia in the absence of Lar and microtubules get recruited to bulbous tips in the absence of Liprin- α even though they are not stabilized there. These continuous probabilistic interactions insure robustness as this stepwise process guarantees the stabilization of the formed pre-postsynaptic contacts as long as all the required stabilizing proteins are recruited while eliminating all contacts that lack any of the elements.

This suggests that Lar and Liprin- α , *per se*, are dispensable for synapses to form but are required in R7s to stabilize their contacts with their postsynaptic partners to form synapses, providing an explanation why both the proteins are not required for synapse formation in R1-6

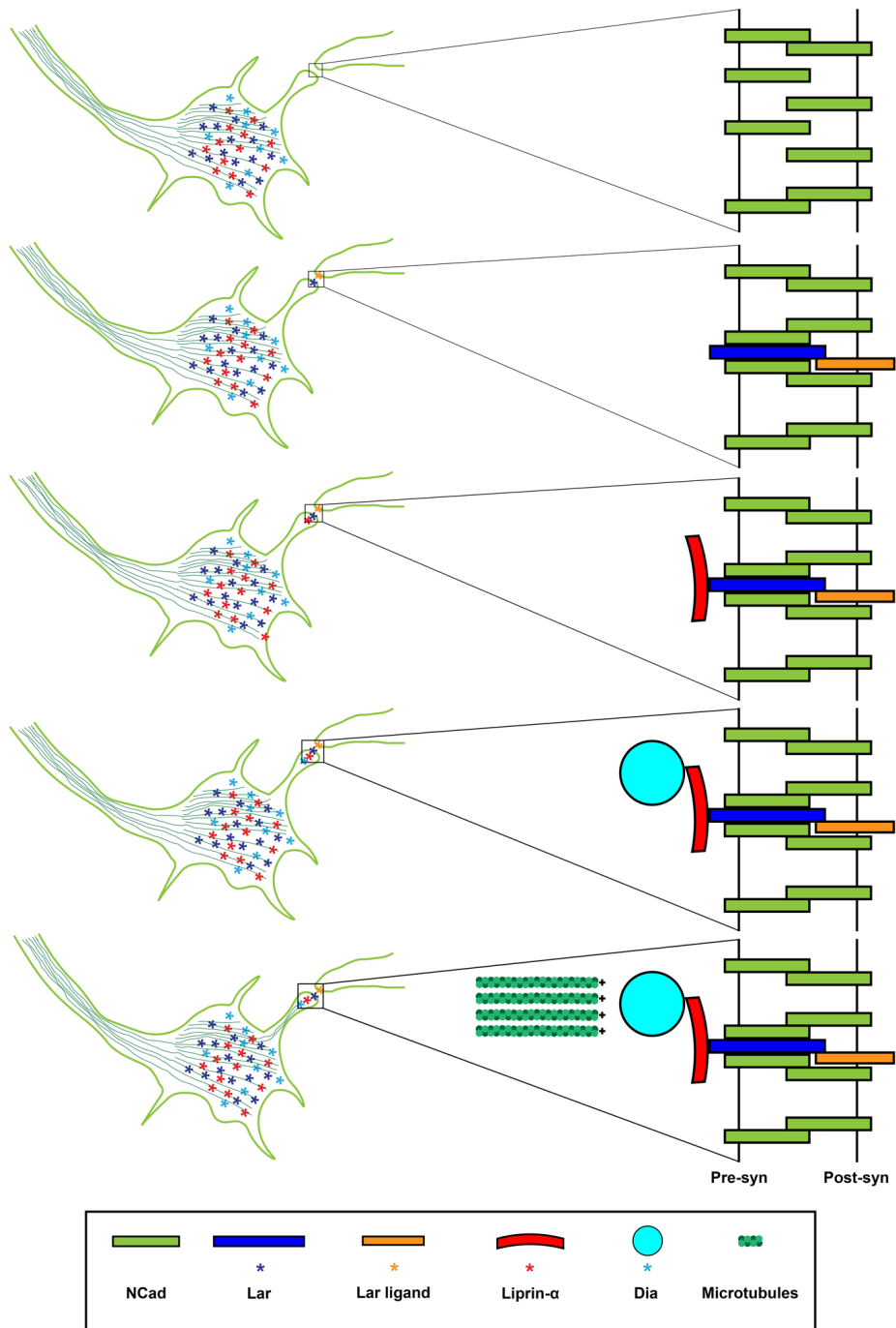


Fig. 3.3.6. A Model suggesting the function of Lar and Liprin- α in R7 bulbous tip stabilization.

A non-comprehensive, step-wise mechanism of R7 bulbous tip stabilization. R7 growth cones form a bulbous tip that binds the post-synaptic side initially through the NCad homophilic adhesion. Then Lar binds its postsynaptic ligand and clusters NCad around that contact point for consolidation. Lar then recruits Liprin- α which, in turn, recruits Dia that promotes microtubule polymerization to support the bulbous tip and maintain its stability. This model suggests that these steps are probabilistic and they can take place at any order, any formed bulbous tip can be eliminated and is stabilized only when all the necessary proteins are recruited in the right order.

that are in close contact with their postsynaptic lamina cells within the cartridges. They are also not required in DRA R7s as they rely on DRA R8s for targeting, and possibly form synapses with, although it is not clear whether the DRA R7s can still form synapses with Dm8s. This supports the assumption that synapse formation is a probabilistic process that is facilitated by establishing pre-postsynaptic contact and maintaining it long enough until all the synaptic components are recruited and functional synapses are formed.

To my knowledge, this is the first molecular mechanism that explains the role of active zone proteins in facilitating synapse formation. This mechanism, however, is by far incomprehensive as both Lar and Liprin- α are known to interact with several other proteins that can also play a role in facilitating targeting and synapse formation.

PART | 4 PTP69D

Role of PTP69D in R7 Targeting
and Synapse Formation

4.1. Contribution

I designed and generated all the fly lines in this section. I also performed all the experiments and analyzed the results myself.

4.2. Results

PTP69D was reported to play a role in the NMJ and in R7 targeting. Its role in targeting was considered as redundant to the action of other members of the PTP family (Sun et al. 2001). Photoreceptors mutant of *ptp69d* were reported to target their correct layer before they retracted to M3, a phenotype that was enhanced by the additive effect of *lar* loss of function (Hakeda-Suzuki et al. 2017). However, the effect of *ptp69d* loss on R7s' dynamics during development and its effect on synapse formation were not known.

4.2.1. PTP69D is not required for R7 layer targeting but is required for filopodia formation

PTP69D's role in R7 targeting was previously reported where R7s initially targeted correctly but then they probabilistically retract to M3. To follow the progression of the phenotype during development I used the null allele *ptp69d*^{D1689} (Newsome et al. 2000a) for my analysis. This allele is homozygous lethal and was reported to have a point mutation that created a premature stop-codon in the second exon that produces a truncated protein (red line in Fig. 4.2.1-1, A). To test for the correct allele, I amplified the region flanking the reported stop-codon from genomic DNA of heterozygous flies. I then sequenced the PCR products with the right band size and confirmed having the G to A point mutation that led to the reported stop-codon. Since I extracted DNA from heterozygous flies, the traces showed two peaks for both the wildtype (G) and the mutant (A) bases (Fig. 4.2.1-1, B).

To check the effect of *ptp69d* loss on R7 targeting, I generated whole-eyes mutant of the gene and the respective control. Subsequently, I quantified the retracted R7s in adult flies. Unlike the previously reported penetrance of 50% (Newsome et al. 2000a) or 20% (Hakeda-Suzuki et al. 2017), the calculated penetrance, assuming all the quantified eyes contained 800 ommatidia, was slightly higher than 2% (Fig. 4.2.1-2, A-B). I then attempted to find another solution to reproduce the reported retraction penetrance, hence I sought using *ptp69d* RNAi lines which were reported to cause a quantitatively comparable R7 retraction phenotype to the null mutant allele (Hakeda-Suzuki et al. 2017). However, driving the two available RNAi lines with GMR-Gal4 caused even fewer retracted R7s than the mutant did, bringing the penetrance to about 0.5% (Fig. 4.2.1-2, A-B).

To find how *ptp69d* mutant R7s behave during development, I generated sparse R7 mutant clones and performed long term live imaging as described in (Özel et al. 2019). Mutant R7s targeted correctly and adopted a normal morphology similar to wildtype R7s (controls not

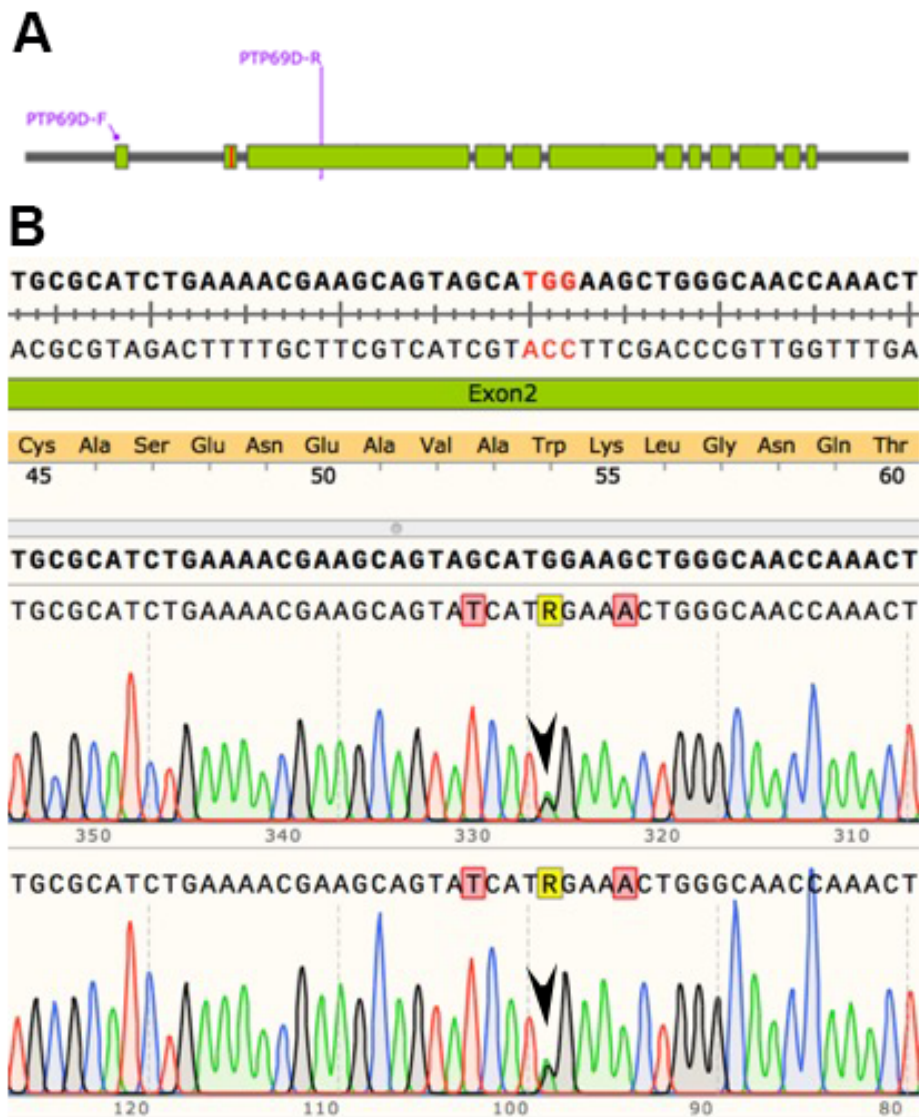


Fig. 4.2.1-1. Confirming the *ptp69d*^{D1689} allele.

The *ptp69d*^{D1689} is a null allele with a point mutation in the second exon that introduces a premature stop codon. **(A)** Schematic representation of the *ptp69d* genomic locus that show the exons in green and the site of the point mutation (red line in exon 2). The primers used to amplify the genomic region for sequencing are marked. **(B)** The genomic sequence that contains the mutated base (red). Traces of the sequencing genomic DNA from heterozygous flies show the mutated base and the wildtype base (arrow head).

shown here). However, due to the very low penetrance, I did not manage to capture a retracting R7 during four live imaging sessions. The only observed change in *ptp69d* mutant R7s was that the growth cones were much smoother and carried fewer filopodia, but not bulbous tips, than normally observed with wildtype R7s (Fig. 4.2.1-2, C). This behavior was also observed in fast filopodia dynamics; R7 growth cones carried one stable bulbous tip and formed transient

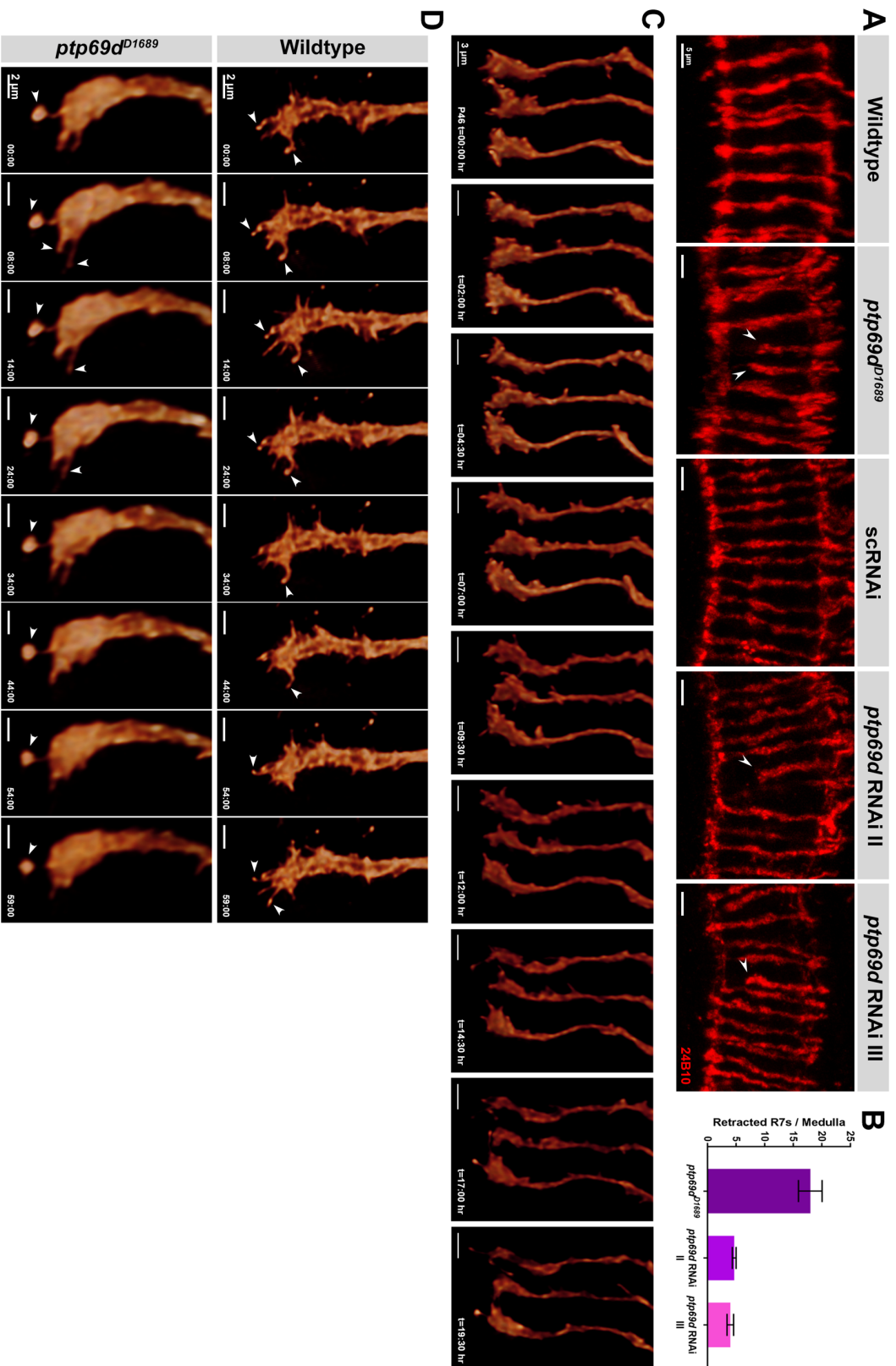


Fig. 4.2.1-2. *ptp69d* loss cause R7 retraction and a filopodia formation defect. (Figure legend continues in the next page)

PART | 4 PTP69D

ptp69d R7s initially target correctly before they retract to M3 with a much lower penetrance than previously reported. Mutant R7s form stable bulbous tips but fail to form filopodia. **(A)** Fixed preparations of adult whole-eyes mutant of *ptp69d* and those expressing *ptp69d* RNAi in all photoreceptors with their respective controls. Photoreceptors were stained with anti-Chaoptin (red), scale bar = 5 μ m. Mutant R7s retracted to M3 (arrow heads) with a low penetrance. **(B)** Quantification of the retracted R7s in (A), bars show mean \pm SEM retracted R7s per medulla. *ptp69d*: 18 \pm 2.08 R7s. *ptp69d* RNAi II: 4.66 \pm 0.33. *ptp69d* III: 4 \pm 0.57 R7s. 3 brains were quantified for each condition. **(C)** Long term live imaging of *ptp69d* R7s showed that they target correctly and developed normally as they extended with no morphological changes during development. Start stage the stage (P) in which live imaging started is indicated in the first frame, time resolution = 30 minutes, scale bar = 3 μ m. **(D)** Live imaging of fast filopodial dynamics of wildtype and *ptp69d* R7s at P60. Compared to wildtype, *ptp69d* R7s formed fewer transient filopodia but bulbous tip formation and stabilization was not affected (arrow heads). Time resolution = 1 minute, scale bar = 2 μ m.

ones during a one-hour imaging window. However, the growth cones formed very few filopodia suggesting the requirement of PTP69D for this function (Fig. 4.2.1-2, D).

4.2.2. PTP69D is not required for synapse formation in photoreceptors

The proposed functional redundancy between PTP69D and Lar in R7 targeting and the role of the PTP69D vertebrate homologue in synapse formation suggested a potential role of PTP69D in synapse formation as well. To test this, I generated *ptp69d* sparse mutant R7s clones while using Brp-D3 as a presynaptic active zone marker. Quantification of the synapse number did not show any synaptic defect in *ptp69d* mutant R7s compared to wildtype ones at P70 (Fig. 4.2.2, A-B).

ERG recording of newly-hatched adult flies with either whole-eyes mutant of *ptp69d* or expressing *ptp69d* RNAi were used as a measure of synaptic transmission in photoreceptors to their postsynaptic partners. Both groups did not show any changes in the On-transient but rather a decreased depolarization level. This eliminates synaptic transmission defects upon loss of *ptp69d*. Nonetheless mutant photoreceptors were found unhealthy (Fig. 4.2.2, C-D).

4.3. Discussion

Loss of *ptp69d* destabilized R7s contact in M6 and caused them to retract to M3. It interacts with, and thought to be redundant to, the other PTP member Lar for such a role (Hakeda-Suzuki et al. 2017). The findings at hand suggest a unique role of PTP69D in R7s targeting, but not synapse formation, which is distinct from Lar's function.

4.3.1. PTP69D function in R7s is not redundant to Lar

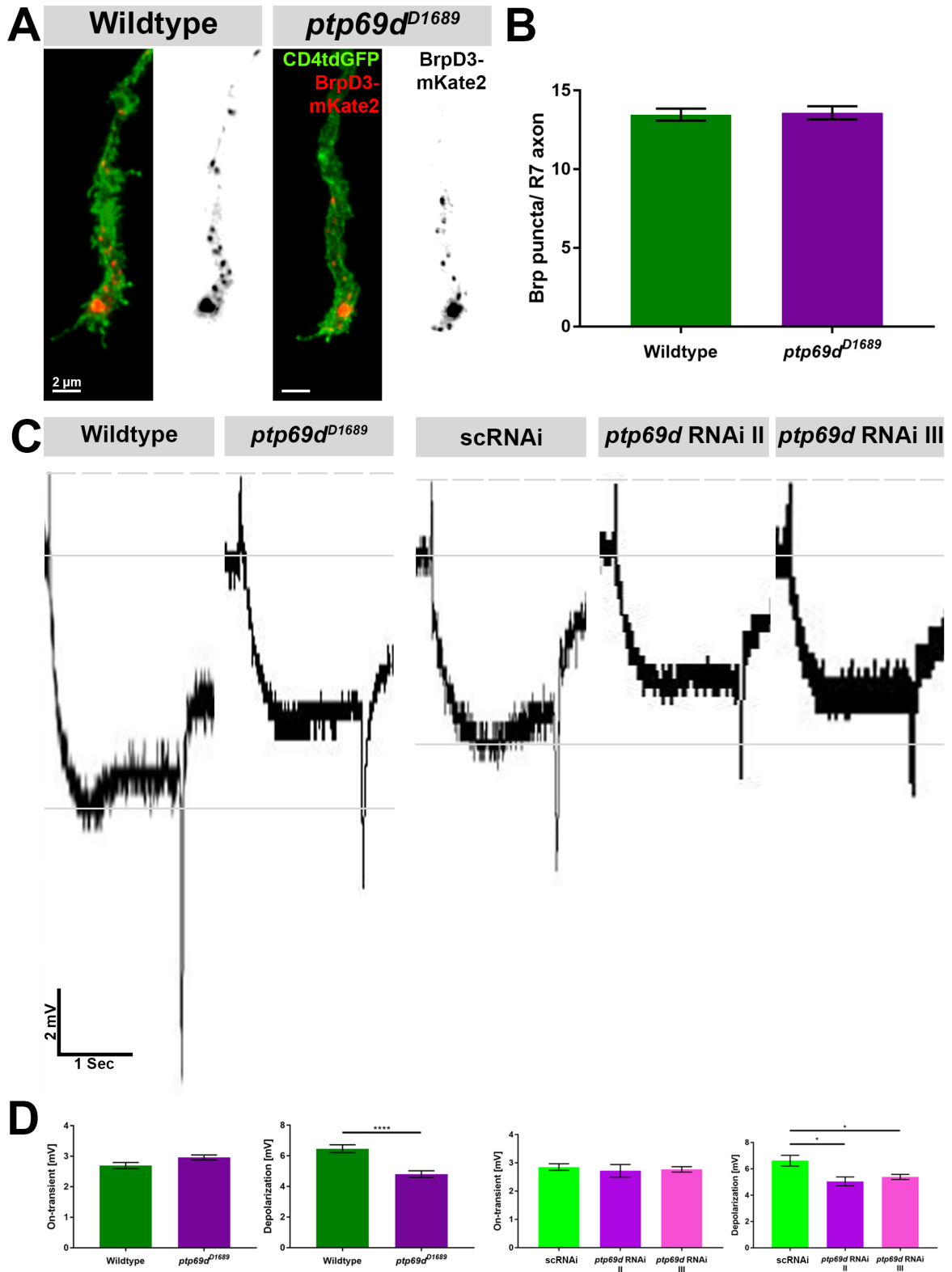


Fig. 4.2.2. PTP69D is not required for synapse formation in photoreceptors.

Loss of *ptp69d* does not cause a synaptic formation defect in R7s nor a synaptic transmission as recorded by ERG. (Figure legend continues in the next page)

PART | 4 PTP69D

(A) Wildtype and *ptp69d* R7s clones at P70 with their membrane labelled with CD4tdGFP (green) and the active zones marked with Brp-mKate2 (red) which is also shown in a separate panel. Scale bar = 2 μ m. **(B)** Quantification of R7 synapses in wildtype and *ptp69d* R7s. Bars represent mean \pm SEM synapses/R7 axon. Wildtype: 13.47 \pm 0.37 synapses, n=19 R7s. *ptp69d*: 13.58 \pm 0.41 synapses, n=12 R7s (P=0.8513). **(C)** Representative ERG traces recorded from flies with whole-eye mutant of *ptp69d* and the respective control, together with flies expressing scRNAi, *ptp69d* II and III RNAi in all photoreceptors. The solid lines mark the baseline (middle line) and the control depolarization level (bottom line), the dashed line marks the control On-transient level. Although photoreceptors lacking *ptp69d* were unhealthy, their synaptic transmission was not affected. **(D)** Quantification of ERG On-transient and depolarization amplitudes shown in (C). Graph bars represent mean \pm SEM mV. Wildtype; On-transient: 2.69 \pm 0.1 mV, depolarization: 6.46 \pm 0.25 mV, n=12 flies. *ptp69d*; On-transient: 2.96 \pm 0.08 mV (P=0.0552), depolarization: 4.8 \pm 0.21 mV (P<0.0001), n=11 flies. scRNAi; On-transient: 2.85 \pm 0.11 mV, depolarization: 6.62 \pm 0.41 mV, n=22 flies. *ptp69d* RNAi II; On-transient: 2.72 \pm 0.22 mV (P=0.5717), depolarization: 5.05 \pm 0.33 mV (P=0.0221), n=10 flies. *ptp69d* RNAi III; On-transient: 2.76 \pm 0.09 mV (P=0.6124), depolarization: 5.38 \pm 0.19 mV (P=0.0235), n=15 flies.

The subtle R7 retraction phenotype observed in *ptp69d* R7s is surprising and suggests a compensatory mechanism, possibly involving Lar or other PTPs. Since mutant R7s formed normal number of synapses and only a few filopodia, the phenotype could, however, be explained in light of our recent computational modeling of probability of R7 retraction predicting that R7 stabilization is caused by the combined effect of transient filopodia and the number of synapses (Özel et al. 2019).

PTP69D localization in developing R7s could shed light on its function. It is not known whether it localizes in bulbous tips or in filopodia, although the results suggest that it localizes in filopodia. It also remains a question whether PTP69D is an active zone protein similar to its vertebrate homologue.

The phenotypes associated with loss of *ptp69d* in R7s are qualitatively and quantitatively different from those of *lar*. While loss of *lar* causes a defect in bulbous tip formation and synapse formation, loss of *ptp69d* causes only defect in a filopodial formation with no effect on synapse formation nor bulbous tip formation or stabilization. Such dynamic differences could only be unraveled using live imaging. Although this result does not shed light on what role PTP69D have in filopodia formation, it highlights a distinct function of PTP69D in R7 development negating its functional redundancy to Lar.

PART | 5 NEUREXIN-1

Functional Requirement of Nrx for Photoreceptor Synapse Formation and Synaptic-Partner Specification

5.1. Contribution

I designed and generated all the fly lines in this section, except for the *trans*-Tango flies that were designed and generated by F. Ridvan Kiral, which I then modified for the experiments in this section. I also performed all the experiments and analyzed the results myself.

5.2. Results

Nrx is a presynaptic active zone protein that mediates pre-postsynaptic apposition through its interaction with Neuroligin (Nlg). The role of the *Drosophila* Nrx was described in the NMJ; it was found to be required in the NMJ to form synaptic boutons and for pre-postsynaptic differentiation, but has no effect on targeting (Li et al. 2007). Nrx was also reported to be important for columnar restriction in L4 axon terminals (Liu et al. 2017). However, Nrx's role in photoreceptor targeting and synapse formation was not studied before.

5.2.1. Nrx is not required for R7 correct targeting

For the available *nrx* mutant alleles were homozygous lethal, I sought generating mutant clones in otherwise heterozygous animals. For that I initially recombined the *nrx*²⁴¹ null allele to an FRT site. I confirmed having the FRT site in the candidate lines before testing for the *nrx*²⁴¹ molecularly using PCR (Fig. 5.2.1, A). As expected, the control PCR resulted in bands in all the candidate lines (short fragment) while only one candidate line resulted in a band for the long fragment (lane 3 in Fig. 5.2.1, B). I then further confirmed the candidate line by crossing it to a deficiency line lacking Nrx which results in viable flies that stained negative for Nrx (Fig. 5.2.1, C).

Using the confirmed line, I generated flies with whole-eyes mutant of *nrx*. Photoreceptors in the medulla showed no targeting or morphological defects compared to wildtype (Fig. 5.2.1, D). Sparse clones of R7s mutant of *nrx* also developed normally with no changes in their dynamics as shown by long term live imaging (data not shown).

5.2.2. Loss of *nrx* in photoreceptors causes an increase in neurotransmission

To assay the function of photoreceptors mutant of *nrx*, I recorded ERG from eyes of newly hatched flies with whole-eyes mutant of *nrx* and the respective control. Surprisingly, synaptic transmission, as measured by the On-transient amplitudes, from *nrx* mutant photoreceptors showed nearly a 1.5-fold increase compared to wildtype ones. Depolarization, however, was reduced to almost half that of the wildtype indicating severely unhealthy neurons (Fig. 5.2.2). This result opposes findings in the NMJ where loss of *nrx* caused defective synaptic transmission (Li et al. 2007).

5.2.3. *nrx* R7s form contacts with incorrect postsynaptic neurons

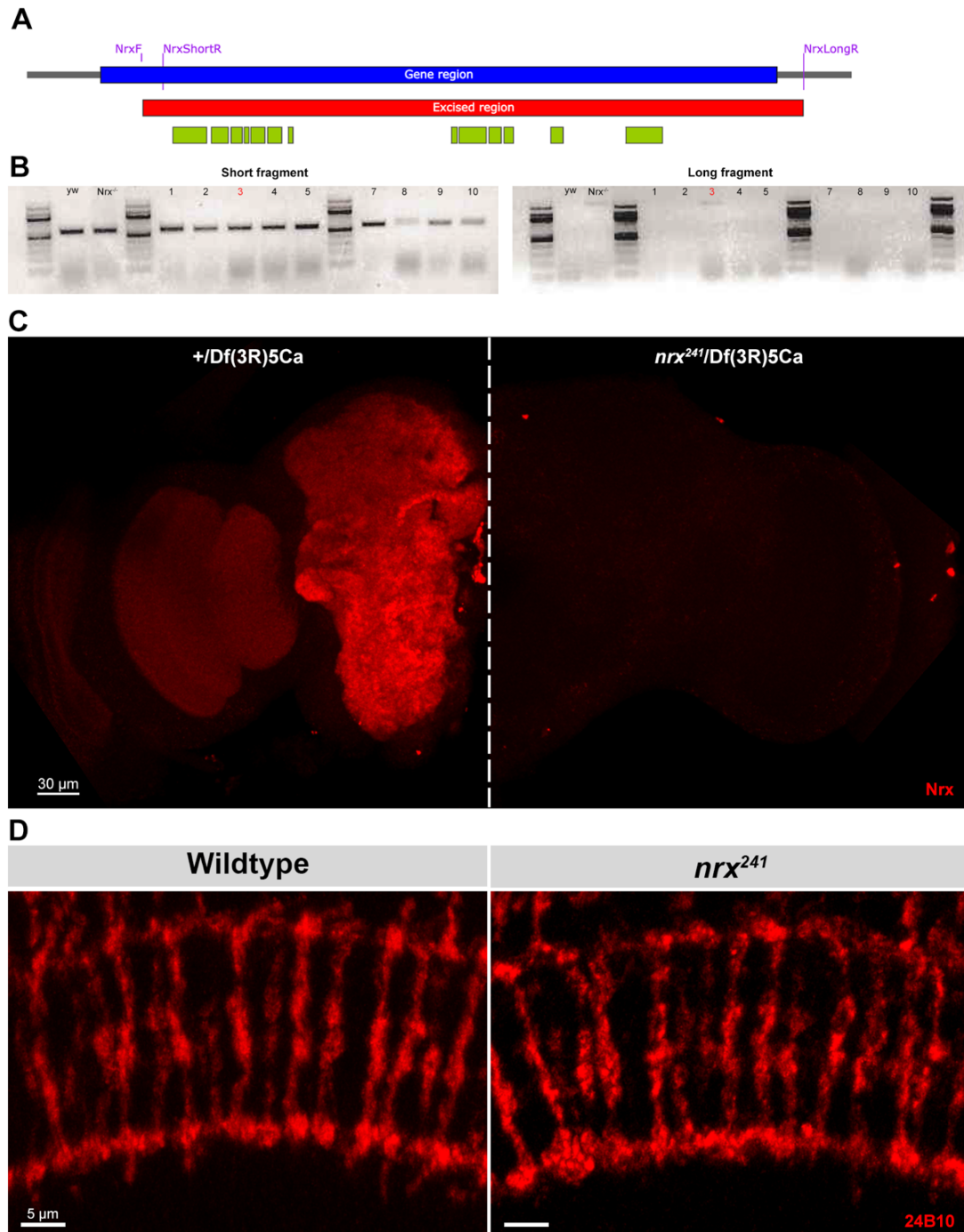


Fig. 5.2.1. NrX is not required for R7 targeting.

(A) Schematic representation of the *nrX* genomic locus (blue), protein coding region (green), and the reported excised fragment of the *nrX*²⁴¹ allele (red). The primers used to test the candidate recombinant lines are indicated. (B) PCR products bands from the two reactions. Short fragment was used as a control and gave a band in all lines while the long fragment gave a band only in line 3 similar to *nrX*^{+/+} control. (C) NrX antibody staining of newly-hatched adult brains from *nrX*-deficient (right) and control animals (left). NrX marked all neuropils in control brains (red) while the staining was completely missing from *nrX*-deficient brains. Scale bar = 30 μm. (D) Photoreceptor projections terminated in their correct layers in the medulla in *nrX* mutant eyes similar to the respective control eyes. Photoreceptors stained with anti-Chaoptin (red), scale bar = 5 μm.

PART | 5 NRX

To find if the increase in synaptic transmission described before is concomitant with an increase of R7s synapses as reported in (Kiral et al. 2019). It was not possible to use Brp-D3 to quantify presynaptic active zones since it showed a smear of fluorescence along R7 axons instead of distinct puncta (data not shown). It was not possible to confirm the observed phenotype until the point of writing this.

Alternatively, I sought using trans-Tango (Talay et al. 2017) as an unbiased method to identify the postsynaptic neurons that *nrx* R7s contacted. This, again, was motivated by the findings in (Kiral et al. 2019) where autophagy-deficient R7s formed synapses on more and incorrect postsynaptic neurons compared to wildtype R7s. For that, I generated sparse R7 *nrx* mutant clones in which I expressed the R7 specific driver Rhodopsin4-Gal4 (Rh4-Gal4) instead of GMR-Gal4 to restrict the analysis only to neurons postsynaptic to R7s as GMRflp generates clones in R1 and R6 as well as R7s.

The postsynaptic partners of R7s were previously characterized. EM reconstruction of medulla columns showed that R7s formed most their synapses on Dm8s and fewer synapses on Tm5s (Takemura et al. 2013; Karuppururai et al. 2014). Consistently, trans-tango identified Dm8s as the major synaptic partner of wildtype R7s and labelled Tm5s as well. On the other hand, loss of *nrx* in R7s led to a drastic, 2-fold increase in the number of labelled postsynaptic neurons they contacted as shown by the cell body count of the labelled cells (Fig. 5.2.3, A-B). Although the experimental genetic approach only allowed labeling of postsynaptic partners of a sparse population of R7s, the large number and dense projections of the postsynaptic partners of *nrx* mutant R7s made it difficult to identify all the labelled neurons. However, some of the frequently-labelled incorrect postsynaptic targets were Lawf, C2, C3, T1, Mi4, and Mi1, based on their described morphology in (Fischbach and Dittrich 1989), and were not previously reported as synaptic partners of R7s (Fig. 5.2.3, C).

5.2.4. *nrx* R7s fail to stabilize bulbous tips

The previous results where *nrx* mutant photoreceptors showed an increase of synaptic transmission and R7s contacted incorrect postsynaptic neurons suggested that loss of *nrx* in R7s phenocopied autophagy-deficient R7s (Kiral et al. 2019). Hence, I performed live imaging of fast filopodial dynamics of *nrx* R7s at P60 during the peak of synapse formation. Mutant R7s were of normal morphology, although, unexpectedly, they failed to form any stable bulbous tips and rather formed numerous transient ones with lifetimes not exceeding 15 minutes (yellow arrowheads in Fig. 5.2.4).

5.3. Discussion

The requirement of *Nrx* in vertebrate systems for synaptic development and function was previously described. The *Drosophila* *Nrx* is important for the proliferation of synaptic boutons

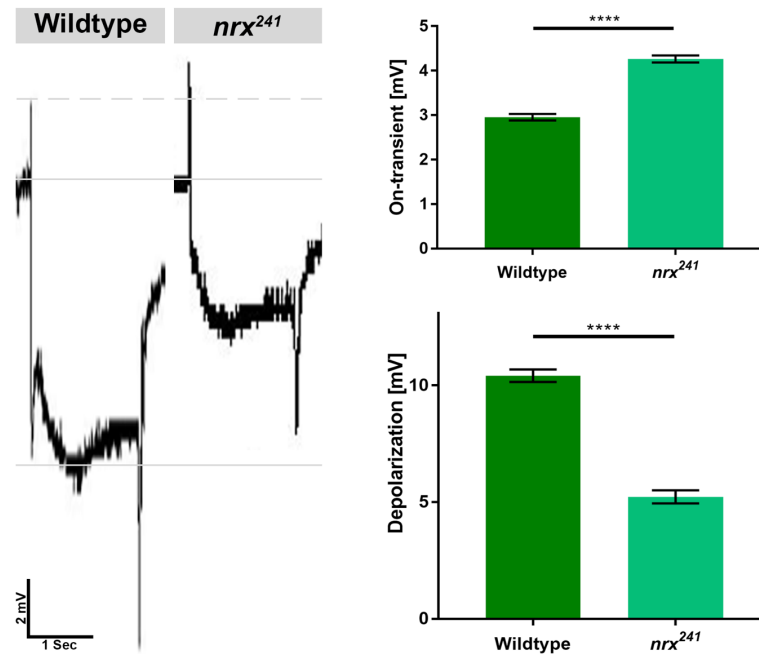


Fig. 5.2.2. Loss of *nrx* leads to an increase in synaptic transmission.

ERG recording from whole-eyes mutant of *nrx* and its respective control. Representative ERG traces recorded from wildtype and *nrx* eyes (left). The solid lines mark the baseline (middle line) and the control depolarization level (bottom line), the dashed line marks the control On-transient level. *nrx* mutant photoreceptors were not healthy but showed an increase of synaptic transmission.

ERG On-transient and depolarization amplitudes were quantified (right), bars represent mean ± SEM mV. Wildtype; On-transient: 2.95 ± 0.07 mV, depolarization: 10.42 ± 0.26 mV, n=38 flies. *nrx*; On-transient: 4.26 ± 0.07 mV (P < 0.0001), depolarization: 1042 ± 0.26 mV (P < 0.0001), n=32 flies.

in the NMJs. Here, I studied the function of NrX in targeting and synapse formation in photoreceptors. While NrX had no effect on R7 targeting, its loss of function affected R7 synaptic partner specification and enhanced synaptic transmission in photoreceptors.

5.3.1. Loss of *nrx* increases R7s filopodial dynamics

Targeting and stabilization of R7s mutant of *nrx* is not affected similar to mutant NMJs. The dynamics of mutant terminals are not distinguishable from wildtype R7s. Filopodial dynamics, however, are severely affected, the overall dynamics of filopodia and bulbous tips were upregulated and growth cones failed to form stable bulbous tips. This dynamic defect resembles that observed in *syd-1* R7s as we recently reported; analysis and simulation of bulbous tip distribution in *syd-1* R7s showed that the inhibitory feedback during bulbous tip formation and the bulbous tip stabilization rate were reduced which eventually increased the frequency of transient bulbous tips (Özel et al. 2019). Syd-1 is a multi-domain active zone protein that binds the PDZ-binding domain of NrX and recruits it to the presynaptic active zone

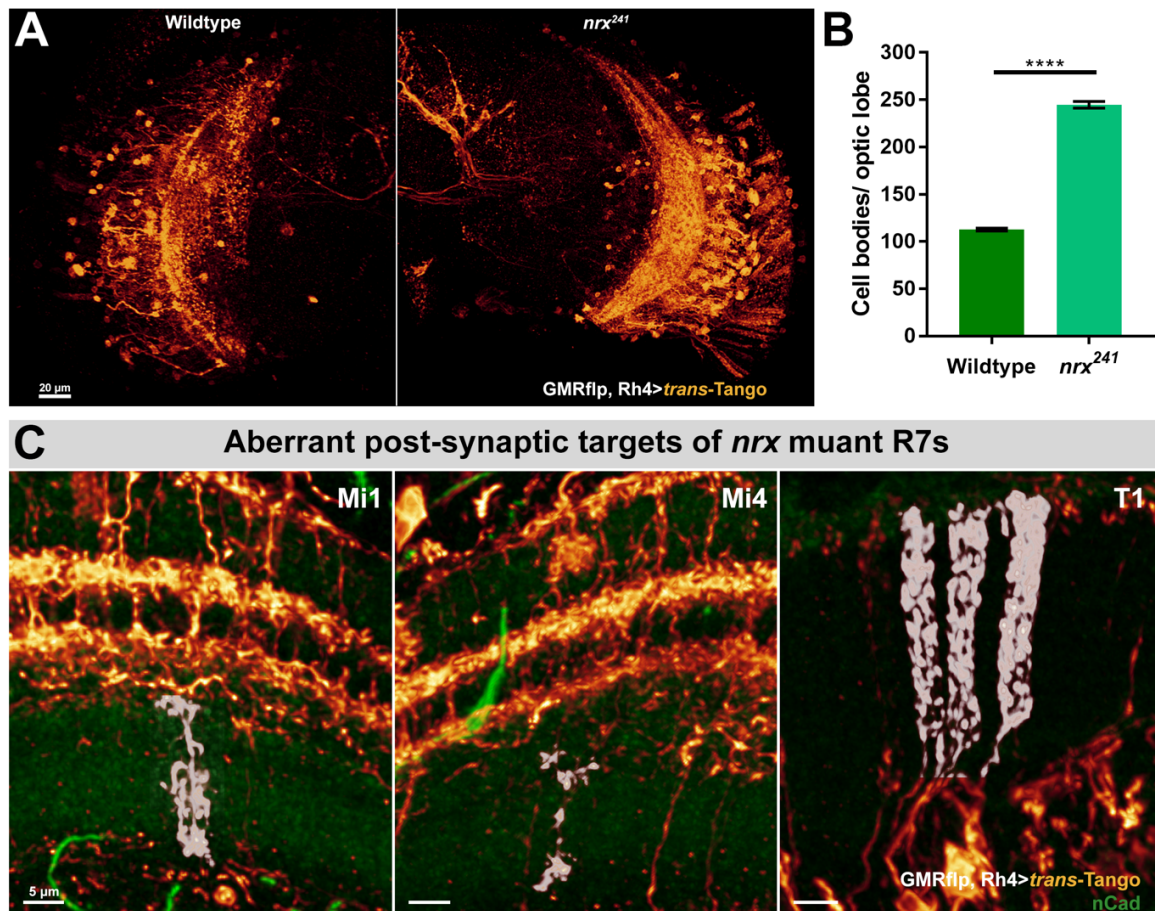


Fig. 5.2.3. *nrx* R7s form contacts with aberrant synaptic partners.

Anterograde trans-synaptic circuit tracing of the neurons postsynaptic to *nrx* R7s. **(A)** Maximum projection images of adult optic lobes showing postsynaptic neurons of wildtype (left) and *nrx* (right) R7s. *nrx* R7s formed contacts with more postsynaptic neurons that show denser projections. Scale bar = 20 μ m. **(B)** Quantification of the postsynaptic neurons contacted by wildtype and *nrx* R7s based on trans-Tango-labelled cell body counts. Bars represent mean \pm SEM cell bodies per optic lobe. Wildtype: 112.7 \pm 1.45 cell bodies, n=3 optic lobes. *nrx*: 244.7 \pm 3.48 cell bodies, n=3 optic lobes (P<0.0001). **(C)** Examples of aberrant postsynaptic neurons that contact *nrx* R7s that are false-colored in white while all the postsynaptic cells are labelled in glow. NCad staining was used to mark the neuropil layers (green).

(Owald et al. 2012), suggesting that the PDZ domain of Syd-1 is required for bulbous tip stabilization and to maintain the inhibitory feedback through its interaction with Nr_x.

5.3.2. Nr_x restricts synapse formation in photoreceptors

The increased synaptic transmission recorded from *nrx* mutant photoreceptors and the increased number of postsynaptic partners of *nrx* R7s were counter-intuitive results, as a synaptic defect was initially expected in photoreceptors similar to the findings in the NMJ.

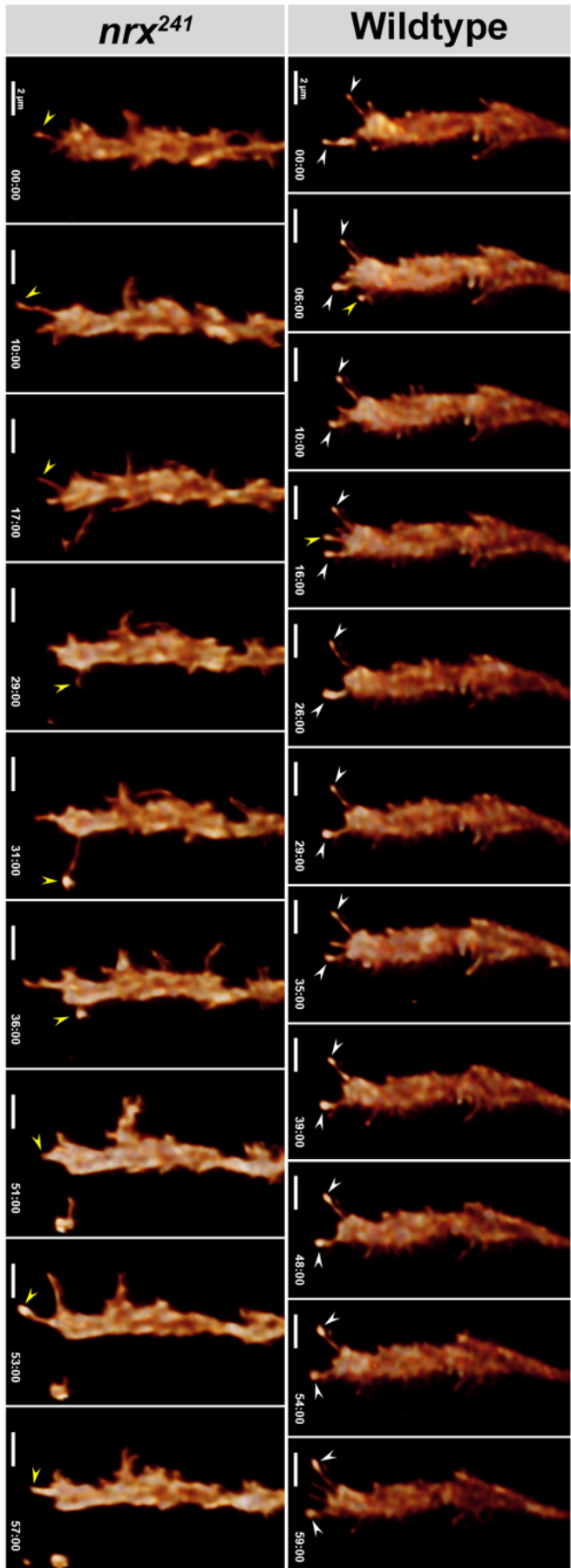


Fig. 5.2.4. *nrx* R7s form numerous unstable bulbous tips.

Live imaging of fast filopodial dynamics of wild type and *nrx* R7s at P60. Wildtype R7s formed bulbous tips (white arrow heads) that were stable longer than 40 minutes and transient bulbous tips (yellow arrow heads) with a shorter lifetime. On the other hand, *nrx* R7s formed more bulbous tips that were all transient and their lifetimes did not exceed 20 minutes (yellow arrow heads). *nrx* R7s all terminated in M6 and adopted a normal morphology.

PART | 5 NRX

Specially the result in R7s as they failed to stabilize bulbous tips which should predict a synaptic defect (Özel et al. 2019).

A proposed explanation to the enhanced synapse formation in *nrx* photoreceptors relies on two pieces of information: 1) The vertebrate Nr_x homologue, α -neurexin, is not required to form synapses (Missler et al. 2003), and 2) The *Drosophila* Nr_x interacts with Syd-1 and Spinophilin (Spn) through their PDZ domains. The interaction of Spn with Nr_x antagonizes Syd-1 and limits synapse formation, Spn also downregulates both Nr_x and Syd-1 in presynaptic compartments (Muhammad et al. 2015). In the absence of Nr_x, the negative regulatory role of Spn is abolished and Syd-1 is not downregulated in axons further promoting synapse formation.

The finding that *nrx* R7s contacted wrong postsynaptic neurons was surprising, specially that synaptic tracing showed that R7s formed synapses on almost all neurons with dendritic arbors in contact with R7 axons. This goes against the idea of a molecular match-making code that specifies pre-postsynaptic connections, since Nr_x localizes in presynaptic active zones of all neurons. One concern, however, about this result is that the trans-Tango presynaptic component is comprised of the human glucagon receptor fused to the transmembrane and intracellular domains of the *Drosophila* Nr_x to localize it to the synapse (Talay et al. 2017). Expressing the Nr_x transmembrane and intracellular domains might produce artefacts in a *nrx* mutant background. This result should be complimented with activity-dependent GRASP and Brp-D3 puncta distribution analysis to confirm the formation of ectopic functional synapses.

PART | 6 AMYLOID PRECURSOR PROTEIN-LIKE

Role of APPL in R7 Targeting and
Synapse Formation

*And an APPL Side-Story: Dynamics of the APPL Proteolytic
Cleavage Products*

6.1. Contribution

I designed and generated all the fly lines in this section. I also performed all the experiments and analyzed the results myself, except for the experiment in Fig. 6.2.1.3, B which was blindly quantified by E. Jennifer Jin.

6.2. Results

6.2.1. Role of APPL in R7 targeting and synapse formation

Animals mutant of *appl* are viable and show subtle defects in learning and in the formation of mushroom body lobes. During development, APPL is expressed in photoreceptor precursor cells and is enriched in R7s in the eye imaginal discs of third instar larvae. Loss of *appl* caused 2% of R7s to terminate in the distal layer M3 instead of M6 and sensitizing the *appl* mutant

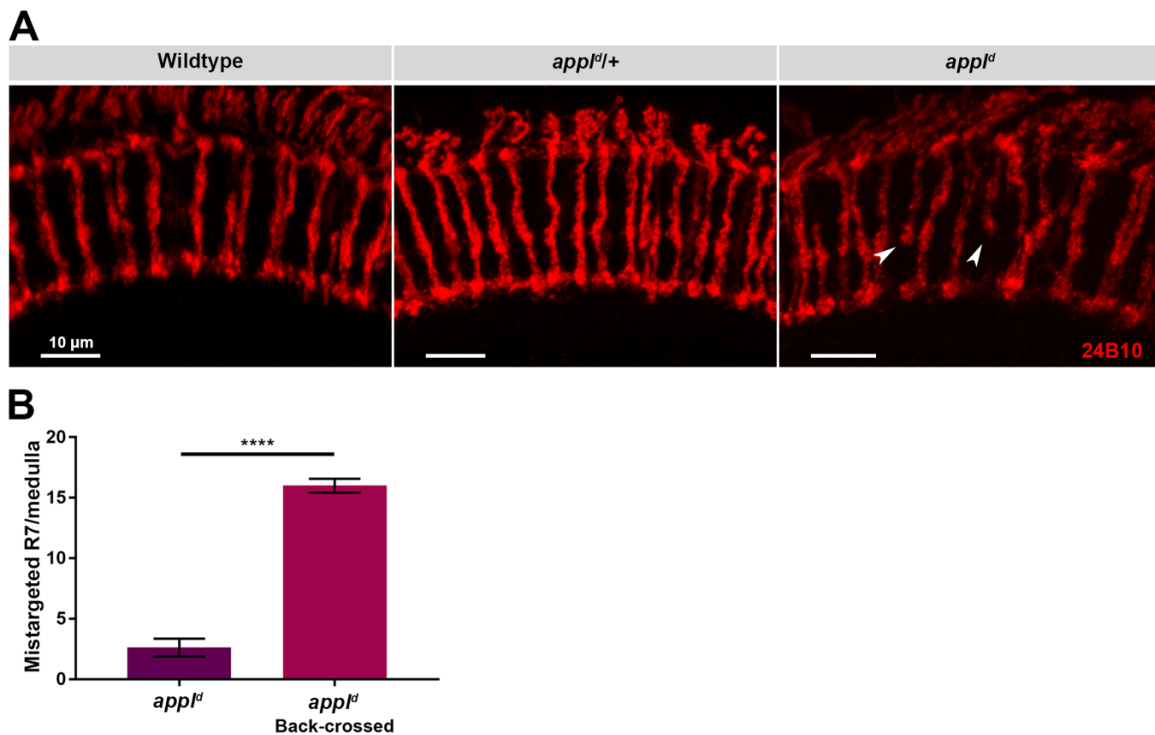


Fig. 6.2.1.1-1. R7s terminate in M3 in *appl^d* flies.

R7s of adult *appl^d* flies show a mild mistargeting defect that cause them to terminate in M3. **(A)** Representative images with photoreceptors of wildtype, animals heterozygous of *appl^d*, and animals mutant of *appl^d*. Mistargeted R7s are only found in mutant animals and marked with arrow heads. Photoreceptors are stained with anti-Chaoptin (Red), and scale bar = 10 μ m. **(B)** Quantification of the number of mistargeting R7s in the whole medulla of *appl^d*, *hsflp* mutant animals (referred to as *appl^d*). The mild mistargeting phenotype was enhanced by back-crossing and brought to the previously reported penetrance. Graph bars represent mean \pm SEM mistargeting R7s per medulla. *appl^d*: 2.62 \pm 0.73 R7, n=8 flies. Back-crossed *appl^d*: 16 \pm 0.57 R7s, n=3 flies (P<0.0001).

flies with genetic heterozygous backgrounds of mutant alleles of membrane proteins enhanced the R7 mistargeting phenotype, suggesting that APPL interacts with other membrane proteins for correct R7 targeting.

Here, I aimed at investigating the R7 mistargeting phenotype associated with *appl* loss of function and whether it has a role in synapse formation. I also tested if APPL's interaction with membrane, synaptic, and endolysosomal proteins is required to achieve correct R7 targeting.

6.2.1.1. *appl^d* R7s initially target correctly before retracting to M3

appl^d is a null mutant allele of *appl*. In the visual system of *appl^d* flies, R7s were reported to terminate in M3 with a very mild penetrance. I initially confirmed the reported R7 mistargeting phenotype in *appl^d* flies. I tested two *appl^d* lines; one contained only the mutant allele and the other was recombined to *hsflp* on the same chromosome. Both lines caused R7 mistargeting in mutant adult animals without any effect in heterozygosity (Fig. 6.2.1.1-1, A), however, the

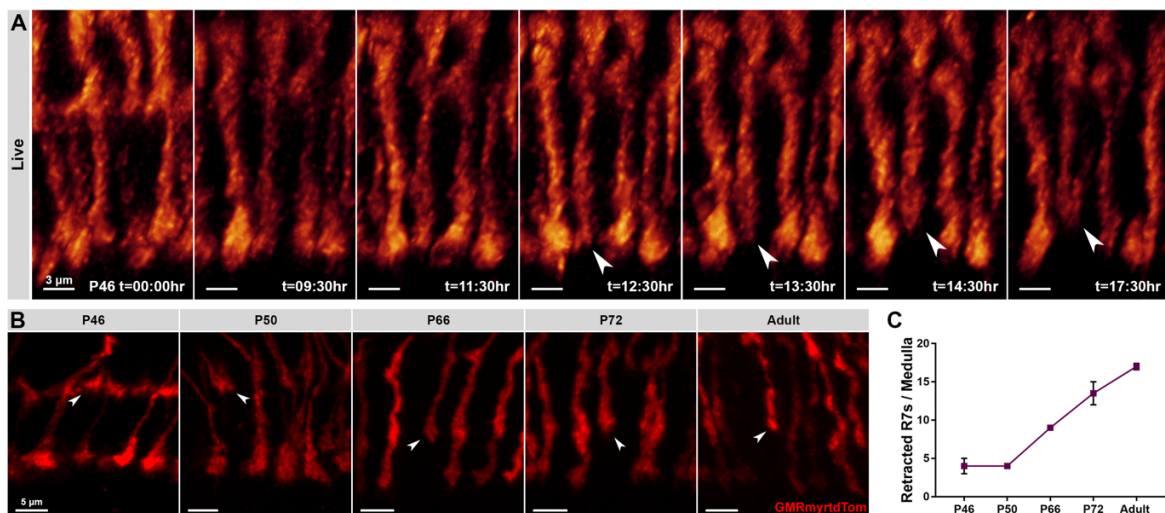


Fig. 6.2.1.1-2. *appl^d* R7s initially target correctly before they retract.

The mild R7 targeting defect in *appl^d* flies is a retraction phenotype. R7s targeting to their correct layer is not affected and then they probabilistically destabilize and retract to the layer which R8s are in. **(A)** Live imaging of *ex vivo* cultured brains of *appl^d* flies with all photoreceptors labelled with GMRmyrdTom. R7s correctly reach their target layer before they destabilize and retract. Arrow heads mark the retracting R7s. Imaging was performed with a time resolution of 30 minutes and the stage (P) in which imaging started is indicated in the first frame. Scale bar = 3 μ m. **(B)** Fixed preparations from *appl^d* flies in different developmental stages with photoreceptors labelled with GMRmyrdTom. R7s start retracting before P46 and more retractions take place with development until flies reach the adult stage. Arrow heads mark the retracted R7s, scale bar = 5 μ m. **(C)** Quantification of the retracted R7s in the stages shown in (B). Data points represent mean \pm SEM retracted R7s per medulla. P46: 4 \pm 1 R7s, n=2 flies. P50: 4 \pm 0 R7s, n=2 flies. P66: 9 R7s, n=1 fly. P72: 13.5 \pm 1.5 R7s, n=2 flies. Adult: 17 \pm 0.4 R7s, n=4 flies.

quantified R7 mistargeting phenotype was much milder compared to the previous report. *appl*-related phenotypes are sensitive to the genetic background and they are prone to accumulate suppressor genes (B. Hassan; personal communication). Therefore, I back-crossed the two lines to Canton S flies to clear the background. The R7 mistargeting phenotype was only enhanced in the flies with *appl^d* recombined to *hsflp* and reached a similar penetrance to the reported phenotype (Fig. 6.2.1.1-1, B). This line will be used in the following experiments and will be referred to as *appl^d* flies.

To understand the nature of the R7 mistargeting phenotype, I performed long term live imaging of photoreceptors in *appl^d* animals. Since *appl* is on the X chromosome and mutant flies are viable, I sorted *appl^d* 3rd instar male larvae, then I selected and staged white pupae in humid chambers until dissection. For these experiments, male animals with *hsflp* on the X chromosome were used as controls. Live imaging revealed that, as seen with many other mutants, *appl^d* R7s initially targeted correctly before they retracted to the R8 layer (Fig. 6.2.1.1-2, A). Since R7s retracted with such a subtle penetrance, live imaging was not reliable to identify when R7s destabilize from their correct layer and retract. Therefore, I used fixed preparations to quantify the progression of R7 retraction. The earliest time point was P46 and a few R7s were already retracted to the edge of the medulla, the number of retracted R7s remained constant until P50 before it gradually increased during the second half of pupal stage (Fig. 6.2.1.1-2, B-C).

6.2.1.2. *appl^d* R7s form fewer and unstable bulbous tips together with fewer synapses

To perform live imaging of R7 fast filopodial dynamics, I used the *hsflp*, recombined to *appl^d*, to generate sparse photoreceptor clones. At P60, *appl^d* R7s infrequently adopted an abnormal morphology with some axon terminals bifurcated and formed protrusions invading adjacent columns. All R7s, however, showed a bulbous tip formation and stabilization defects with bulbous tip lifetime not exceeding five minutes (Fig. 6.2.1.2, A).

Consequently, I generated sparse photoreceptor clones that expressed Brp-D3 as an active zone marker while labelling the photoreceptor membrane with CD4tdTom to test if the R7 bulbous tip dynamic defects had an effect on synapse formation. The analysis was restricted to that area of R7 axons between M3 and M6 since using *hsflp* to generate the photoreceptor clones labels R8s as well (red box in Fig. 6.2.1.2, B). As suggested in (Özel et al. 2019), failure of *appl^d* R7s to stabilize bulbous tips caused a synapse formation defect (Fig. 6.2.1.2, B-C).

6.2.1.3. Sensitizing the *appl* mutant flies with genetic heterozygous backgrounds changes the R7 retraction phenotype

APP was shown to interact with plenty of membrane and synaptic proteins in developing neurons. Additionally, the fly homologue of APP, APPL, was suggested to interact with other

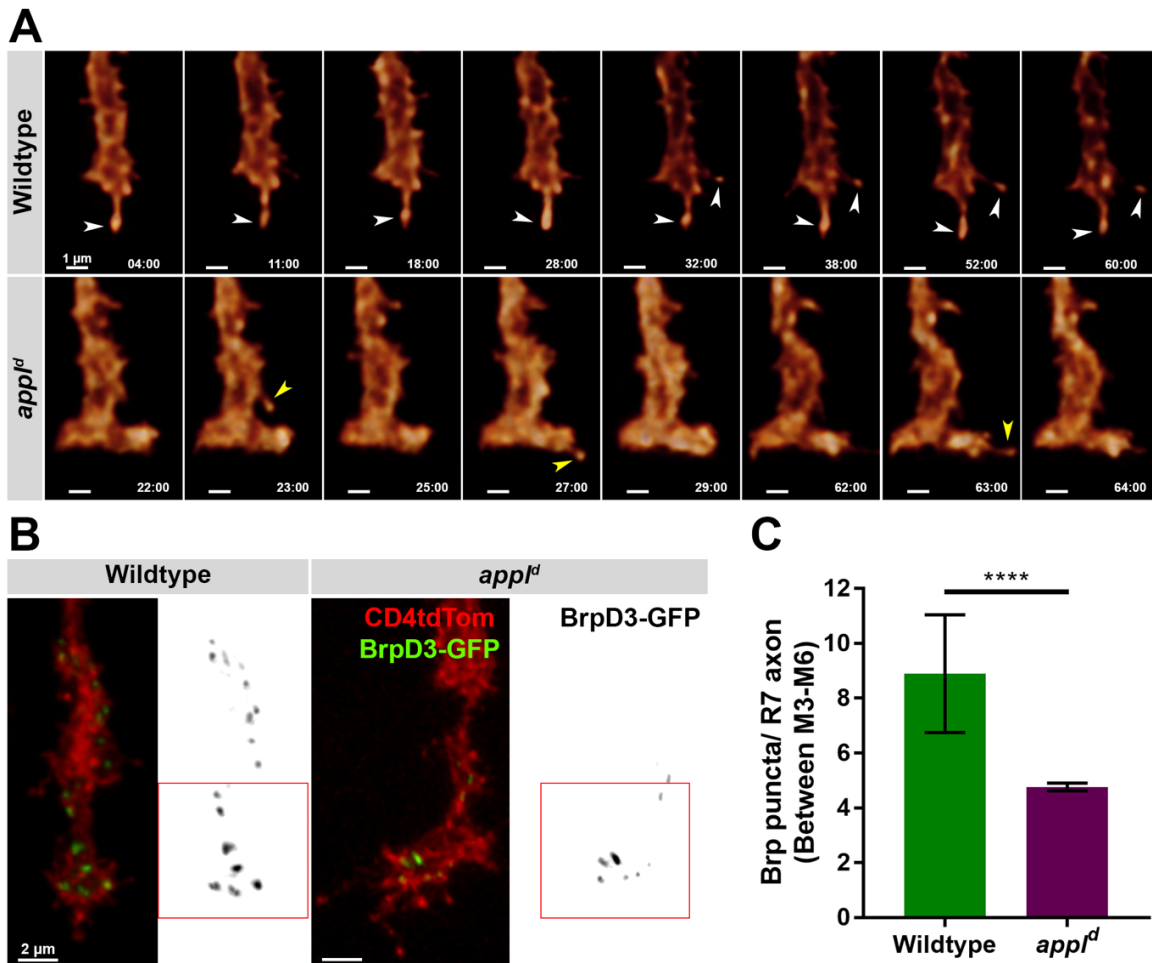


Fig. 6.2.1.2. *appI^d* R7s do not form stable bulbous tips and have a synaptic defect.

Bulbous tip formation and stabilization is affected in *appI^d* R7s which is reflected in the reduced number of synapses they form. **(A)** Live imaging of wildtype and *appI^d* R7 terminals fast dynamics at P60. Wildtype R7s form a bulbous tip that is stable for the whole duration of the 1-hour imaging window (white arrow heads), while *appI^d* R7s form fewer bulbous tips that were all transient with lifetimes not exceeding 5 minutes (yellow arrow heads). Scale bar = 1 μ m. **(B)** Representative single R7 terminals at P70 of wildtype and *appI^d* R7s, the membranes are labelled with CD4tdTom (red) and active zones are marked with Brp-D3 (green). Brp-D3 is shown in a separate panel in black for better contrast, and depicts fewer number of Brp-D3 dots in *appI^d* compared to wildtype R7s. Line marks M6. Red boxes mark the area between M3 and M6, scale bar = 2 μ m. **(C)** Quantification of Brp-D3 dots from (B), compared to wildtype, *appI^d* R7s show a significant reduction in the number of synapses formed between M3 and M6. Bars represent mean \pm SEM synapses per R7 terminal. Wildtype; 8.9 \pm 0.33 synapses, n=40 R7s. *appI^d*: 4.77 \pm 0.13, n=126 R7s (P<0.0001).

membrane proteins to facilitate correct R7 layer targeting (Mora et al. 2013). This was shown as the R7 mistargeting phenotype was enhanced in flies with heterozygous genetic backgrounds of membrane proteins and mutant of *appl*.

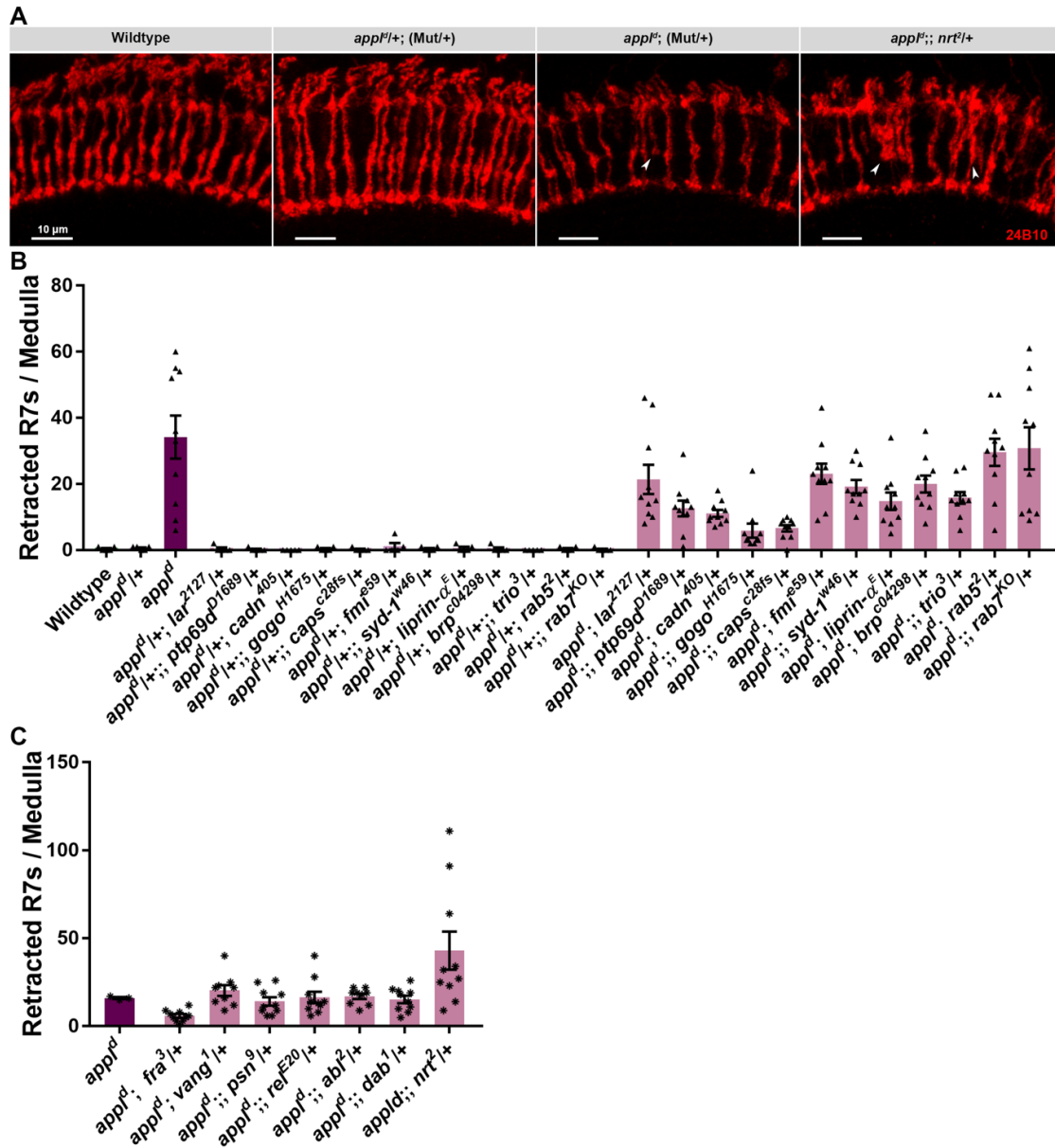


Fig. 6.2.1.3. Sensitizing the *app1d* mutant with genetic heterozygous backgrounds does not enhance the R7 retraction phenotype.

The variable R7 retraction phenotype in *app1d* flies is not altered when the mutant allele is combined with genetic heterozygous backgrounds of membrane proteins, synaptic proteins, endolysosomal proteins, and APPL-interacting proteins. **(A)** Representative photoreceptor images of wildtype, double-heterozygous flies of *app1d* and the tested genes, *app1d* mutant flies sensitized for the tested genes, and *app1d* mutant flies sensitized for *nrt*. Retracted R7s are only found in *app1d* flies (arrow heads) and sensitizing the background with *nrt* heterozygosity infrequently causes massive R7 retractions and disrupts the photoreceptor organization in the medulla (arrow heads). Photoreceptors are stained with anti-Chaoptin (Red), scale bars = 10 μ m **(B,C)** Quantification of the retracted R7s in each of the specified genotype showing the variable distribution of the number of retracted R7s only in the *app1d* mutant background but not in heterozygosity. Bars represent mean \pm SEM retracted R7s per medulla. At least 10 flies were quantified in the *app1d* mutant conditions and individual data points are plotted in each bar.

I followed a similar approach and sought to identify potential membrane, synaptic, and endolysosomal proteins that interact with APPL for R7 targeting. In a screen for potential interactors, I chose membrane proteins that were known to affect photoreceptor targeting (Lar, PTP69D, NCad, Gogo, Caps, and Fmi), synaptic proteins (Syd-1, Liprin- α , Brp, and Trio), and endolysosomal proteins (Rab5 and Rab7). The experiment was independently quantified by E.J. Jin that was blinded to the genotypes to avoid any bias interpreting the result.

Quantifying the total number of retracted R7s in each medulla showed that R7s did not retract in wildtype and in flies heterozygous of *app^d* or any of the tested genes (data not shown) or when heterozygous of both the genes with only a very few exceptions of R7 retractions in these flies (Fig. 6.2.1.3, A-B). Quantifying medullas from at least ten different flies for each condition showed that *app^d* flies either alone or sensitized for other genes exhibited a broad variability in the number of retracted R7s with none of the sensitizing genes enhanced the already-variable phenotype (Fig. 6.2.1.3, B). Only exception to that is sensitizing the *app^d* background with removing one copy of the membrane proteins Gogo and Caps, which slightly ameliorated the retraction phenotype. This was surprising since both of the proteins were not known to affect R7 targeting (Berger-Müller et al. 2013) and Caps is not expressed in R7s nor its target layer (Shinza-Kameda et al. 2006).

I then expanded the screen to sensitize the background with the membrane proteins reported to enhance the retraction phenotype (Fra and Nrt) together with a component of the immune deficiency pathway (Rel) and a component of the planar-cell-polarity complex (Vang) that were reported to interact with APPL to regulate neurite outgrowth, and other known interactors of APPL (Psn, Abl, and Dab). These results were quantified by me; hence, they were shown separately from the previous screen, I also omitted quantifying the double heterozygous animals. As before, the tested genes did not enhance the *app^d* R7 retraction phenotype, even *fra* heterozygous genetic background did not cause any effect contradicting the reported findings reported by Mora et al. (Fig. 6.2.1.3, C). Sensitizing the *app^d* background with *nrt* heterozygosity still created the wide variability seen with other mutants. In some rare occasions, however, the photoreceptor organization in the medulla was completely disrupted, with plenty of retracted R7s and several bundled columns to form clumps of photoreceptor terminals in the medulla (Fig. 6.2.1.3, A-C).

6.2.1.4. Overexpression of APPL in *app^d* flies does not rescue the R7 retraction phenotype

APPL was previously shown to be required for the mushroom body axonal outgrowth; cell autonomously for the β lobe and non-cell autonomously for the α lobe formation (Soldano et al. 2013). The described R7 retraction phenotype was analyzed in whole *app^d* animals which

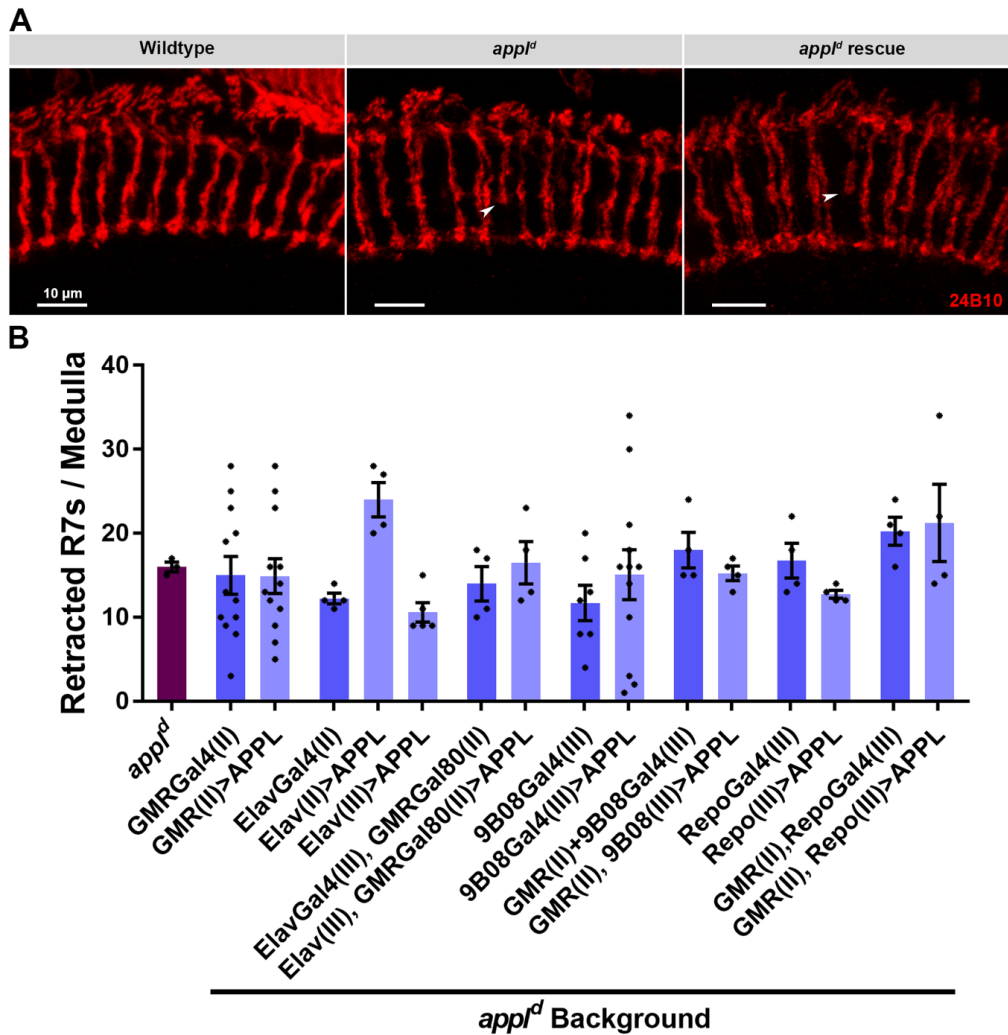


Fig. 6.2.1.4. Expression of full-length APPL does not rescue R7 retraction in *app^{ld}* flies.

Expression of full-length APPL in photoreceptors, lamina cells, all neurons, and glia in *app^{ld}* flies does not rescue the R7 retraction phenotype. **(A)** Representative images of adult photoreceptor terminals in the medulla of wildtype, *app^{ld}* flies, and *app^{ld}* flies expressing full-length APPL. The R7 retractions in *app^{ld}* are not rescued with the expression of APPL in neurons or glia in the visual system. Retracted R7s are marked with arrowheads. Photoreceptors are stained with anti-Chaoptin (red), scale bar = 10 μ m. **(B)** Quantification of the retracted R7s in the *app^{ld}* mutants and flies expressing APPL under the respective Gal4s. Bars represent mean \pm SEM retracted R7s per medulla and the individual data points are plotted in each bar.

does not provide an answer to whether such a phenotype is due to APPL's cell autonomous or non-cell autonomous function in photoreceptors.

Therefore, I expressed the full-length APPL in the photoreceptors, lamina cells, glia cells, and all neurons and combinations thereof in *app^{ld}* animals. This aimed at introducing the protein in all the cells present and terminating in the medulla throughout development. And since introducing any transgenic construct could sensitize the *app^{ld}* background and affect the R7 retraction phenotype, I used *app^{ld}* with the used Gal4(s) as control animals. Surprisingly,

overexpression of APPL did not rescue the R7 retraction phenotype irrespective of the Gal4(s) used, but rather increased the variability around the same mean number of retracted R7s (Fig. 6.4.1.4, A-B). Even more, overexpressing APPL in all neurons using the second chromosome Elav-Gal4 insert enhanced the R7 retraction phenotype compared to the respective control which was completely unexpected.

6.2.1.5. *appl* mutant alleles, other than *appl^d*, do not cause R7 retractions

In search of a Gal4 line that would rescue the R7 retraction phenotype in *appl^d* flies, I used the APPL Trojan Gal4 (APPL-TG4) which is a Gal4 insertion in the first intron of the *appl* gene. APPL-TG4 is homozygous lethal but is viable in heterozygosity over *appl^d* and lacks the distinct APPL antibody staining in the mushroom body of adult flies compared to APPL-TG4 heterozygous flies (Fig. 6.2.1.5, A). This *appl* mutant trans-heterozygous background was intended to function as an *appl*-null background in which APPL would be expressed at the right level and the spatio-temporal pattern. Surprisingly, R7s did not show any retractions in the *appl* trans-heterozygous flies without APPL expression. (Fig. 6.2.1.5, C).

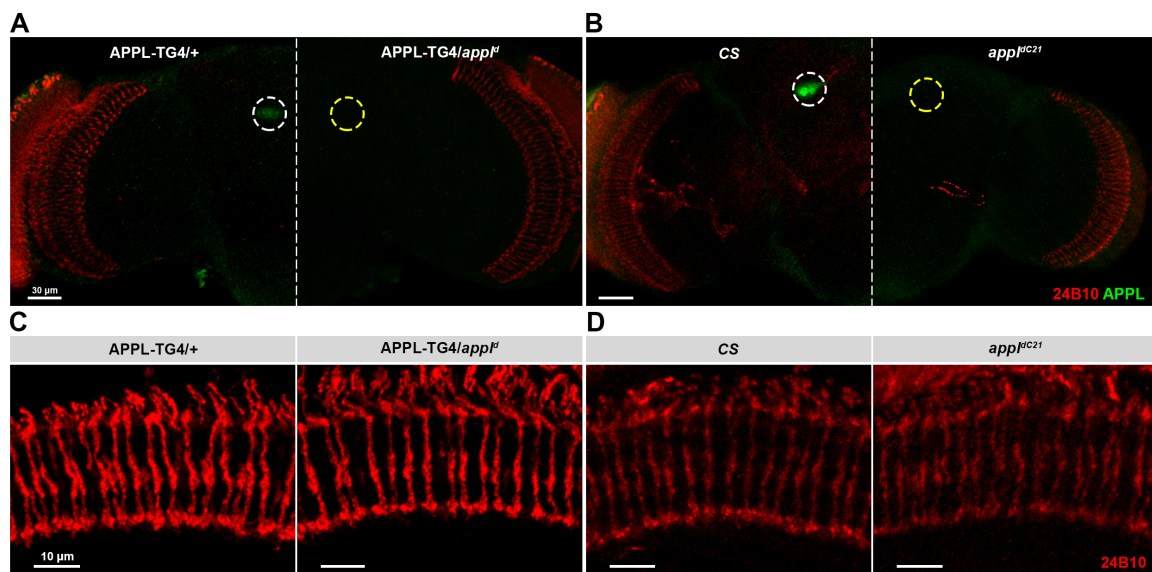


Fig. 6.2.1.5. Loss of *appl* does not cause R7 retraction.

R7 targeting is not affected in two lines mutant of *appl*, other than *appl^d*. (**A,B**) Antibody staining of APPL in *appl* trans-heterozygous mutant (A) and *appl^{dC21}* mutant flies (B) and their respective controls confirming the used flies are full mutants of *appl* as protein is not detected in the mushroom body (yellow circles) compared to the control flies (white circles). APPL (green) and photoreceptors are stained with anti-Chaoptin (red), scale bar = 30 μm. (**C,D**) Photoreceptor terminals in the medulla of the *appl* trans-heterozygous mutant (C) and *appl^{dC21}* mutant flies (D) and their controls showing correct targeting and normal organization. Photoreceptors are stained with anti-Chaoptin (red), scale bar = 10 μm.

PART | 6 APPL

To confirm this finding, I used another *appl* mutant allele (*appl^{dC21}*) which was recently generated by CRISPR-Cas9. This mutant also stained negative for APPL in the mushroom body of adult flies compared to Canton S flies as its corresponding genetic background (Fig. 6.2.1.5, B). Again, all R7s in this background terminated in M6 with no targeting defect (Fig. 6.2.1.5, D). Suggesting that the R7 retraction phenotype in *appl^d* flies is not due to loss of *appl* but rather for genetic background in the *appl^d* artificial chromosome that was generated by Luo et al. 1992.

6.2.2. *An APPL side-story: Expression pattern, dynamics of APPL's proteolytic cleavage products, and their effect on neuronal and non-neuronal tissues*

APPL is a transmembrane protein that, similar to the vertebrate APP, is exposed to proteolytic cleavage. APPL is cleaved either by Kuzbanian (Kuz), the fly homologue of α -secretase, or β -site amyloid precursor protein cleaving enzyme (BACE) to release the secreted α - or β -fragment, respectively. This is then followed by γ -secretase cleavage to release the APPL intracellular domain (AICD). Distinct functions were reported for each of the APPL proteolytic fragments that included neuronal outgrowth and survival.

Here, I aimed at characterizing APPL's expression in different neuronal tissues during development. And I also studied the dynamics of APPL's proteolytic cleavage products in developing photoreceptors.

6.2.2.1. APPL is a neuron-specific protein in flies

Expression of APPL in developing flies was reported to be restricted to the nervous system. To confirm this, I used the APPL-TG4 to drive the expression of CD4tdGFP to label the membranes of neurons that produce APPL. In the same fly I also labelled the nervous system by using the glia-specific driver Repo-LexA to drive the expression of CD4tdTom.

At the gross morphological level, APPL was mostly expressed in the nervous system as the APPL producing neurons overlapped with glia in the nervous system, with the exception that it was also expressed in the hind-gut and the anal pads in 3rd instar larva as well. In pupal stages, APPL expression gradually decreased in extra-neuronal tissues and became restricted to the nervous system starting P24 onwards until the end of development (Fig. 6.2.2.1-1).

I then used the same fly to look at APPL's expression in different regions of the nervous system. On top of labelling APPL-expressing neurons and glia, I also stained for the neuronal transcription factor Elav to label the cell bodies of neurons and for the endogenously expressed APPL to confirm the specificity of APPL-TG4. Maximum intensity projection images of 3rd instar and newly-hatched adult fly brains and ventral nerve cords (VNC) showed that APPL-TG4 labelled neurons and their projections in all the neuropils while neuronal cell bodies and glia were, as expected, located in the cortical regions (Fig. 6.2.2.1-2).

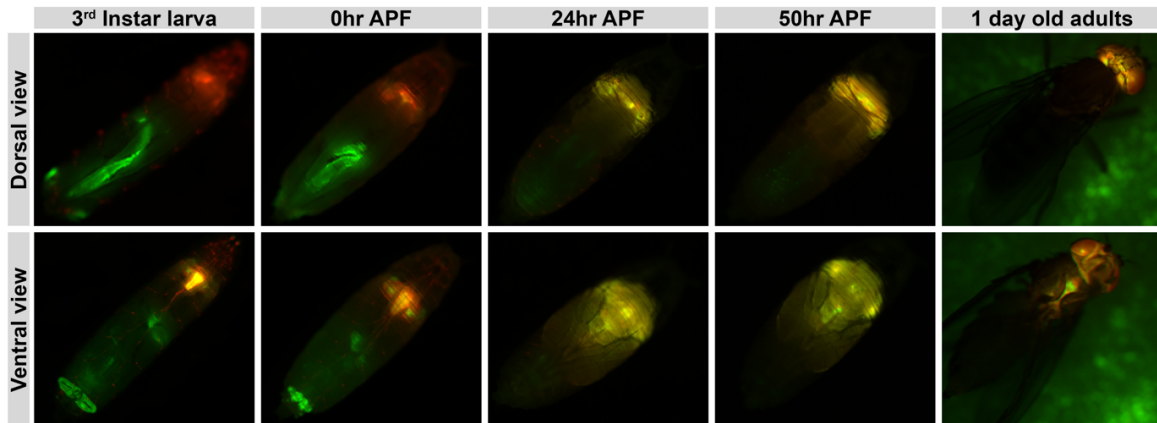


Fig. 6.2.2.1-1. APPL is expressed in the nervous system of developing and adult flies.

APPL expression pattern in intact animals at different developmental and adult stages shows its localization in the nervous system. APPL-producing cells (green) overlap with glia (red) in the nervous system throughout development except for the hind-gut and anal pads that produce APPL in larval and early pupal stages. Images of the dorsal and the ventral sides of intact animals are shown with their anterior ends in the top right and posterior ends in the bottom left of each panel.

To gain more details about APPL's expression, I acquired zoomed-in images of different regions of the brains and the VNCs (boxed regions in Fig. 6.2.2.1-2). The 3rd instar eye imaginal disc showed APPL expression in all photoreceptors (Fig. 6.2.2.1-2, A). APPL-TG4 labelling of APPL-expressing neurons perfectly matched the antibody staining of the endogenous protein, indicating the driver's specificity. Interestingly, APPL expression level was not uniform among all the photoreceptors of the same ommatidium. The mushroom body peduncle of the 3rd instar larval brain showed strong labelling of neurons expressing APPL, the mushroom body neuronal projections formed bundles wrapped with glia that did not show any APPL expression. The mushroom body peduncle region is devoid of neuronal cell bodies which explains the absence of Elav staining (Fig. 6.2.2.1-2, C). The cortical region of the 3rd instar larval VNC showed strong antibody staining of APPL concentrated in the cell bodies of motor neurons (arrow heads in Fig. 6.2.2.1-2, E).

On the other hand, the Kenyon cell bodies of the adult brain were labelled with APPL-TG4 and stained for APPL as well (Fig. 6.2.2.1-2, B). Surprisingly, a glia cell was found to contain APPL, this cell was relatively large compared to other glia cells which suggested it potentially engulfed other APPL-expressing neurons that is detected by antibody staining (yellow arrow head in Fig. 6.2.2.1-2, B). The adult mushroom body lobes expressed high levels of APPL which was not present in the surrounding glia cells (Fig. 6.2.2.1-2, D). Finally, in the adult VNC, neurons were labelled by APPL-TG4 and not all of them showed APPL staining in their cell bodies as opposed to the case in the 3rd instar VNC (Fig. 6.2.2.1-2, F).

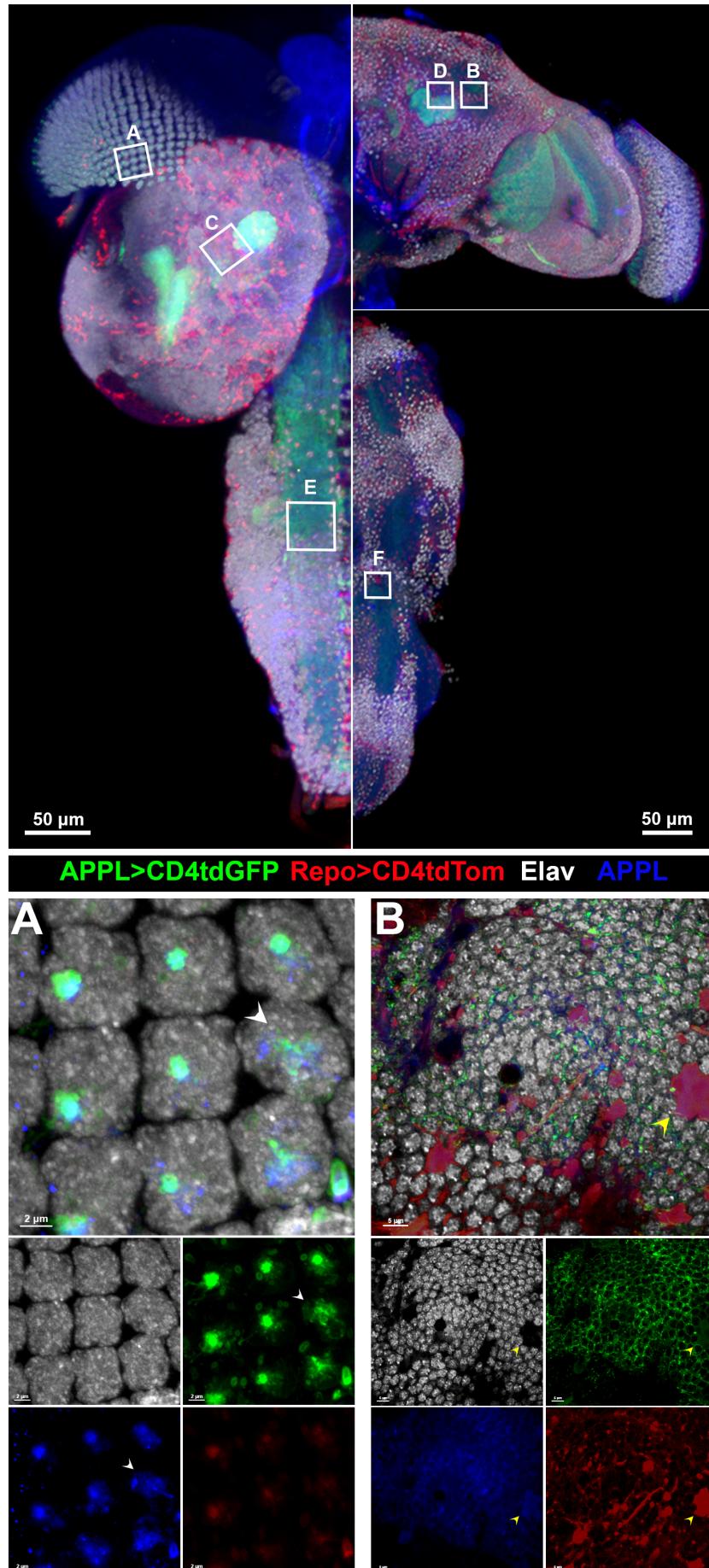


Fig. 6.2.2.1-2. (Figure continues in the next page)

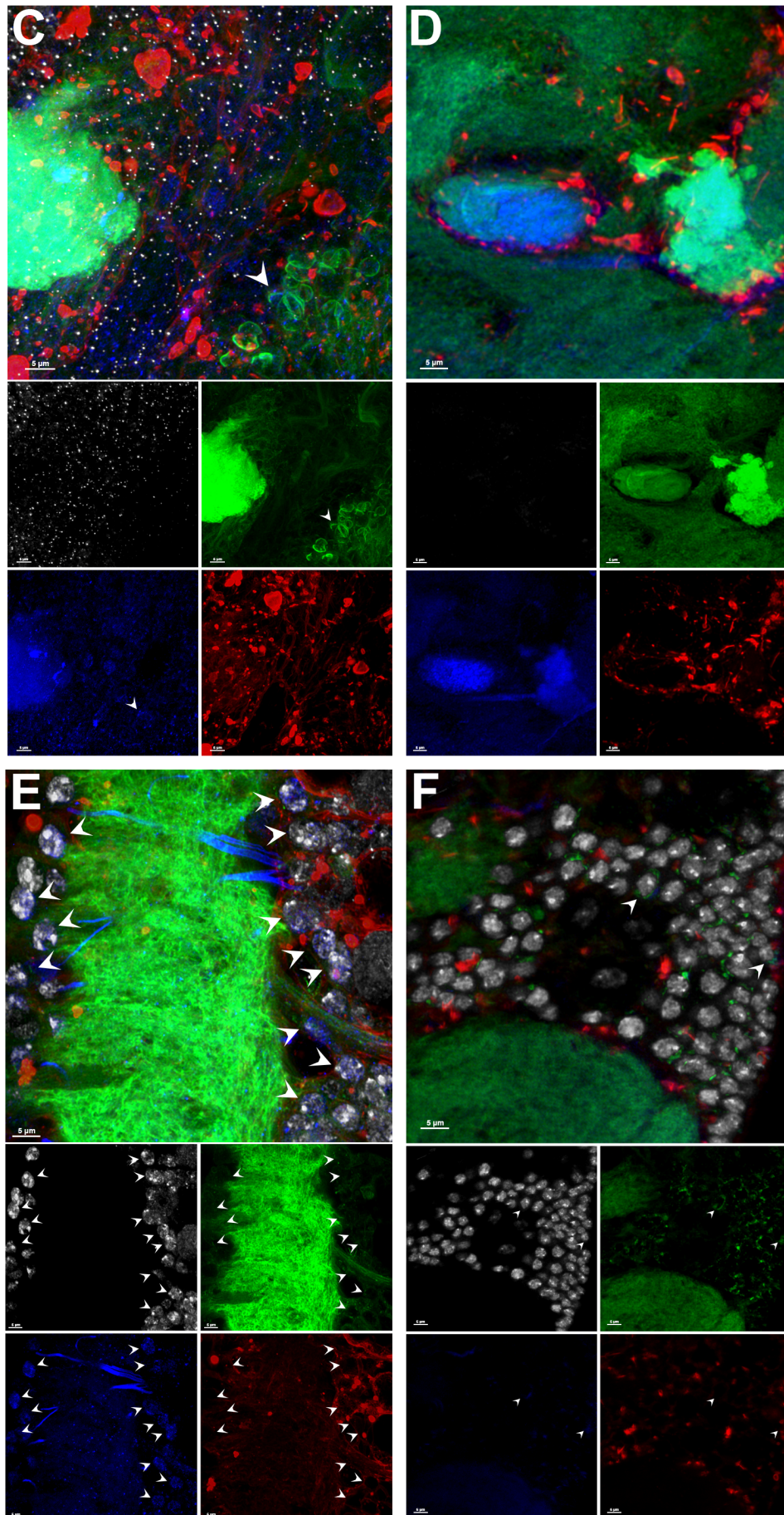


Fig. 6.2.2.1-2. APPL is a neuron-specific protein. (Figure legend in the next page)

PART | 6 APPL

APPL is produced in neurons in the fly nervous system. Maximum intensity projection images of 3rd instar larval (left) and adult (right) brain and VNC. APPL-producing cells are labelled with APPL-TG4 driving CD4tdGFP (green), glial cells are labelled with CD4tdTom (red), neuronal cell bodies are labelled with anti-Elav staining (grey), and endogenous APPL is stained with anti-APPL (blue). Zoom-in pictures of different regions in the following panels are marked with boxes. Scale bar = 50 μm . **(A)** Zoom-in pictures of the eye-imaginal disc showing organized ommatidia with photoreceptor precursor neurons labelled with Elav with only neurons, not glia, produce APPL and the APPL antibody staining overlaps with the APPL-TG4 expression (arrow head). Scale bar = 2 μm . **(B)** Cell bodies of Kenyon cells in the adult brain showing APPL expression in neurons and devoid of wrapping glia processes. APPL antibody staining is not uniform in all the neurons while all are express APPL-TG4. Exceptionally, APPL is found in an enlarged glial cell possibly because it engulfed an APPL-producing neuron (yellow arrow head). Scale bar = 5 μm . **(C)** Kenyon cells dendritic projections show strong expression of APPL that is strictly present in neurons and neuronal projections but completely absent in glia (arrow heads). Scale bar = 5 μm . **(D)** Mushroom body lobe of adult brains shows the distinct strong APPL expression that localizes to neuronal axons and not in the surrounding glia cells. Scale bar = 5 μm . **(E)** 3rd instar larval VNC with strong, localized APPL expression in the neuronal cell bodies in the VNC cortex (arrow heads). The neuropil is occupied by axons of APPL-producing cells with APPL concentrated in neuronal cell bodies. As before, APPL is not produced in glial cells. Scale bar = 5 μm . **(F)** In the adult VNC, APPL is expressed at a lower level compared to its level in larval VNC. Antibody staining is found in sparse cell bodies in the cortex whose projections are in the neuropil (arrow heads). APPL is also not found in glial cells. Scale bar = 5 μm .

Taken together, APPL was confirmed to be neuron-specific and is a pan-neuronal protein in developmental and adult stages. APPL-TG4 expression reflected the pattern of APPL antibody staining in 3rd instar larvae, but not in the adult brain. One explanation to this discrepancy could be that APPL is still produced pan-neuronally in the adult brain, the full-length protein is constantly cleaved releasing the AICD that is directly degraded and secreting the extracellular fragments. APPL-TG4 activity is not affected in these neurons while the anti-APPL antibody will not detect the endogenous APPL in such neurons since it was raised against the AICD.

6.2.2.2. APPL is proteolytically cleaved to release the secreted fragments to glia

APPL is cleaved by different secretases to produce the α - and β - secreted fragments (sAPPL) and the AICD. These different fragments are produced, trafficked and processed differentially during different stages of neurons development. Here, I used a double fluorophore-tagged APPL transgenic construct (APPL-DT) that is tagged at the extracellular N-terminus with mCherry and with GFP at the C-terminus to study the dynamics and localization of sAPPL and the AICD during different developmental and adult stages of photoreceptors.

PART | 6 APPL

Expression of APPL-DT using the photoreceptor driver GMR-Gal4 did not cause any developmental or targeting defects (data not shown). In developing photoreceptors, full-length APPL-DT was never detected but sAPPL and AICD were rather cleaved and localized to different compartments. AICD was strongly concentrated in the cell bodies and axon terminals of photoreceptors at P20, its level in axon terminals gradually diminished until almost undetected in newly-hatched adults before it increased again with age and accumulated in terminals of 7-day-old adults. sAPPL, however, was not localized inside photoreceptors but was always in the region surrounding photoreceptor axons and terminals as early as P20. As pupal development progressed, sAPPL levels kept increasing in the cortical region of the medulla and even reached the inner chiasma region between the proximal medulla and the lobula and lobula plate by P70. Interestingly, in newly-hatched adults, sAPPL was found wrapping the entire brain cortical region and the central brain, a pattern that was maintained with age (Fig. 6.2.2.2-1).

To find if other neuronal drivers also cause a similar sAPPL pattern in the brain cortex, I expressed APPL-DT using the pan-neuronal driver Elav-Gal4 and in a subset of R7s using the late driver Rh3-Gal4. Expressing APPL-DT in all neurons cause sAPPL accumulation in the brain cortex similar to expressing it using GMR-Gal4. However, using Rh3-Gal4 caused small accumulations of sAPPL in the cortical region primarily clustered around the dorsal part of the medulla cortex, these accumulations increased and spread to cover a larger area as the flies aged (Fig. 6.2.2.2-2, A). Surprisingly, using the R1-6-specific late driver Rh1-Gal4 did not cause any detectable sAPPL accumulations in cortices of adult brains even 14 days after hatching (data not shown). This suggested that sAPPL needed to be released by neurons whose axons are in contact with the cortex region in order to spread and cover the entire brain cortex. It was not possible to identify if the sAPPL cortical accumulations were of the α - or β -secreted fragments for the lack of the genetic tools. Expressing *kuz* and *bace* RNAis together in photoreceptors was not sufficient to block APPL-DT cleavage and sAPPL release (Fig. 6.2.2.2-2, B), this prevented investigating the dynamics of the α - and β -sAPPL separately.

To understand how sAPPL spreads to cover the entire brain cortical region when APPL-DT is expressed in photoreceptors, I performed live imaging of a developing brain using a resonant-scanner confocal microscope. For this experiment, I chose to start imaging at P24 with a time-resolution of 20 minutes to cover the initial phase of sAPPL spreading before it accumulated in the medulla cortex. Maximum intensity projection images of the developing brain showed that at P24 already, the cortical region surrounding the optic lobe (edge marked by the dashed line in Fig. 6.2.2.2-3) was full of sAPPL, which was also found sparsely in the cortex surrounding the central brain. On the other hand, the AICD was restricted to the cell bodies and was never released from photoreceptors. With time, more sAPPL moved away from the optic lobe towards the central brain (exemplified by the dashed circle in Fig. 6.2.2.2-3) than

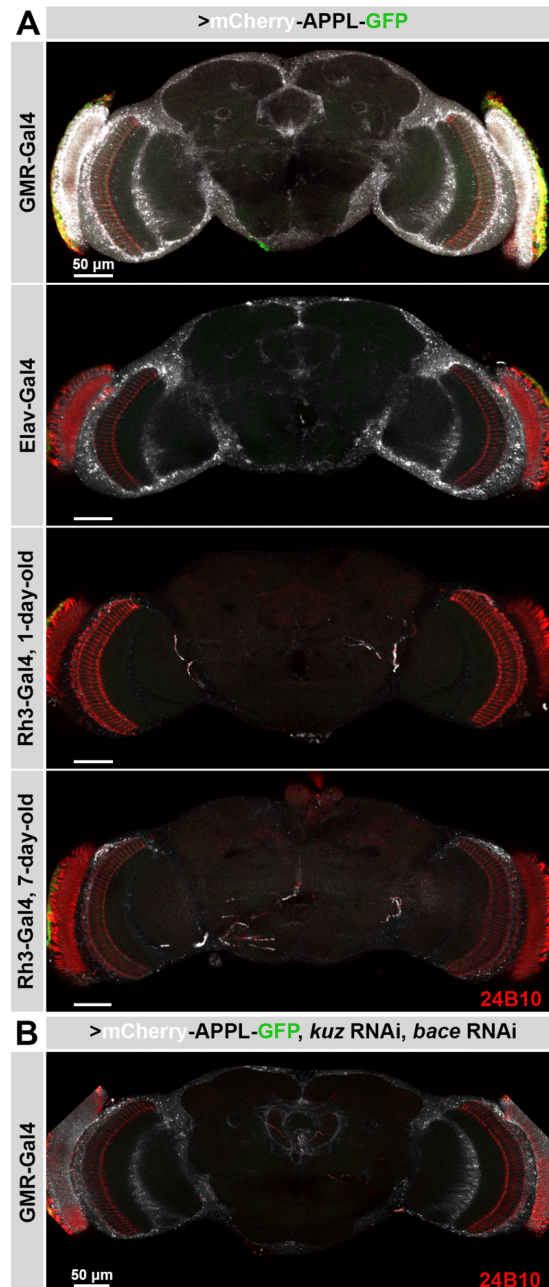


Fig. 6.2.2.2-2. sAPPL covers brain cortices when APPL-DT is expressed in different neuronal tissues.

Expression of APPL-DT using different drivers causes sAPPL to cover the cortical areas of adult brains. The full pattern is achieved in newly-hatched flies with early developmental drivers while the expansion is gradual with late drivers. sAPPL (grey), AICD (green), and photoreceptors stained with anti-Chaoptin (red). Scale bar = 50 μm. **(A)** 3 μm sections of adult brains showing the sAPPL pattern when APPL-DT is expressed in photoreceptors using GMR-Gal4, pan-neuronally using Elav-gal4, and in a subset of R7s using the late Rh3-Gal4 driver. sAPPL covered the entire brain cortex in newly-hatched flies in the case of GMR-Gal4 and Elav-Gal4 while it gradually increased to cover the cortex region of the optic lobe with aging in the case of Rh3-Gal4. **(B)** Using *kuz* and *bace* RNAi is not sufficient to block APPL proteolytic cleavage in photoreceptor and sAPPL formed its usual pattern in the brain cortex.

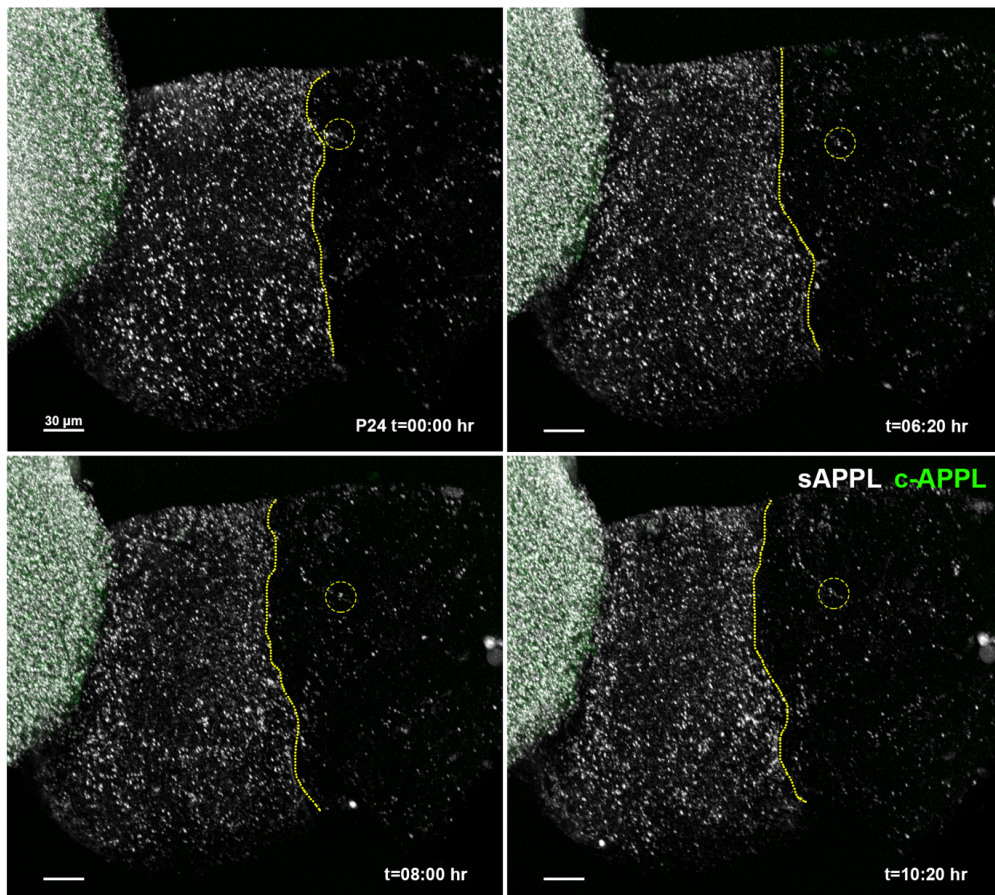


Fig. 6.2.2.2-3. sAPPL gradually migrates away from photoreceptors in the optic lobe towards the central brain.

Live imaging of the sAPPL dynamics when APPL-DT is expressed in photoreceptors. sAPPL concentrates in the cortical region of the optic lobe (edges marked with a dashed line) with less dense accumulations around the central brain. sAPPL primarily moves away from the optic lobe and travels towards the central brain (circled dots) with some compartments moving towards the optic lobes. Imaging was performed with a time resolution of 30 minutes and the stage (P) in which imaging started is indicated in the first frame. sAPPL (grey), AICD (green), scale bar = 20 μm .

the other direction. This suggested that sAPPL release from photoreceptors and migration to cover the brain cortex is a gradual dynamic process.

Based on the previous results, sAPPL spreading to cover the brain cortex was most-likely a result of it being taken up by other migratory cells. The brain cortex is packed with neuronal cell bodies and different glia sub-types. In order to find where sAPPL localizes after release from neurons, I expressed APPL-DT in photoreceptors, labelled the membranes of glia with CD4tdGFP, and Elav antibody to mark the cell bodies of the neurons. Since GFP-tagged AICD was restricted to photoreceptors and its level was very low in newly-hatched flies, it was possible to use CD4tdGFP to label glia. As shown before, sAPPL covered the entire adult brain cortex which, as expected, overlapped with the glia and the neuronal cell bodies (Fig. 6.2.2.4,

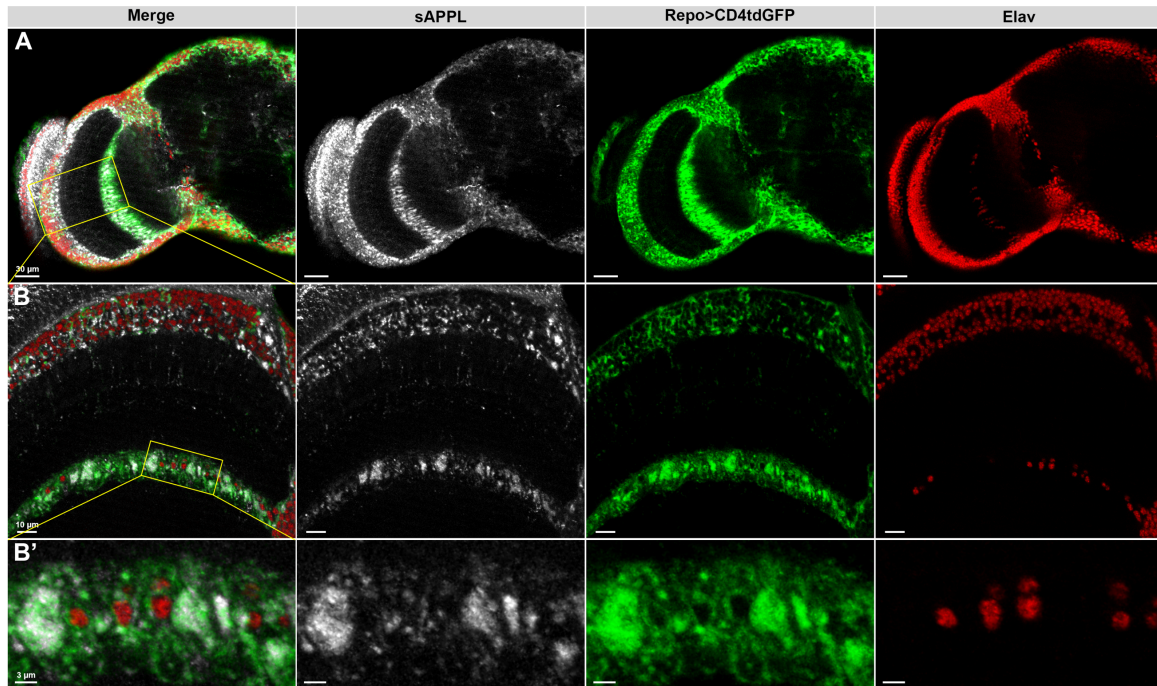


Fig. 6.2.2.2-4. sAPPL is released from neurons and picked up by glia.

Expression of APPL-DT in photoreceptors releases sAPPL that is taken up by glia and spreads with it to cover the entire cortex of adult brains. sAPPL (grey), glia (green), neuronal cell bodies stained with anti-Elav (red). (A) Overview of sAPPL localization in the adult brain as it covers the cortex where cortical glia and neuronal cell bodies are. Scale bar = 30 μm . (B) Higher magnification of the optic lobe showing sAPPL accumulating in the medulla cortex and the inner chiasm that are occupied by neuronal cell bodies and glia cells. Scale bar = 10 μm . (C) Higher magnification of the inner chiasm region that is predominantly composed of glia with the presence of a few neuronal cell bodies. sAPPL localizes in glia cells and is completely devoid of neuronal cell bodies. Scale bar = 3 μm .

A). Higher magnification images showed that sAPPL localized with glia but not with neurons (Fig. 6.2.2.4, B-B'). This was clearly seen in the inner chiasma that is occupied with glia cells and contained only a few neuronal cell bodies, sAPPL was completely devoid of the regions where neuronal cell bodies were while highly overlapping with glia.

Taken together, APPL was found to be expressed in neurons before it underwent proteolytic cleavage to release the sAPPL and the AICD which adopt different dynamics and localization within neurons. While AICD remained localized inside neurons, sAPPL was released from neurons and picked up by glia in the brain cortex before it gradually expanded to cover the entire brain.

6.2.2.3. APPL expression in neurons has cell autonomous and non-cell autonomous effects on endolysosomal trafficking

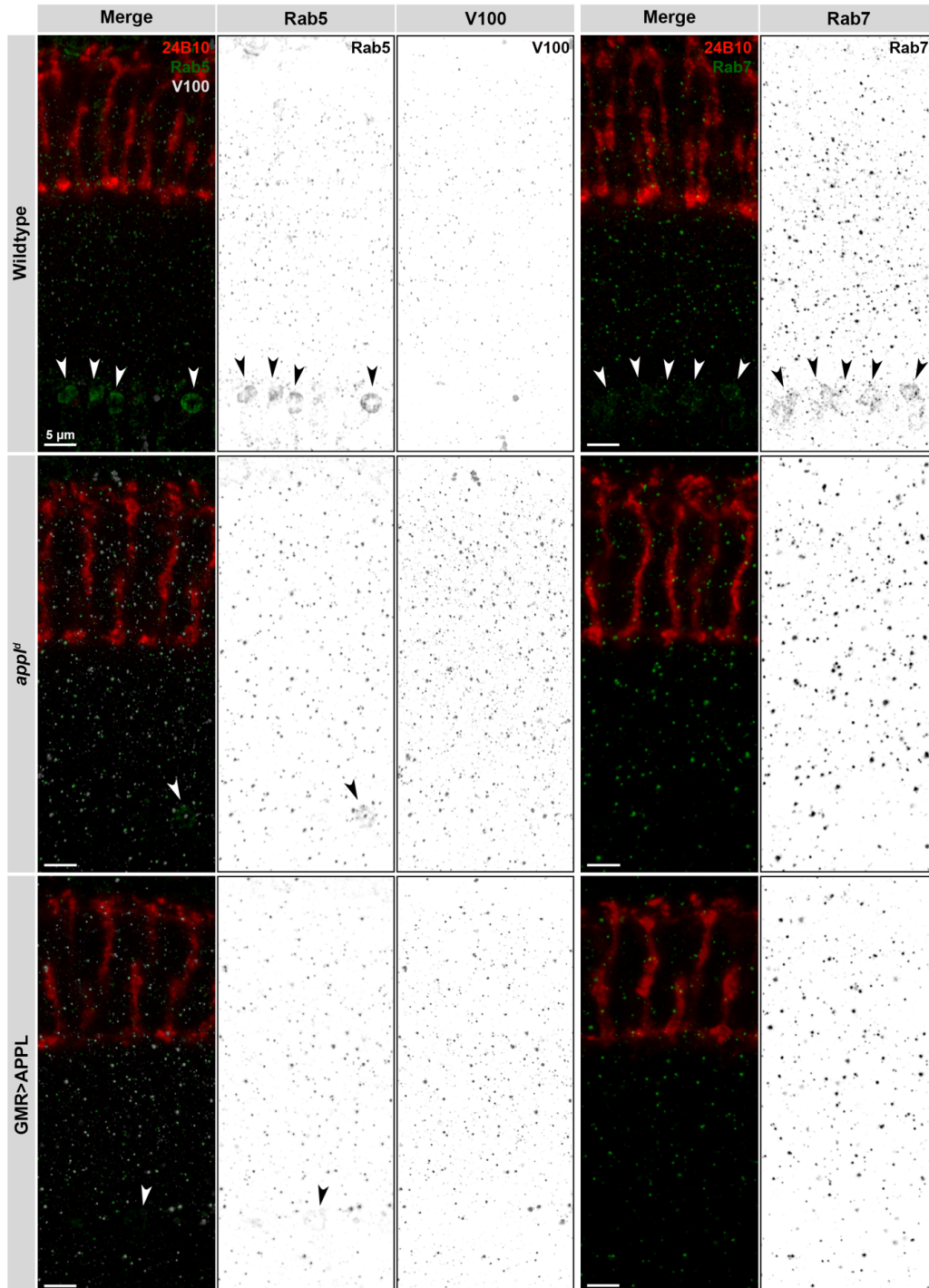


Fig. 6.2.2.3-1. APPL overexpression in photoreceptors and loss of function affects endolysosomal trafficking in inner chiasm glia.

The inner chiasm of adult brains is predominantly occupied by glia where sAPPL from neurons accumulate. Glia in the chiasm of wildtype brains show strong labelling of early endosomes (stained with anti-Rab5, left panel, green) and late endosomes (stained with anti-Rab7, right panel, green) with no accumulation of acidified compartments (stained with anti-V100, right panel, grey). The chiasm glia in *app^Δ* flies and flies overexpressing full-length APPL in photoreceptors show a severe reduction of early endosomes and a complete loss of late endosomes in both the cases (arrow heads). Acidified compartments do not show any noticeable changes. Images are of 2 μ m sections with photoreceptors visualized with anti-Chaoptin staining (red), scale bar = 5 μ m.

APPL shares the same functional domain as its vertebrate homologues, including the conserved YENPTY endocytic domain in the AICD that regulates Clathrin-mediated endocytosis. With APPL being a neuron-specific protein that is cleaved into an intracellular domain and a secreted fragment that is taken up by glia, I sought to test APPL effect on endolysosomal trafficking in neurons and glia; as a non-comprehensive test, I tested APPL's effect on Rab5 that marks early endosomes, Rab7 that marks late endosomes, and V100 that marks acidified compartments.

Therefore, I used brains of newly-hatched adult flies that were wildtype, mutant of *appl*, and overexpressing APPL in photoreceptors. All the brains were immobilized on charged plates and were stained with the same antibody solutions and imaged using the same confocal parameters.

In wildtype brains, the inner-chiasm region is dominated by glia, as shown before, that had large accumulations of rab5⁺ and Rab7⁺ compartments with few acidified compartments in that region (arrow heads in Fig. 6.2.2.3-1). Interestingly, flies mutant of *appl* and those that overexpressed APPL in photoreceptors showed a drastic reduction of Rab5⁺ compartments while Rab7⁺ compartments were completely abolished in inner-chiasma glia. The change in V100⁺ compartments was not visually discernable, nevertheless (Fig. 6.2.2.3-1).

To quantify the number and volume changes in the compartments in such a complex field (Fig. 6.2.2.3-2, A), I used the spot generation function of Imaris to get unbiased, uniform results across the three genotypes. For the compartments inside photoreceptors, I generated a surface to mark photoreceptors using the photoreceptor membrane channel (stained by anti-Chaoptin), then eliminated all the signal outside of the surface area, and finally generated spots for the remaining compartments inside photoreceptors (process summarized in Fig. 6.2.2.3-2, B-B'). For the compartments in the proximal medulla between photoreceptors and inner-chiasma glia, I assigned regions of interest (ROI) with a fixed size in all the brains and then generated spots for the compartments within these pre-defined regions (Process summarized in Fig. 6.2.2.3-2, C-C').

Inside photoreceptors, the numbers of all the three compartments did not show any significant changes among the different genotypes, except for Rab5⁺ compartments that slightly decreased upon APPL overexpression (Fig. 6.2.2.3-2, D). However, the volume of the compartments changed significantly in the three states; rab5⁺ and V100⁺ compartments were smaller in brains mutant of *appl* and upon APPL overexpression in photoreceptors compared to wildtype ones, while Rab7⁺ compartments were larger (Fig. 6.2.2.3-2, F). On the other hand, the compartments in the ROIs also showed changes in number and volume. The ROIs contained fewer and smaller Rab5⁺ compartments in both the *appl* mutant brains and with APPL overexpression in photoreceptors. The number of Rab7⁺ and V100⁺ compartments,

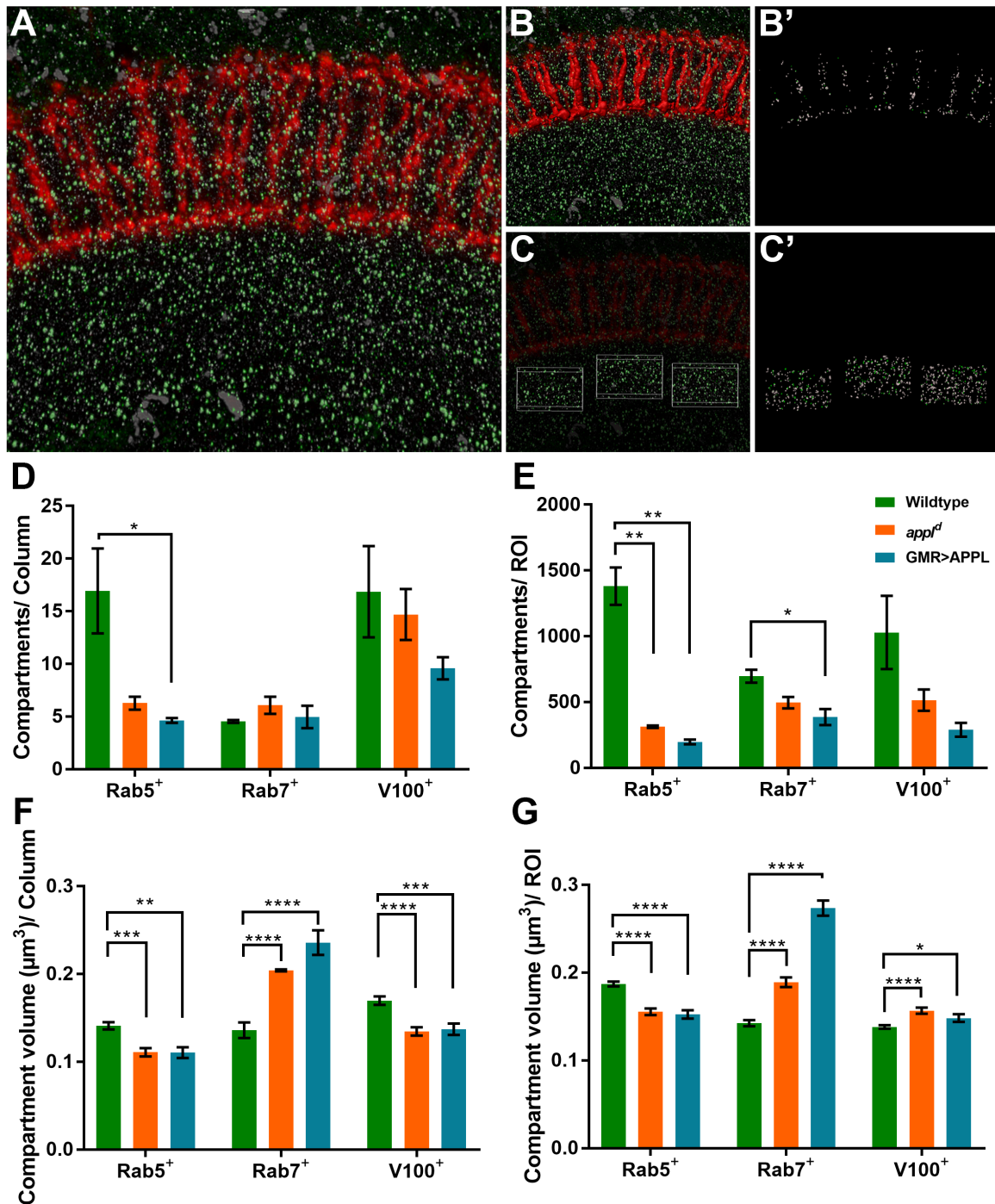


Fig. 6.2.2.3-2. APPL overexpression in photoreceptors and loss of function affect endolysosomal trafficking in photoreceptors and medulla neurons.

Early, late, and acidified compartments are affected in photoreceptors upon *appl* loss of function and overexpression. These compartments are also affected in axons and terminals of other medulla neurons in the same conditions. **(A)** Example sections of imaging data that are processed for automatic quantification. **(B,B')** Processing of compartments in photoreceptors: Surface was generated using the Chaoptin channel (B) and the signal was eliminated outside the defined surface (B'). Automatic spots were generated and their number and volume were automatically quantified.

(Figure legend continues on the next page)

(C,C') Processing of compartments outside of photoreceptors in axons and terminals of medulla neurons: Three regions of interest (ROI) with equal sizes were defined per brain and spots were automatically generated within the ROIs and quantified. **(D)** Quantification of the number of compartments within photoreceptors. Graph represents mean±SEM compartments per photoreceptor column. Number of Rab7⁺ compartments; Wildtype: 4.53±0.13 compartments. *app^{fl}*: 6.07±0.81 compartments, (P=0.1347). GMR>APPL: 4.97±1.05 compartments, (P=0.7041). Number of Rab5⁺ compartments; Wildtype: 16.94±4.03 compartments. *app^{fl}*: 6.27±0.61 compartments, (P=0.0591). GMR>APPL: 4.62±0.23 compartments, (P=0.0381). Number of V100⁺ compartments; Wildtype: 16.86±4.33 compartments. *app^{fl}*: 14.7±2.42 compartments, (P=0.6854). GMR>APPL: 9.58±1.05 compartments, (P=0.1783). **(E)** Quantification of the number of compartments in the axons and terminals of medulla neurons. Graph represents mean±SEM compartments per photoreceptor column. Number of Rab7⁺ compartments; Wildtype: 697±49 compartments. *app^{fl}*: 495±43.71 compartments, (P=0.0581). GMR>APPL: 386.7±61.2 compartments (P=0.0377). Number of Rab5⁺ compartments; Wildtype: 1381±141.3 compartments, *app^{fl}*: 313,3±9.02 compartments, (P=0.0017). GMR>APPL: 197.7±17.9 compartments, (P=0.0011). Number of V100⁺ compartments; Wildtype: 1029±278 compartments. *app^{fl}*: 514.7±80.83 compartments, (P=0.1501). GMR>APPL: 290.3±2.64 compartments, (P=0.0593). **(F)** Quantification of the volume of compartments within photoreceptors. Graph represents mean±SEM μm^3 . Volume of Rab7⁺ compartments; Wildtype: 0.136±0.0088 μm^3 , n=327 compartments. *app^{fl}*: 0.2043±0.0118 μm^3 , n=401 compartments, (P<0.0001). GMR>APPL: 0.2359±0.0139 μm^3 , n=328 compartments, (P<0.0001). Volume of Rab5⁺ compartments; Wildtype: 0.141±0.0042 μm^3 , n=1118 compartments. *app^{fl}*: 0.1109±0.0047 μm^3 , n=329 compartments, (P=0.0002). GMR>APPL: 0.1105±0.0062 μm^3 , n=215 compartments, (P=0.0022). Volume of V100⁺ compartments; Wildtype: 0.1698±0.0049 μm^3 , n=1113 compartments. *app^{fl}*: 0.1346±0.0048 μm^3 , n=768 compartments, (P<0.0001). GMR>APPL: 0.1372±0.0064 μm^3 , n=447 compartments, (P=0.0002). **(G)** Quantification of the volume of compartments in the axons and terminals of medulla neurons. Graph represents mean±SEM μm^3 . Volume of Rab7⁺ compartments; Wildtype: 0.1424±0.0035 μm^3 , n=1740 compartments. *app^{fl}*: 0.1891±0.0055 μm^3 , n=1488 compartments, (P<0.0001). GMR>APPL: 0.2734±0.0086 μm^3 , n=1160 compartments, (P<0.0001). Volume of Rab5⁺ compartments; Wildtype: 0.1871±0.0027 μm^3 , n=4142 compartments. *app^{fl}*: 0.1553±0.0037 μm^3 , n=940 compartments, (P<0.0001). GMR>APPL: 0.1523±0.0047 μm^3 , n=593 compartments, (P<0.0001). Volume of V100⁺ compartments; Wildtype: 0.1382±0.0019 μm^3 , n=3086 compartments. *app^{fl}*: 0.1566±0.0035 μm^3 , n=1544 compartments (P<0.0001). GMR>APPL: 0.1482±0.0043 μm^3 , n=871 compartments, (P=0.222).

however, was not significantly altered, yet both showed an increase in volume in the aforementioned states of APPL compared to wildtype brains (Fig. 6.2.2.3-2, E-G).

It is noteworthy to mention that all the brains of the three conditions were exposed to the same experimental conditions and images were acquired and processed similarly, this excluded any influence of technical variability on the results. Another point to clarify, which was surprising, is that the changes seen in the ROIs upon APPL overexpression in photoreceptors were quantified from axons and terminals of wildtype cells whose cell bodies were surrounded by

PART | 6 APPL

glia that took up more sAPPL as it was released from the photoreceptors. Finally, loss or gain of APPL caused the same trend, with a different extent, in the number and volume the tested endolysosomal compartments. Suggesting that both APPL's expression and level play a role in trafficking cell autonomously and non-cell autonomously.

6.2.2.4. Neuronal sAPPL accumulates in the nephrocytes

APPL function in flies has only been studied in neurons where it is known to be expressed. As demonstrated before, APPL is cleaved and its secreted fragments were taken up by glia where it affected endolysosomal trafficking.

The expression APPL-DT in photoreceptors did not only cause sAPPL to accumulate in glia, but it was also detected in the dorsal abdomen as early as 2nd instar larval stage until adult flies hatch. sAPPL in the abdomen was concentrated in beads organized in two parallel strands along either side of the midline, the strands were constantly moving following the movement of the heart. The same pattern was also seen when APPL-DT was expressed with APPL-TG4 and even Repo-Gal4, but a fluorescent membrane marker did not replicate this pattern when expressed by the same drivers (Fig. 6.2.2.4).

To find where sAPPL accumulate in the abdomen and taking clues from the tissues in that area, I expressed APPL-DT in photoreceptors while using Hand-GFP to label the nephrocytes (Han et al. 2006). As predicted, sAPPL fluorescent signal perfectly colocalized with Hand-GFP, suggesting it accumulated in nephrocytes.

This surprising observation was found by complete coincidence and it suggests that sAPPL is not just restricted within the nervous system. As it is taken up by glia from the neurons, where APPL is produced and cleaved, before it gets released to the hemolymph and then gets filtered out by the nephrocytes where it accumulates. And so far, it remains an open question whether sAPPL accumulation in nephrocytes is required for their development or function.

6.3. Discussion

APPL is required in neurons for outgrowth, synapse formation, and survival. It is expressed in photoreceptor progenitors and enriched in the UV-sensitive R7s where it was reported to affect layer targeting and UV responsiveness. The findings of this chapter suggest that even though R7s in flies with the *app^l* mutant allele retract from their target layer, the phenotype was found to not be due to APPL loss of function. APPL is produced pan-neuronally and its proteolytic cleavage products were found to be trafficked differentially. It secretes the extracellular fragment that accumulates in non-neuronal cells.

6.3.1. APPL is not required for R7 targeting

The vertebrate and the fly APP homologues interact with several membrane and synaptic proteins and regulate their trafficking. As numerous membrane proteins are required for R7 stabilization, this led to hypothesize that APPL regulates endolysosomal trafficking of membrane proteins which affects their role in R7 stabilization as an explanation to the reported subtle targeting defect associated with *appl* loss of function.

R7s in flies with the *appl^d* mutant allele were found to target correctly before they destabilized and retracted similar to the phenotype observed with loss of other membrane proteins.

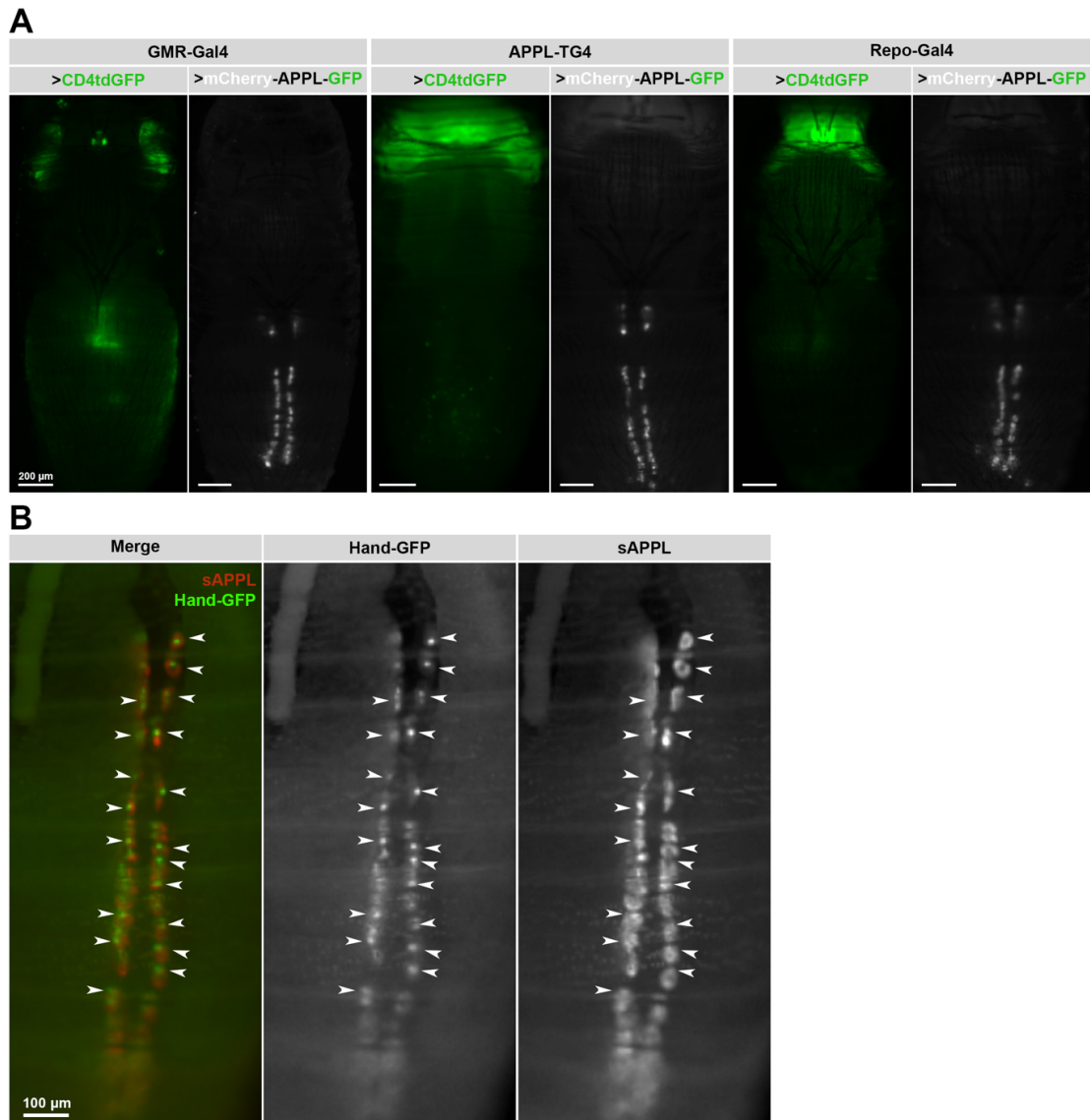


Fig. 6.2.2.4. Secreted APPL from neurons accumulates in nephrocytes.

Expression of APPL-DT in neurons and in glia leads to sAPPL accumulation in nephrocytes. **(A)** Intact late pupa expressing APPL-DT and the membrane marker CD4tdGFP in photoreceptors, in APPL-producing neurons, and in glia. The fluorescently-tagged sAPPL accumulates in the nephrocytes unlike the membrane marker that only labels the nervous system where it is produced. Scale bar = 200 μ m. **(B)** Late pupa with sAPPL released from photoreceptors colocalizes with Hand-GFP that labels nephrocytes (arrow heads). Scale bar = 100 μ m.

PART | 6 APPL

Filopodial dynamics and bulbous tip formation and stabilization were reduced and resulted in a synaptic defect which explains the flies reduced preference for UV light as reported by Mora et al. (Mora et al. 2013).

The penetrance of the R7 retraction phenotype was sensitive to the genetic background. It was ameliorated by suppressor genes that *appl* mutant flies are prone to accumulate, the suppression was eliminated when flies were backcrossed for three generations. On the other hand, sensitizing the *appl* mutant flies with genetic heterozygous backgrounds did not enhance the R7 retraction phenotype except when sensitized with a heterozygous background of *nrt* similar to the findings in (Mora et al. 2013). This effect, however, could be attributed to *nrt* heterozygosity as its loss of function phenotype in growth cones could only be revealed when combined with other neuronal cell adhesion molecules (Merdes et al. 2004).

The findings in this section suggest that the R7 retraction phenotype in *appl^d* flies is not caused due to loss of *appl* but rather due to other genetic elements in the background. There are two pieces of evidence to support this claim: 1) It was not possible to rescue the R7 retraction phenotype in *appl^d* flies by expressing APPL in photoreceptors or in other neurons or glia in the optic lobe. 2) More importantly, other *appl* null backgrounds did not cause R7 retractions suggesting the phenotype is related to the *appl^d* allele rather than APPL's function in photoreceptors. *appl^d* mutant allele was generated by Y chromosome translocation onto an X chromosome terminal deficiency line which resulted in a synthetic X chromosome lacking the *appl* gene (Luo et al. 1992). *appl* is located in a region of the X chromosome that is required for neuronal development, it is flanked by the genes *vnd* and *elav* that are possibly affected in the *appl^d* chromosome which contribute to, if not cause, the subtle R7 retraction phenotype.

6.3.2. Neuronal and non-neuronal functions of APPL

APPL expression and function in neurons has been studied for decades. It has been shown that it is strictly-expressed in fly neurons with roles in outgrowth, synapse formation, and neuronal survival. However, the release of its extracellular fragment to glia has never been detected before. APPL release from neurons and accumulation in glia occurs starting early pupal stages and gradually extends to glia cells covering the entire brain cortex. The exact glia subtypes that take up APPL remain unknown, although based on their location in the brain it is likely that it accumulates in perineural, sub-perineural, or cortex glia whose pattern was demonstrated in (Kremer et al. 2017). It is not clear how sAPPL accumulate in glia, there are two possible scenarios for this process; photoreceptors release APPL (e.g. in exosomes) that are then engulfed by glia, or sAPPL interacts with other membrane proteins on the surface of glia and then endocytosed. The data suggest the first scenario is more likely as sAPPL compartments accumulate adjacent to photoreceptor axons in the lamina plexus as early as P20 and then gradually spread to cover the whole brain. Another intriguing question about

sAPPL spread is whether they migrate within glia cells that circulate around the brain or it is taken up by glia that are in proximity of photoreceptors and, in turn, release it to be taken up by adjacent glia until sAPPL covers the entire brain cortex. The results show that sAPPL must be secreted from neurons whose axons pass the brain cortex in order for sAPPL to spread in the brain cortex and there are two observations that support this claim: 1) expression of APPL-DT in R1-6 that terminate in the lamina using Rh1-Gal4 does not lead to sAPPL accumulation in the brain cortex, and 2) expression of APPL-DT in a subset of R7s using the late driver Rh3-Gal4 leads to sAPPL accumulation in the medulla cortex which spreads with time to a larger area of the brain cortex. This suggests that sAPPL is taken up by glia that migrate to cover the brain cortex carrying the released fragment along, it is not known, however, whether *Drosophila* glia are migratory cells, although this question could be readily answered using live imaging.

The effect of APPL loss and gain of function on endolysosomal trafficking in photoreceptors was not surprising as it contains the endocytic YENPTY motif in the AICD. What was not expected though, is that both the states caused the tested endolysosomal compartments to change in the same direction to a varying extent contrary to what would have been expected of such a manipulation. Suggesting that the observed changes in endolysosomal trafficking are rather due to changing the level of APPL from the wildtype level and not the protein's expression state, yet it is still not clear whether these endolysosomal changes have any physiological effects on the development of function of photoreceptors, or neurons in general. Similar to the changes in photoreceptors, changing the level of sAPPL in glia also changed endolysosomal trafficking as both APPL loss and gain of function drastically reduced the Rab5⁺ and Rab7⁺ compartments. Knowing that APPL is produced only in neurons, the observed changes, especially in mutant animals, could only be explained by the reduction of sAPPL release from neurons and not due to APPL expression in glia. Although glia cells were not labelled in the performed experiments, the location and the size of the compartments in the inner chiasma strongly suggest that they are in glia and not in neuronal cell bodies.

Moreover, APPL overexpression in photoreceptors affected endolysosomal trafficking in axons and terminals of medulla neurons. This is a surprising finding since APPL was overexpressed only in photoreceptors in a wildtype background and, as shown before, the secreted fragment accumulates in glia in the brain cortex where the cell bodies of the medulla neurons are, suggesting a feedback regulatory mechanism where neurons release sAPPL that is taken up by glia where it affects endolysosomal trafficking, these glia cells, in turn, affect endolysosomal trafficking in the neurons in their proximity. These observations could explain the reported function of APPL in neuronal survival where the α -sAPPL is neuroprotective while the β -sAPPL promotes neurodegeneration (Wentzell et al. 2012; Bolkan et al. 2012).

PART | 6 APPL

The release of sAPPL from neurons caused it to not only accumulate in glia but also in the pericardial nephrocytes. Unlike mammalian system, flies do not have a blood-brain-barrier but rather a layer of glia cells in the brain cortex that function as their blood-brain-barrier. These glia cells take up sAPPL from neurons and then release it to the hemolymph to reach the nephrocytes. This is an interesting observation since the mammalian APP is expressed in the kidneys where it plays developmental and physiological roles, which begs the question whether sAPPL also plays a role in the development or function of the *Drosophila* nephrocytes.

PART | 7 CONCLUDING REMARKS

PART | 7 CONCLUDING REMARKS

Sperry's chemoaffinity hypothesis speculated that neurons are guided to and recognize their targets through the combined function of contact-mediated short-range and diffusible long-range guidance cues that are either attractant or repellent (Sperry 1963).

Layer targeting of R7s, which was the main focus of investigation in this study, is not known to require the function of any diffusible guidance cue but rather the function of several membrane-associated proteins, namely, NCad, Lar, and PTP69D. However, these proteins are known to be expressed in all photoreceptors, and even in all neurons, and were found to be important for stabilizing R7s at their target layer rather than cause the correct targeting to start with (Özel et al. 2015; Hakeda-Suzuki et al. 2017; and this study). This brings the question, if not layer targeting, what functions do such membrane proteins have in R7, and ideally in all photoreceptors, development? And also, how do these proteins function together to regulate synapse formation and synaptic partner specification?

7.1. When is a protein considered as a guidance cue?

Previous studies of brain wiring focused primarily on the final developmental outcome of either wildtype or mutant neurons. Mutations in many genes were reported to cause wiring defects in adult brains, which led to interpreting their functions as attractive or repulsive guidance cues. Such analyses, however, reveal little about the dynamic events that take place during development as a process. Using NCad role in R7 targeting as an example; its loss of function causes R7s to terminate in M3 as seen in adult brains. Yet, *ncad* mutant R7s are found to target their correct layer before retracting to eventually terminate in M3. This perspective brings the question: could NCad be considered a guidance cue?

In order not to argue semantics, it is important to first define what a 'guidance cue' is. The definition here-proposed suggests that for a protein to be considered a guidance cue, it needs to comply with three criteria: 1) It should be a membrane-associated or a secreted protein in order for it to be used by neurons to communicate with and identify other neurons. 2) Its loss and gain of function should cause a targeting defect throughout development. 3) Its guidance function should be instructive rather than permissive.

Using these criteria, NCad, together with all the tested CAMs in this study, cannot be considered as guidance cues for R7s. Although their loss of function causes R7s to terminate in the wrong layer, this phenotype is preceded by correct targeting followed by destabilization and retraction. This also applies to Caps as it causes R7s to retract from their correct layer to M3 when ectopically expressed. Additionally, cytosolic proteins that affect R7 targeting as Liprin- α , Liprin- β , and Sequoia should also not be considered as guidance cues.

The recently reported role of the membrane protein Klingon in preventing R7s from extending beyond M6 could be interpreted as a guidance function (Shimozono et al. 2019). However, the

analysis only reported the adult phenotype with no information on the dynamic developmental events that led to the reported defect which could be a point of further investigation.

7.2. The developmental rules that control R7 targeting

Detailed analysis of R7 wiring defects associated with loss of function of genes encoding CAMs indicate that they do not instruct R7 targeting to M6 but rather execute a variety of functions to stabilize R7 contacts in M6, as explained earlier for the function of *Lar*. Guidance of R7 axons to terminate in M6 does not require the function of any of the so far studied CAMs. Hence, it is important to understand the molecular mechanisms by which CAMs stabilize R7 terminals in M6 rather than focusing on the developmental outcomes of their loss of function experiments. The current knowledge does not provide evidence that R7s use a complex molecular code for correct wiring, they rather use a set of broadly-expressed CAMs to stabilize their contacts with their target layer. Alternatively, R7 targeting can be explained using simple developmental rules (Hassan and Hiesinger 2015); R7 axons extend along R8 axons in their respective columns then they terminate right after R8 terminals in the medulla. R7s achieve contact with their main postsynaptic targets (Dm8s) as soon as they arrive in the medulla (Ting et al. 2014), then passively-extend to M6 as the medulla expands. Live imaging of retracting R7s that are mutant of *lar* provided an explanation to their layer targeting. As R7s expand, they use defined certain landmarks to trail their path as they extend to their target layer, and they remain in that layer as long as they maintain their contact in M6. When R7 axons are destabilized, they retract to the previous landmark along their axons, with the first landmark being R8 terminals, irrespective of the layer they terminate in, followed by M0 and finally retract all the way to the lamina.

All the tested CAMs appear to execute the simple developmental rule of stabilizing R7s in their correct layer through different molecular mechanisms that are not fully understood yet. This, however, should not exclude the possibility that R7 targeting is instructed by a guidance cue that is not known yet. Therefore, a screen could be conducted to identify novel receptors or ligands that affect R7 targeting. An approach similar to the recently reported study that used a proteome-instructed screen which identified several CAMs, not previously linked to brain wiring, that affected the wiring of the *Drosophila* olfactory projection neurons (Li et al. 2020).

7.3. Synapse formation in R7s is a probabilistic process

The evidence presented here favors the assumption that synapse formation and synaptic specificity in R7s are not the result of matching molecular codes. However, In order for R7s to reproducibly form the correct number of synapses with the correct synaptic partners, two rules need to be met: 1) R7s stabilize their contacts with their synaptic partners, and 2) an internal feedback mechanism to control the number of synapses.

PART | 7 CONCLUDING REMARKS

The importance of stable contact is shown in the direct correlation between bulbous tip stability (the presumed pre-postsynaptic contact site) and the number of synapses R7s form. This is further supported by the finding that bulbous tips recruit microtubules for stabilization, failure to stabilize microtubules in bulbous tips is associated with decreased bulbous tip stability (less contact time) and the resulting synaptic defect. Thus, stable contacts allow long-enough time for R7s in order to build the synapse. The process of building a synapse requires the function of many proteins that are expressed at high levels throughout the time photoreceptors form synapses (Zhang et al. 2016). These components are thought to be in constant motion in growth cones and are probabilistically recruited to the nascent synapse each executing a certain function required for synapse formation and maturation. Given that the process is probabilistic, proteins are recruited to the nascent synapse at a random order and the contacts remain stable only when the components are recruited at the correct order. This is shown for the reported interaction of Lar, Liprin- α , and microtubules, where the recruitment of Liprin- α or microtubules to bulbous tips was not affected by the presence of the other components, but their stabilization was. In addition, a regulatory mechanism that constantly, and randomly, eliminates nascent synapses that have not reached the 'point of no return' will ensure the robustness of synapse formation and drastically limits the number of synapses R7s eventually form without the requirement of pre-specifying the exact number.

Another mechanism that controls synapse formation is the presence of a feedback function, as reported to be executed by Syd-1 in R7s (Özel et al. 2019), that only allows stabilizing one contact point at a time. This mechanism functions as an internal timer that restricts the number of synapses R7s can form within the time window of synaptogenesis. However, when the feedback mechanism is lost in R7s while still maintaining the capacity to form synapses, as in the proposed function of Nr x , R7s form more synapses.

The findings in this study and in the work of Kiral and colleagues (Kiral et al. 2019) support the assumption that synaptic-partner specification in R7s is not molecularly-encoded but it is rather a result of developmental rules. R7s found to form synapses with incorrect synaptic partners by affecting their dynamics (as with the case of autophagy deficient R7s) or the feedback machinery (as proposed for Nr x deficient R7s). Suggesting that R7s can form synapses with all neurons they form stable contacts with irrespective of molecular codes.

7.4. Do glia have a role in targeting and synapse formation in R7s?

Neuron-glia interaction in the fly visual system was reported to be required for the differentiation of lamina cells (Fernandes et al. 2017). However, glial cells are not known to play any role in R7 targeting or synapse formation. In vertebrates, glia were reported to function as contact hubs between pre- and postsynaptic neurons for synaptic remodeling in developing

PART | 7 CONCLUDING REMARKS

hippocampal neurons (Weinhard et al. 2018). Interactions between cell surface proteins from glia and neurons control synaptic connectivity (Apóstolo and de Wit 2019).

Evidence presented here and in previous studies suggested neuron-glia communication during development through secretion or shedding of the ectodomain of membrane proteins that localize in glia as observed for APPL and previously-reported for PTP69D (Garrity et al. 1999). The developmental relevance of these observations and whether they are important for R7s targeting or synapse formation are compelling questions that can add to our understanding of brain wiring.

REFERENCES

- Agi E, Kulkarni A, Hiesinger PR (2020) Neuronal strategies for meeting the right partner during brain wiring. *Curr Opin Neurobiol* 63:1–8. doi: <https://doi.org/10.1016/j.conb.2020.01.002>
- Aizawa H, Wakatsuki S, Ishii A, et al (2001) Phosphorylation of cofilin by LIM-kinase is necessary for semaphorin 3A-induced growth cone collapse. *Nat Neurosci* 4:367–373. doi: 10.1038/86011
- Akin O, Zipursky SL (2016) Frazzled promotes growth cone attachment at the source of a Netrin gradient in the *Drosophila* visual system. *Elife* 5:e20762. doi: 10.7554/eLife.20762
- Alves-Silva J, Sánchez-Soriano N, Beaven R, et al (2012) Spectraplakins Promote Microtubule-Mediated Axonal Growth by Functioning As Structural Microtubule-Associated Proteins and EB1-Dependent +TIPs (Tip Interacting Proteins). *J Neurosci* 32:9143 LP – 9158. doi: 10.1523/JNEUROSCI.0416-12.2012
- Apitz H, Salecker I (2014) A Challenge of Numbers and Diversity: Neurogenesis in the *Drosophila* Optic Lobe. *J Neurogenet* 28:233–249. doi: 10.3109/01677063.2014.922558
- Apóstolo N, de Wit J (2019) Compartmentalized distributions of neuronal and glial cell-surface proteins pattern the synaptic network. *Curr Opin Neurobiol* 57:126–133. doi: <https://doi.org/10.1016/j.conb.2019.01.025>
- Ashley J, Packard M, Ataman B, Budnik V (2005) Fasciclin II Signals New Synapse Formation through Amyloid Precursor Protein and the Scaffolding Protein dX11/Mint. *J Neurosci* 25:5943 LP – 5955. doi: 10.1523/JNEUROSCI.1144-05.2005
- Astigarraga S, Hofmeyer K, Farajian R, Treisman JE (2010) Three *Drosophila* liprins interact to control synapse formation. *J Neurosci* 30:15358–15368. doi: 10.1523/JNEUROSCI.1862-10.2010
- Ayaz D, Leyssen M, Koch M, et al (2008) Axonal Injury and Regeneration in the Adult Brain of *Drosophila*. *J Neurosci* 28:6010 LP – 6021. doi: 10.1523/JNEUROSCI.0101-08.2008
- Bamburg JR, Bray D (1987) Distribution and cellular localization of actin depolymerizing factor. *J Cell Biol* 105:2817 LP – 2825. doi: 10.1083/jcb.105.6.2817
- Bekkers JM, Stevens CF (1991) Excitatory and inhibitory autaptic currents in isolated hippocampal neurons maintained in cell culture. *Proc Natl Acad Sci* 88:7834 LP – 7838. doi:

REFERENCES

10.1073/pnas.88.17.7834

Bellen HJ, Tong C, Tsuda H (2010) 100 years of Drosophila research and its impact on vertebrate neuroscience: a history lesson for the future. *Nat Rev Neurosci* 11:514–522. doi: 10.1038/nrn2839

Bentley D, Toroian-Raymond A (1986) Disoriented pathfinding by pioneer neurone growth cones deprived of filopodia by cytochalasin treatment. *Nature* 323:712–715. doi: 10.1038/323712a0

Berger-Müller S, Sugie A, Takahashi F, et al (2013) Assessing the role of cell-surface molecules in central synaptogenesis in the Drosophila visual system. *PLoS One* 8:1–14. doi: 10.1371/journal.pone.0083732

Biswas S, Kalil K (2018) The Microtubule-Associated Protein Tau Mediates the Organization of Microtubules and Their Dynamic Exploration of Actin-Rich Lamellipodia and Filopodia of Cortical Growth Cones. *J Neurosci* 38:291 LP – 307. doi: 10.1523/JNEUROSCI.2281-17.2017

Bolkan BJ, Triphan T, Kretzschmar D (2012) β -Secretase Cleavage of the Fly Amyloid Precursor Protein Is Required for Glial Survival. *J Neurosci* 32:16181 LP – 16192. doi: 10.1523/JNEUROSCI.0228-12.2012

Braitenberg V (1967) Patterns of projection in the visual system of the fly. I. Retina-lamina projections. *Exp Brain Res* 3:271–298. doi: 10.1007/BF00235589

Braitenberg V, Schüz A (1998) Peters' Rule and White's Exceptions BT - Cortex: Statistics and Geometry of Neuronal Connectivity. In: Braitenberg V, Schüz A (eds). Springer Berlin Heidelberg, Berlin, Heidelberg, pp 99–101

Brand AH, Perrimon N (1993) Targeted gene expression as a means of altering cell fates and generating dominant phenotypes. *Development* 118:401 LP – 415

Cagan RL, Ready DF (1989) The emergence of order in the Drosophila pupal retina. *Dev Biol* 136:346–362. doi: [https://doi.org/10.1016/0012-1606\(89\)90261-3](https://doi.org/10.1016/0012-1606(89)90261-3)

Campos-Ortega JA (1980) Chapter 10 On Compound Eye Development In *Drosophila melanogaster*. In: Moscona AA, Monroy ABT-CT in DB (eds) *Neural Development Part I*. Academic Press, pp 347–371

Chen Y, Akin O, Nern A, et al (2014) Cell-type-Specific Labeling of Synapses In Vivo through

REFERENCES

Synaptic Tagging with Recombination. *Neuron* 81:280–293. doi: <https://doi.org/10.1016/j.neuron.2013.12.021>

Cherry S, Jin EJ, Özel MN, et al (2013) Charcot-Marie-Tooth 2B mutations in rab7 cause dosage-dependent neurodegeneration due to partial loss of function. *Elife* 2:e01064. doi: 10.7554/eLife.01064

Choe K-M, Prakash S, Bright A, Clandinin TR (2006) Liprin- α is required for photoreceptor target selection in *Drosophila*. *Proc Natl Acad Sci* 103:11601 LP – 11606. doi: 10.1073/pnas.0601185103

Chotard C, Leung W, Salecker I (2005) glial cells missing and gcm2 Cell Autonomously Regulate Both Glial and Neuronal Development in the Visual System of *Drosophila*. *Neuron* 48:237–251. doi: 10.1016/j.neuron.2005.09.019

Chow RW, Almeida AD, Randlett O, et al (2015) Inhibitory neuron migration and IPL formation in the developing zebrafish retina. *Development* 142:2665 LP – 2677. doi: 10.1242/dev.122473

Clandinin TR, Lee C-H, Herman T, et al (2001) *Drosophila* LAR Regulates R1-R6 and R7 Target Specificity in the Visual System. *Neuron* 32:237–248. doi: [https://doi.org/10.1016/S0896-6273\(01\)00474-3](https://doi.org/10.1016/S0896-6273(01)00474-3)

Clandinin TR, Zipursky SL (2002) Making Connections in the Fly Visual System. *Neuron* 35:827–841. doi: 10.1016/S0896-6273(02)00876-0

Craig EM (2018) Model for Coordination of Microtubule and Actin Dynamics in Growth Cone Turning. *Front. Cell. Neurosci.* 12:394

D’Aiuto L, Naciri J, Radio N, et al (2018) Generation of three-dimensional human neuronal cultures: application to modeling CNS viral infections. *Stem Cell Res Ther* 9:134. doi: 10.1186/s13287-018-0881-6

Dascenco D, Erfurth M-L, Izadifar A, et al (2015) Slit and Receptor Tyrosine Phosphatase 69D Confer Spatial Specificity to Axon Branching via Dscam1. *Cell* 162:1140–1154. doi: 10.1016/j.cell.2015.08.003

Delorme-Walker V, Seo J-Y, Gohla A, et al (2015) Chronophin coordinates cell leading edge dynamics by controlling active cofilin levels. *Proc Natl Acad Sci* 112:E5150 LP-E5159. doi: 10.1073/pnas.1510945112

REFERENCES

- Desai C, Purdy J (2003) The Neural Receptor Protein Tyrosine Phosphatase DPTP69D Is Required During Periods of Axon Outgrowth in *Drosophila*. *Genetics* 164:575 LP – 588
- Dickson BJ (2002) Molecular Mechanisms of Axon Guidance. *Science* (80-) 298:1959 LP – 1964. doi: 10.1126/science.1072165
- Drescher U, Kremoser C, Handwerker C, et al (1995) In vitro guidance of retinal ganglion cell axons by RAGS, a 25 kDa tectal protein related to ligands for Eph receptor tyrosine kinases. *Cell* 82:359–370. doi: [https://doi.org/10.1016/0092-8674\(95\)90425-5](https://doi.org/10.1016/0092-8674(95)90425-5)
- Egger B, Boone JQ, Stevens NR, et al (2007) Regulation of spindle orientation and neural stem cell fate in the *Drosophila* optic lobe. *Neural Dev* 2:1. doi: 10.1186/1749-8104-2-1
- Endo M, Ohashi K, Sasaki Y, et al (2003) Control of Growth Cone Motility and Morphology by LIM Kinase and Slingshot via Phosphorylation and Dephosphorylation of Cofilin. *J Neurosci* 23:2527 LP – 2537. doi: 10.1523/JNEUROSCI.23-07-02527.2003
- Faivre-Sarrailh C, Banerjee S, Li J, et al (2004) *Drosophila* contactin, a homolog of vertebrate contactin, is required for septate junction organization and paracellular barrier function. *Development* 131:4931 LP – 4942. doi: 10.1242/dev.01372
- Fernandes VM, Chen Z, Rossi AM, et al (2017) Glia relay differentiation cues to coordinate neuronal development in *Drosophila*. *Science* (80-) 357:886 LP – 891. doi: 10.1126/science.aan3174
- Fischbach K-F, Dittrich APM (1989) The optic lobe of *Drosophila melanogaster*. I. A Golgi analysis of wild-type structure. *Cell Tissue Res* 258:441–475. doi: 10.1007/BF00218858
- Fortini ME, Rubin GM (1991) The optic lobe projection pattern of polarization-sensitive photoreceptor cells in *Drosophila melanogaster*. *Cell Tissue Res* 265:185–191. doi: 10.1007/BF00318153
- Fouquet W, Oswald D, Wichmann C, et al (2009) Maturation of active zone assembly by *Drosophila* Bruchpilot. *J Cell Biol* 186:129 LP – 145. doi: 10.1083/jcb.200812150
- Gao S, Takemura S, Ting C-Y, et al (2008) The Neural Substrate of Spectral Preference in *Drosophila*. *Neuron* 60:328–342. doi: 10.1016/j.neuron.2008.08.010
- Garrity PA, Lee C-H, Salecker I, et al (1999) Retinal Axon Target Selection in *Drosophila* Is Regulated by a Receptor Protein Tyrosine Phosphatase. *Neuron* 22:707–717. doi:

REFERENCES

10.1016/S0896-6273(00)80730-8

Goguel V, Belair A-L, Ayaz D, et al (2011) Drosophila Amyloid Precursor Protein-Like Is Required for Long-Term Memory. *J Neurosci* 31:1032 LP – 1037. doi: 10.1523/JNEUROSCI.2896-10.2011

Gohla A, Birkenfeld J, Bokoch GM (2005) Chronophin, a novel HAD-type serine protein phosphatase, regulates cofilin-dependent actin dynamics. *Nat Cell Biol* 7:21–29. doi: 10.1038/ncb1201

Golic KG (1991) Site-specific recombination between homologous chromosomes in Drosophila. *Science* (80-) 252:958 LP – 961. doi: 10.1126/science.2035025

Golic KG, Lindquist S (1989) The FLP recombinase of yeast catalyzes site-specific recombination in the drosophila genome. *Cell* 59:499–509. doi: 10.1016/0092-8674(89)90033-0

Green P, Hartenstein AY, Hartenstein V (1993) The embryonic development of the Drosophila visual system. *Cell Tissue Res* 273:583–598. doi: 10.1007/BF00333712

Gunawardena S, Yang G, Goldstein LSB (2013) Presenilin controls kinesin-1 and dynein function during APP-vesicle transport in vivo. *Hum Mol Genet* 22:3828–3843. doi: 10.1093/hmg/ddt237

Gundersen RW, Barrett JN (1979) Neuronal chemotaxis: chick dorsal-root axons turn toward high concentrations of nerve growth factor. *Science* (80-) 206:1079 LP – 1080. doi: 10.1126/science.493992

Hadjieconomou D, Timofeev K, Salecker I (2011) A step-by-step guide to visual circuit assembly in Drosophila. *Curr Opin Neurobiol* 21:76–84. doi: 10.1016/J.CONB.2010.07.012

Hakeda-Suzuki S, Takechi H, Kawamura H, Suzuki T (2017) Two receptor tyrosine phosphatases dictate the depth of axonal stabilizing layer in the visual system. *Elife* 6:e31812. doi: 10.7554/eLife.31812

Han Z, Yi P, Li X, Olson EN (2006) Hand, an evolutionarily conserved bHLH transcription factor required for Drosophila cardiogenesis and hematopoiesis. *Development* 133:1175 LP – 1182. doi: 10.1242/dev.02285

Hassan BA, Hiesinger PR (2015) Beyond Molecular Codes: Simple Rules to Wire Complex

REFERENCES

Brains. *Cell* 163:285–291. doi: <https://doi.org/10.1016/j.cell.2015.09.031>

Hattori D, Chen Y, Matthews BJ, et al (2009) Robust discrimination between self and non-self neurites requires thousands of Dscam1 isoforms. *Nature* 461:644–648. doi: [10.1038/nature08431](https://doi.org/10.1038/nature08431)

Hattori D, Millard SS, Wojtowicz WM, Zipursky SL (2008) Dscam-Mediated Cell Recognition Regulates Neural Circuit Formation. *Annu Rev Cell Dev Biol* 24:597–620. doi: [10.1146/annurev.cellbio.24.110707.175250](https://doi.org/10.1146/annurev.cellbio.24.110707.175250)

He H, Kise Y, Izadifar A, et al (2014) Cell-intrinsic requirement of Dscam1 isoform diversity for axon collateral formation. *Science* (80-) 344:1182 LP – 1186. doi: [10.1126/science.1251852](https://doi.org/10.1126/science.1251852)

Hiesinger PR, Fayyazuddin A, Mehta SQ, et al (2005) The v-ATPase V0 Subunit a1 Is Required for a Late Step in Synaptic Vesicle Exocytosis in *Drosophila*. *Cell* 121:607–620. doi: <https://doi.org/10.1016/j.cell.2005.03.012>

Hiesinger PR, Zhai RG, Zhou Y, et al (2006) Activity-Independent Prespecification of Synaptic Partners in the Visual Map of *Drosophila*. *Curr Biol* 16:1835–1843. doi: <https://doi.org/10.1016/j.cub.2006.07.047>

Hofbauer A, Campos-Ortega JA (1990) Proliferation pattern and early differentiation of the optic lobes in *Drosophila melanogaster*. *Roux's Arch Dev Biol* 198:264–274. doi: [10.1007/BF00377393](https://doi.org/10.1007/BF00377393)

Hofmeyer K, Maurel-Zaffran C, Sink H, Treisman JE (2006) Liprin- α has LAR-independent functions in R7 photoreceptor axon targeting. *Proc Natl Acad Sci* 103:11595 LP – 11600. doi: [10.1073/pnas.0604766103](https://doi.org/10.1073/pnas.0604766103)

Hofmeyer K, Treisman JE (2009) The receptor protein tyrosine phosphatase LAR promotes R7 photoreceptor axon targeting by a phosphatase-independent signaling mechanism. *Proc Natl Acad Sci* 106:19399 LP – 19404. doi: [10.1073/pnas.0903961106](https://doi.org/10.1073/pnas.0903961106)

Holbrook S, Finley JK, Lyons EL, Herman TG (2012) Loss of *syd-1* from R7 Neurons Disrupts Two Distinct Phases of Presynaptic Development. *J Neurosci* 32:18101 LP – 18111. doi: [10.1523/JNEUROSCI.1350-12.2012](https://doi.org/10.1523/JNEUROSCI.1350-12.2012)

Holguera I, Desplan C (2018) Neuronal specification in space and time. *Science* (80-) 362:176 LP – 180. doi: [10.1126/science.aas9435](https://doi.org/10.1126/science.aas9435)

REFERENCES

- Huang Z, Kunes S (1996) Hedgehog, Transmitted along Retinal Axons, Triggers Neurogenesis in the Developing Visual Centers of the *Drosophila* Brain. *Cell* 86:411–422. doi: 10.1016/S0092-8674(00)80114-2
- Huber AB, Kolodkin AL, Ginty DD, Cloutier J-F (2003) SIGNALING AT THE GROWTH CONE: Ligand-Receptor Complexes and the Control of Axon Growth and Guidance. *Annu Rev Neurosci* 26:509–563. doi: 10.1146/annurev.neuro.26.010302.081139
- Juliano RL (2002) Signal Transduction by Cell Adhesion Receptors and the Cytoskeleton: Functions of Integrins, Cadherins, Selectins, and Immunoglobulin-Superfamily Members. *Annu Rev Pharmacol Toxicol* 42:283–323. doi: 10.1146/annurev.pharmtox.42.090401.151133
- Karuppudurai T, Lin T-Y, Ting C-Y, et al (2014) A Hard-Wired Glutamatergic Circuit Pools and Relays UV Signals to Mediate Spectral Preference in *Drosophila*. *Neuron* 81:603–615. doi: 10.1016/j.neuron.2013.12.010
- Kaufmann N, DeProto J, Ranjan R, et al (2002) *Drosophila* Liprin- α and the Receptor Phosphatase Dlar Control Synapse Morphogenesis. *Neuron* 34:27–38. doi: [https://doi.org/10.1016/S0896-6273\(02\)00643-8](https://doi.org/10.1016/S0896-6273(02)00643-8)
- Kim J-E, Kim Y-J, Lee D-S, et al (2016) PLPP/CIN regulates bidirectional synaptic plasticity via GluN2A interaction with postsynaptic proteins. *Sci Rep* 6:26576
- King GD, Perez RG, Steinhilb ML, et al (2003) X11 α modulates secretory and endocytic trafficking and metabolism of amyloid precursor protein: mutational analysis of the yenyty sequence. *Neuroscience* 120:143–154. doi: [https://doi.org/10.1016/S0306-4522\(03\)00284-7](https://doi.org/10.1016/S0306-4522(03)00284-7)
- Kiral FR, Linneweber GA, Georgiev SV, et al (2019) Autophagy-dependent filopodial kinetics restrict synaptic partner choice during *Drosophila* brain wiring. *bioRxiv* 762179. doi: 10.1101/762179
- Kolodkin AL, Hiesinger PR (2017) Wiring visual systems: common and divergent mechanisms and principles. *Curr Opin Neurobiol* 42:128–135. doi: <https://doi.org/10.1016/j.conb.2016.12.006>
- Kolodkin AL, Tessier-Lavigne M (2011) Mechanisms and Molecules of Neuronal Wiring: A Primer. *Cold Spring Harb Perspect Biol* 3:. doi: 10.1101/cshperspect.a001727
- Kremer MC, Jung C, Batelli S, et al (2017) The glia of the adult *Drosophila* nervous system. *Glia* 65:606–638. doi: 10.1002/glia.23115

REFERENCES

- Krueger NX, Van Vactor D, Wan HI, et al (1996) The Transmembrane Tyrosine Phosphatase DLAR Controls Motor Axon Guidance in *Drosophila*. *Cell* 84:611–622. doi: 10.1016/S0092-8674(00)81036-3
- Kulkarni A, Ertekin D, Lee C-H, Hummel T (2016) Birth order dependent growth cone segregation determines synaptic layer identity in the *Drosophila* visual system. *Elife* 5:e13715. doi: 10.7554/eLife.13715
- Langen M, Agi E, Altschuler DJ, et al (2015) The Developmental Rules of Neural Superposition in *Drosophila*. *Cell* 162:120–133. doi: 10.1016/j.cell.2015.05.055
- Lawrence Zipursky S, Grueber WB (2013) The Molecular Basis of Self-Avoidance. *Annu Rev Neurosci* 36:547–568. doi: 10.1146/annurev-neuro-062111-150414
- Lee C-H, Herman T, Clandinin TR, et al (2001) N-Cadherin Regulates Target Specificity in the *Drosophila* Visual System. *Neuron* 30:437–450. doi: [https://doi.org/10.1016/S0896-6273\(01\)00291-4](https://doi.org/10.1016/S0896-6273(01)00291-4)
- Lee T, Luo L (1999) Mosaic Analysis with a Repressible Cell Marker for Studies of Gene Function in Neuronal Morphogenesis. *Neuron* 22:451–461. doi: 10.1016/S0896-6273(00)80701-1
- Lefebvre JL, Kostadinov D, Chen W V, et al (2012) Protocadherins mediate dendritic self-avoidance in the mammalian nervous system. *Nature* 488:517–521. doi: 10.1038/nature11305
- Leyssen M, Ayaz D, Hébert SS, et al (2005) Amyloid precursor protein promotes post-developmental neurite arborization in the *Drosophila* brain. *EMBO J* 24:2944–2955. doi: 10.1038/sj.emboj.7600757
- Li J, Ashley J, Budnik V, Bhat MA (2007) Crucial Role of *Drosophila* Neurexin in Proper Active Zone Apposition to Postsynaptic Densities, Synaptic Growth, and Synaptic Transmission. *Neuron* 55:741–755. doi: <https://doi.org/10.1016/j.neuron.2007.08.002>
- Li J, Han S, Li H, et al (2020) Cell-Surface Proteomic Profiling in the Fly Brain Uncovers Wiring Regulators. *Cell*. doi: 10.1016/j.cell.2019.12.029
- Li Y, Liu T, Peng Y, et al (2004) Specific functions of *Drosophila* amyloid precursor-like protein in the development of nervous system and nonneural tissues. *J Neurobiol* 61:343–358. doi: 10.1002/neu.20048

REFERENCES

- Liu L, Tian Y, Zhang X, et al (2017) Neurexin Restricts Axonal Branching in Columns by Promoting Ephrin Clustering. *Dev Cell* 41:94-106.e4. doi: 10.1016/j.devcel.2017.03.004
- Lokmane L, Proville R, Narboux-Nême N, et al (2013) Sensory Map Transfer to the Neocortex Relies on Pretarget Ordering of Thalamic Axons. *Curr Biol* 23:810–816. doi: 10.1016/j.cub.2013.03.062
- Lowery LA, Vactor D Van (2009) The trip of the tip: understanding the growth cone machinery. *Nat Rev Mol Cell Biol* 10:332–343. doi: 10.1038/nrm2679
- Luo L, Tully T, White K (1992) Human amyloid precursor protein ameliorates behavioral deficit of flies deleted for *appl* gene. *Neuron* 9:595–605. doi: 10.1016/0896-6273(92)90024-8
- Luo LQ, Martin-Morris LE, White K (1990) Identification, secretion, and neural expression of APPL, a *Drosophila* protein similar to human amyloid protein precursor. *J Neurosci* 10:3849 LP – 3861. doi: 10.1523/JNEUROSCI.10-12-03849.1990
- Martin-Morris LE, White K (1990) The *Drosophila* transcript encoded by the beta-amyloid protein precursor-like gene is restricted to the nervous system. *Development* 110:185 LP – 195
- Mast JD, Prakash S, Chen P-L, Clandinin TR (2006) The mechanisms and molecules that connect photoreceptor axons to their targets in *Drosophila*. *Semin Cell Dev Biol* 17:42–49. doi: <https://doi.org/10.1016/j.semcdb.2005.11.004>
- Maurel-Zaffran C, Suzuki T, Gahmon G, et al (2001) Cell-Autonomous and -Nonautonomous Functions of LAR in R7 Photoreceptor Axon Targeting. *Neuron* 32:225–235. doi: 10.1016/S0896-6273(01)00471-8
- Meinertzhagen IA, Boycott BB (1976) The organization of perpendicular fibre pathways in the insect optic lobe. *Philos Trans R Soc London B, Biol Sci* 274:555–594. doi: 10.1098/rstb.1976.0064
- Meinertzhagen IA, O'Neil SD (1991) Synaptic organization of columnar elements in the lamina of the wild type in *Drosophila melanogaster*. *J Comp Neurol* 305:232–263. doi: 10.1002/cne.903050206
- Meinertzhagen IA, Sorra KEBT-P in BR (2001) Chapter 3 Synaptic organization in the fly's optic lamina: few cells, many synapses and divergent microcircuits. In: *Concepts and Challenges in Retinal Biology (Progress in Brain Research)*. Elsevier, pp 53–69

REFERENCES

- Melnattur K V, Lee C-H (2011) Visual circuit assembly in *Drosophila*. *Dev Neurobiol* 71:1286–1296. doi: 10.1002/dneu.20894
- Menon S, Gupton SL (2016) Chapter Three - Building Blocks of Functioning Brain: Cytoskeletal Dynamics in Neuronal Development. In: Jeon KWBT-IR of C and MB (ed) *International Review of Cell and Molecular Biology*. Academic Press, pp 183–245
- Merdes G, Soba P, Loewer A, et al (2004) Interference of human and *Drosophila* APP and APP-like proteins with PNS development in *Drosophila*. *EMBO J* 23:4082–4095. doi: 10.1038/sj.emboj.7600413
- Meyer RL (1998) Roger Sperry and his chemoaffinity hypothesis. *Neuropsychologia* 36:957–980. doi: [https://doi.org/10.1016/S0028-3932\(98\)00052-9](https://doi.org/10.1016/S0028-3932(98)00052-9)
- Missler M, Zhang W, Rohlmann A, et al (2003) α -Neurexins couple Ca^{2+} channels to synaptic vesicle exocytosis. *Nature* 423:939–948. doi: 10.1038/nature01755
- Miura SK, Martins A, Zhang KX, et al (2013) Probabilistic Splicing of *Dscam1* Establishes Identity at the Level of Single Neurons. *Cell* 155:1166–1177. doi: 10.1016/j.cell.2013.10.018
- Mora N, Almudi I, Alsina B, et al (2013) β amyloid protein precursor-like (APPL) is a Ras1/MAPK-regulated gene required for axonal targeting in *Drosophila* photoreceptor neurons. *J Cell Sci* 126:53 LP – 59
- Morante J, Desplan C (2008) The Color-Vision Circuit in the Medulla of *Drosophila*. *Curr Biol* 18:553–565. doi: 10.1016/j.cub.2008.02.075
- Morgan TH (1910) Sex limited inheritance in *Drosophila*. *Science* (80-) 32:120 LP – 122. doi: 10.1126/science.32.812.120
- Muhammad K, Reddy-Alla S, Driller JH, et al (2015) Presynaptic spinophilin tunes neurexin signalling to control active zone architecture and function. *Nat Commun* 6:8362. doi: 10.1038/ncomms9362
- Müller UC, Deller T, Korte M (2017) Not just amyloid: physiological functions of the amyloid precursor protein family. *Nat Rev Neurosci* 18:281
- Newsome TP, Asling B, Dickson BJ (2000a) Analysis of *Drosophila* photoreceptor axon guidance in eye-specific mosaics. *Development* 127:851 LP – 860

REFERENCES

Newsome TP, Schmidt S, Dietzl G, et al (2000b) Trio Combines with Dock to Regulate Pak Activity during Photoreceptor Axon Pathfinding in *Drosophila*. *Cell* 101:283–294. doi: [https://doi.org/10.1016/S0092-8674\(00\)80838-7](https://doi.org/10.1016/S0092-8674(00)80838-7)

O'Tousa JE, Baehr W, Martin RL, et al (1985) The *Drosophila* *ninaE* gene encodes an opsin. *Cell* 40:839–850. doi: 10.1016/0092-8674(85)90343-5

Oliva C, Soldano A, Mora N, et al (2016) Regulation of *Drosophila* Brain Wiring by Neuropil Interactions via a Slit-Robo-RPTP Signaling Complex. *Dev Cell* 39:267–278. doi: 10.1016/j.devcel.2016.09.028

Owald D, Khorramshahi O, Gupta VK, et al (2012) Cooperation of Syd-1 with Neurexin synchronizes pre- with postsynaptic assembly. *Nat Neurosci* 15:1219–1226. doi: 10.1038/nn.3183

Özel MN, Kulkarni A, Hasan A, et al (2019) Serial Synapse Formation through Filopodial Competition for Synaptic Seeding Factors. *Dev Cell* 50:447-461.e8. doi: <https://doi.org/10.1016/j.devcel.2019.06.014>

Özel MN, Langen M, Hassan BA, Hiesinger PR (2015) Filopodial dynamics and growth cone stabilization in *Drosophila* visual circuit development. *Elife* 4:. doi: 10.7554/eLife.10721

Pawson C, Eaton BA, Davis GW (2008) Formin-Dependent Synaptic Growth: Evidence That Dlar Signals via Diaphanous to Modulate Synaptic Actin and Dynamic Pioneer Microtubules. *J Neurosci* 28:11111 LP – 11123. doi: 10.1523/JNEUROSCI.0833-08.2008

Penserga T, Kudumala SR, Poulos R, Godenschwege TA (2019) A Role for *Drosophila* Amyloid Precursor Protein in Retrograde Trafficking of L1-Type Cell Adhesion Molecule Neuroglian . *Front. Cell. Neurosci.* 13:322

Peters A, Feldman ML (1976) The projection of the lateral geniculate nucleus to area 17 of the rat cerebral cortex. I. General description. *J Neurocytol* 5:63–84. doi: 10.1007/BF01176183

Pollard TD (2016) Actin and Actin-Binding Proteins. *Cold Spring Harb Perspect Biol* 8:. doi: 10.1101/cshperspect.a018226

Pollard TD, Cooper JA (2009) Actin, a Central Player in Cell Shape and Movement. *Science* (80-) 326:1208 LP – 1212. doi: 10.1126/science.1175862

Prakash S, McLendon HM, Dubreuil Cl, et al (2009) Complex interactions amongst N-cadherin,

REFERENCES

- DLAR, and Liprin- α regulate *Drosophila* photoreceptor axon targeting. *Dev Biol* 336:10–19. doi: <https://doi.org/10.1016/j.ydbio.2009.09.016>
- Ramaker JM, Cargill RS, Swanson TL, et al (2016) Amyloid Precursor Proteins Are Dynamically Trafficked and Processed during Neuronal Development . *Front. Mol. Neurosci.* 9:130
- Raper JA, Kapfhammer JR (1990) The enrichment of a neuronal growth cone collapsing activity from embryonic chick brain. *Neuron* 4:21–29. doi: [10.1016/0896-6273\(90\)90440-Q](https://doi.org/10.1016/0896-6273(90)90440-Q)
- Ready DF, Hanson TE, Benzer S (1976) Development of the *Drosophila* retina, a neurocrystalline lattice. *Dev Biol* 53:217–240. doi: [https://doi.org/10.1016/0012-1606\(76\)90225-6](https://doi.org/10.1016/0012-1606(76)90225-6)
- Rister J, Pauls D, Schnell B, et al (2007) Dissection of the Peripheral Motion Channel in the Visual System of *Drosophila melanogaster*. *Neuron* 56:155–170. doi: [10.1016/j.neuron.2007.09.014](https://doi.org/10.1016/j.neuron.2007.09.014)
- Robertson F, Pinal N, Fichelson P, Pichaud F (2012) Atonal and EGFR signalling orchestrate rok and Drak dependent adherens junction remodelling during ommatidia morphogenesis. *Development* 139:3432 LP – 3441. doi: [10.1242/dev.080762](https://doi.org/10.1242/dev.080762)
- Rosen DR, Martin-Morris L, Luo LQ, White K (1989) A *Drosophila* gene encoding a protein resembling the human beta-amyloid protein precursor. *Proc Natl Acad Sci* 86:2478 LP – 2482. doi: [10.1073/pnas.86.7.2478](https://doi.org/10.1073/pnas.86.7.2478)
- Sajnani G, Aricescu AR, Jones EY, et al (2005) PTP σ promotes retinal neurite outgrowth non-cell-autonomously. *J Neurobiol* 65:59–71. doi: [10.1002/neu.20175](https://doi.org/10.1002/neu.20175)
- Sakamoto S, Ishizaki T, Okawa K, et al (2012) Liprin- α controls stress fiber formation by binding to mDia and regulating its membrane localization. *J Cell Sci* 125:108 LP – 120. doi: [10.1242/jcs.087411](https://doi.org/10.1242/jcs.087411)
- Salcedo E, Huber A, Henrich S, et al (1999) Blue- and Green-Absorbing Visual Pigments of *Drosophila*: Ectopic Expression and Physiological Characterization of the R8 Photoreceptor Cell-Specific Rh5 and Rh6 Rhodopsins. *J Neurosci* 19:10716 LP – 10726. doi: [10.1523/JNEUROSCI.19-24-10716.1999](https://doi.org/10.1523/JNEUROSCI.19-24-10716.1999)
- Sancer G, Kind E, Plazaola-Sasieta H, et al (2019) Modality-Specific Circuits for Skylight Orientation in the Fly Visual System. *Curr Biol* 29:2812–2825.e4. doi: [10.1016/j.cub.2019.05.016](https://doi.org/10.1016/j.cub.2019.05.016)

REFERENCES

<https://doi.org/10.1016/j.cub.2019.07.020>

Sato M, Suzuki T, Nakai Y (2013) Waves of differentiation in the fly visual system. *Dev Biol* 380:1–11. doi: <https://doi.org/10.1016/j.ydbio.2013.04.007>

Scheiffele P, Fan J, Choih J, et al (2000) Neuroligin Expressed in Nonneuronal Cells Triggers Presynaptic Development in Contacting Axons. *Cell* 101:657–669. doi: 10.1016/S0092-8674(00)80877-6

Schmid A, Hallermann S, Kittel RJ, et al (2008) Activity-dependent site-specific changes of glutamate receptor composition in vivo. *Nat Neurosci* 11:659–666

Schmucker D, Clemens JC, Shu H, et al (2000) *Drosophila* Dscam Is an Axon Guidance Receptor Exhibiting Extraordinary Molecular Diversity. *Cell* 101:671–684. doi: [https://doi.org/10.1016/S0092-8674\(00\)80878-8](https://doi.org/10.1016/S0092-8674(00)80878-8)

Schwabe T, Borycz JA, Meinertzhagen IA, Clandinin TR (2014) Differential Adhesion Determines the Organization of Synaptic Fascicles in the *drosophila* Visual System. *Curr Biol* 24:1304–1313. doi: 10.1016/j.cub.2014.04.047

Schwabe T, Neuert H, Clandinin TR (2013) A Network of Cadherin-Mediated Interactions Polarizes Growth Cones to Determine Targeting Specificity. *Cell* 154:351–364. doi: <https://doi.org/10.1016/j.cell.2013.06.011>

Selleck SB, Gonzalez C, Glover DM, White K (1992) Regulation of the G1-S transition in postembryonic neuronal precursors by axon ingrowth. *Nature* 355:253–255. doi: 10.1038/355253a0

Shariati SAM, De Strooper B (2013) Redundancy and divergence in the amyloid precursor protein family. *FEBS Lett* 587:2036–2045. doi: 10.1016/j.febslet.2013.05.026

Shimozono M, Osaka J, Kato Y, et al (2019) Cell surface molecule, Klingon, mediates the refinement of synaptic specificity in the *Drosophila* visual system. *Genes to Cells* 24:496–510. doi: 10.1111/gtc.12703

Shinza-Kameda M, Takasu E, Sakurai K, et al (2006) Regulation of Layer-Specific Targeting by Reciprocal Expression of a Cell Adhesion Molecule, Capricious. *Neuron* 49:205–213. doi: <https://doi.org/10.1016/j.neuron.2005.11.013>

Soldano A, Okray Z, Janovska P, et al (2013) The *Drosophila* Homologue of the Amyloid

REFERENCES

- Precursor Protein Is a Conserved Modulator of Wnt PCP Signaling. *PLOS Biol* 11:e1001562
- Sperry RW (1943) Visuomotor coordination in the newt (*triturus viridescens*) after regeneration of the optic nerve. *J Comp Neurol* 79:33–55. doi: 10.1002/cne.900790104
- Sperry RW (1963) CHEMOAFFINITY IN THE ORDERLY GROWTH OF NERVE FIBER PATTERNS AND CONNECTIONS. *Proc Natl Acad Sci* 50:703 LP – 710. doi: 10.1073/pnas.50.4.703
- Stoker AW (2015) RPTPs in axons, synapses and neurology. *Semin Cell Dev Biol* 37:90–97. doi: <https://doi.org/10.1016/j.semcdb.2014.09.006>
- Streuli M, Krueger NX, Tsai AY, Saito H (1989) A family of receptor-linked protein tyrosine phosphatases in humans and *Drosophila*. *Proc Natl Acad Sci* 86:8698 LP – 8702. doi: 10.1073/pnas.86.22.8698
- Südhof TC (2008) Neuroligins and neurexins link synaptic function to cognitive disease. *Nature* 455:903–911. doi: 10.1038/nature07456
- Sullivan LF, Warren TL, Doe CQ (2019) Temporal identity establishes columnar neuron morphology, connectivity, and function in a *Drosophila* navigation circuit. *Elife* 8:e43482. doi: 10.7554/eLife.43482
- Sun Q, Schindelholz B, Knirr M, et al (2001) Complex Genetic Interactions among Four Receptor Tyrosine Phosphatases Regulate Axon Guidance in *Drosophila*. *Mol Cell Neurosci* 17:274–291. doi: <https://doi.org/10.1006/mcne.2000.0939>
- Sun W, You X, Gogol-Döring A, et al (2013) Ultra-deep profiling of alternatively spliced *Drosophila* Dscam isoforms by circularization-assisted multi-segment sequencing. *EMBO J* 32:2029–2038. doi: 10.1038/emboj.2013.144
- Takahashi H, Arstikaitis P, Prasad T, et al (2011) Postsynaptic TrkC and Presynaptic PTP σ Function as a Bidirectional Excitatory Synaptic Organizing Complex. *Neuron* 69:287–303. doi: <https://doi.org/10.1016/j.neuron.2010.12.024>
- Takemura S, Bharioke A, Lu Z, et al (2013) A visual motion detection circuit suggested by *Drosophila* connectomics. *Nature* 500:175–181. doi: 10.1038/nature12450
- Talay M, Richman EB, Snell NJ, et al (2017) Transsynaptic Mapping of Second-Order Taste Neurons in Flies by trans-Tango. *Neuron* 96:783-795.e4. doi:

REFERENCES

<https://doi.org/10.1016/j.neuron.2017.10.011>

Timofeev K, Joly W, Hadjieconomou D, Salecker I (2012) Localized Netrins Act as Positional Cues to Control Layer-Specific Targeting of Photoreceptor Axons in *Drosophila*. *Neuron* 75:80–93. doi: <https://doi.org/10.1016/j.neuron.2012.04.037>

Ting C-Y, McQueen PG, Pandya N, et al (2014) Photoreceptor-Derived Activin Promotes Dendritic Termination and Restricts the Receptive Fields of First-Order Interneurons in *Drosophila*. *Neuron* 81:830–846. doi: <https://doi.org/10.1016/j.neuron.2013.12.012>

Ting C-Y, Yonekura S, Chung P, et al (2005) *Drosophila* N-cadherin functions in the first stage of the two-stage layer-selection process of R7 photoreceptor afferents. *Development* 132:953 LP – 963. doi: 10.1242/dev.01661

Tomasi T, Hakeda-Suzuki S, Ohler S, et al (2008) The Transmembrane Protein Golden Goal Regulates R8 Photoreceptor Axon-Axon and Axon-Target Interactions. *Neuron* 57:691–704. doi: 10.1016/j.neuron.2008.01.012

Tomlinson A, Ready DF (1987) Neuronal differentiation in the *Drosophila* ommatidium. *Dev Biol* 120:366–376. doi: [https://doi.org/10.1016/0012-1606\(87\)90239-9](https://doi.org/10.1016/0012-1606(87)90239-9)

Torroja L, Luo L, White K (1996) APPL, the *Drosophila* Member of the APP-Family, Exhibits Differential Trafficking and Processing in CNS Neurons. *J Neurosci* 16:4638 LP – 4650. doi: 10.1523/JNEUROSCI.16-15-04638.1996

Torroja L, Packard M, Gorczyca M, et al (1999) The *Drosophila* β -Amyloid Precursor Protein Homolog Promotes Synapse Differentiation at the Neuromuscular Junction. *J Neurosci* 19:7793 LP – 7803. doi: 10.1523/JNEUROSCI.19-18-07793.1999

Ullrich B, Ushkaryov YA, Südhof TC (1995) Cartography of neurexins: More than 1000 isoforms generated by alternative splicing and expressed in distinct subsets of neurons. *Neuron* 14:497–507. doi: [https://doi.org/10.1016/0896-6273\(95\)90306-2](https://doi.org/10.1016/0896-6273(95)90306-2)

Urwyler O, Izadifar A, Dascenco D, et al (2015) Investigating CNS synaptogenesis at single-synapse resolution by combining reverse genetics with correlative light and electron microscopy. *Development* 142:394 LP – 405. doi: 10.1242/dev.115071

Van Der Loos H, Glaser EM (1972) Autapses in neocortex cerebri: synapses between a pyramidal cell's axon and its own dendrites. *Brain Res* 48:355–360. doi: [https://doi.org/10.1016/0006-8993\(72\)90189-8](https://doi.org/10.1016/0006-8993(72)90189-8)

REFERENCES

- Weinhard L, di Bartolomei G, Bolasco G, et al (2018) Microglia remodel synapses by presynaptic trogocytosis and spine head filopodia induction. *Nat Commun* 9:1228. doi: 10.1038/s41467-018-03566-5
- Wentzell JS, Bolkan BJ, Carmine-Simmen K, et al (2012) Amyloid precursor proteins are protective in *Drosophila* models of progressive neurodegeneration. *Neurobiol Dis* 46:78–87. doi: <https://doi.org/10.1016/j.nbd.2011.12.047>
- Wernet MF, Desplan C (2014) Homothorax and Extradenticle alter the transcription factor network in *Drosophila* ommatidia at the dorsal rim of the retina. *Development* 141:918 LP – 928. doi: 10.1242/dev.103127
- White K, Kankel DR (1978) Patterns of cell division and cell movement in the formation of the imaginal nervous system in *Drosophila melanogaster*. *Dev Biol* 65:296–321. doi: [https://doi.org/10.1016/0012-1606\(78\)90029-5](https://doi.org/10.1016/0012-1606(78)90029-5)
- Wiggan O, Bernstein BW, Bamberg JR (2005) A phosphatase for cofilin to be HAD. *Nat Cell Biol* 7:8
- Wills Z, Bateman J, Korey CA, et al (1999) The Tyrosine Kinase Abl and Its Substrate Enabled Collaborate with the Receptor Phosphatase Dlar to Control Motor Axon Guidance. *Neuron* 22:301–312. doi: 10.1016/S0896-6273(00)81091-0
- Wolff T, Ready DF (1991) The beginning of pattern formation in the *Drosophila* compound eye: the morphogenetic furrow and the second mitotic wave. *Development* 113:841 LP – 850
- Yam PT, Langlois SD, Morin S, Charron F (2009) Sonic Hedgehog Guides Axons through a Noncanonical, Src-Family-Kinase-Dependent Signaling Pathway. *Neuron* 62:349–362. doi: <https://doi.org/10.1016/j.neuron.2009.03.022>
- Yamaguchi S, Wolf R, Desplan C, Heisenberg M (2008) Motion vision is independent of color in *Drosophila*. *Proc Natl Acad Sci* 105:4910 LP – 4915. doi: 10.1073/pnas.0711484105
- Yuste R (2015) The discovery of dendritic spines by Cajal. *Front. Neuroanat.* 9:18
- Zeng X, Sun M, Liu L, et al (2007) Neurexin-1 is required for synapse formation and larvae associative learning in *Drosophila*. *FEBS Lett* 581:2509–2516. doi: 10.1016/j.febslet.2007.04.068
- Zhang KX, Tan L, Pellegrini M, et al (2016) Rapid Changes in the Transcriptome during the

REFERENCES

Conversion of Growth Cones to Synaptic Terminals. *Cell Rep* 14:1258–1271. doi: 10.1016/j.celrep.2015.12.102

Zhang W, Benson DL (2001) Stages of Synapse Development Defined by Dependence on F-Actin. *J Neurosci* 21:5169 LP – 5181. doi: 10.1523/JNEUROSCI.21-14-05169.2001

Zipursky SL, Sanes JR (2010) Chemoaffinity Revisited: Dscams, Protocadherins, and Neural Circuit Assembly. *Cell* 143:343–353. doi: <https://doi.org/10.1016/j.cell.2010.10.009>

ACKNOWLEDGEMENTS

As I am heading towards the end of my PhD, I would like to express my gratitude to the many people that helped me get this far. Egyptians say that it is more important to pick the right companion before choosing the path. I consider myself very lucky that I got to meet and work with such great people that helped me grow at the scientific, personal, and professional levels. I would like to thank Robin, my supervisor and mentor, for giving me this opportunity and allowing me a great level of freedom in my research. I would also thank my colleagues and friends from the Hiesinger, Wernet, and Hassan labs, you guys rock and it was great fun working with you. A special acknowledgement to our lab manager, Heike, for all her hard work and effort, constantly giving us an example of how a great work ethic should be.

I would like to thank Robin, Gerit, and Marco for taking the time to carefully read and provide feedback on the thesis. I have to apologize that you had to read my long sentences that sometimes made no sense, yet you were always patient and gave the necessary feedback to make sure the thesis was in the best shape possible. I would like to thank Lea Behnke, she was so kind that she offered to translate the summary into German. All the members of the Hiesinger, Wernet, and Hassan labs were very helpful during the writing process, they always offered help and support.

I would have never managed to get this far if it were not for the great friends I consider myself very lucky to have. I would specially mention Ridvan and Gizem that took care of the cats during the time I could not, Gerit and his family for all the help and advice they always offered. The Egyptians in Berlin, Ahmed Samy, Ibrahim Ismael, and Mostafa Amer that always made our gatherings into something unexpectedly funny. My great friends that are spread all over the world were very supportive during my studies, Amgad Ibrahim, Karim Khedr, Anne Jacob, and my best friend, Mohamed Gaafar. I was also lucky to have great neighbors and friends. The Andres family are very warm and kind that I was always treated like a family member. The Keunheim family helped me tremendously, they accepted and supported my work unconditionally and made sure I progressed in my studies and life.

Finally, I would like to thank my family for all what they have done for me and my brother. They spared no effort in making sure we had the best life and education possible, and they do a lot for us. The daily phone calls, the random chats, and the question about what I have eaten that day never failed to make my day a better one. And I am forever indebted to you.

APPENDICES

APPENDIX 1 | LIST OF ABBREVIATIONS

A β : Amyloid- β
Abl: Abelson kinase
aDC: anterior dorsocentral neuron
AICD: APP intracellular domain
APF: After pupal formation
APLP: Amyloid precursor-like protein
APP: Amyloid precursor protein
APPL-DT: Double fluorophore-tagged APPL
APPL-TG4: APPL Trojan-Gal4
APPL: Amyloid precursor protein-like
BACE: β -site amyloid precursor protein cleaving enzyme
BDSC: Bloomington *Drosophila* stock center
Brp: Bruchpilot
C. elegans: *Caenorhabditis elegans*
Ca²⁺: Calcium
CAM: Cell adhesion molecule
Caps: Capricious
CRISPR-Cas9: Clustered regularly interspaced short palindromic repeats-CRISPR-associated protein 9
CS: Canton S
Dab: Disabled
DCC: Devoid in colorectal cancer
dCIN: *Drosophila* Chronophin
Dia: Diaphanous
DNA: Deoxyribonucleic acid
DRA: Dorsal rim area
Dscam: Down syndrome cell adhesion molecule
DSHB: Developmental studies hybridoma bank
EG: Epithelial glia
EJPs: Evoked excitatory potentials
Elav: Embryonic lethal abnormal vision
ERG: Electroretinogram
FA: Formaldehyde
FLP: Flippase
Fmi: Flamingo
Fra: Frazzled

APPENDICES

FRT: Flippase recognition target
GFP-Tub: GFP-tagged α -Tubulin
GMC: Ganglion mother cells
Gogo: Golden Goal
GPC: Glial precursor cells
GRASP: GFP reconstitution across synaptic partners
hsflp: Heat-shock flippase
Hth: Homothorax
Ig: Immunoglobulin
IPC: Inner proliferation center
KD: Knock-down
Kuz: Kuzbanian
Lar: Leukocyte-antigen-related-like
Lawf: lamina wide-field neurons
LF: Lamina furrow
LIMK: LIM kinase
LN: Lamina neurons
LPC: Lamina precursor cells
LRR: Leucine-rich-repeat
M: Medulla layer
MARCM: Mosaic analysis with a repressible cell marker
MEG: Medulla glia
mEJPs: miniature excitatory potentials
MF: Morphogenetic furrow
MG: Marginal glia
MN: Medulla neurons
MNG: Medulla neuropil glia
mV: Millivolt
NB: Neuroblast
NCad: N-Cadherin
NE: Neuroepithelium
Nlg: Neuroligin
NMJ; Neuro-muscular junction
Nrt: Neurotactin
Nrx: Neurexin
OE: Overexpression
OPC: Outer proliferation center

OPO: Optical parametric oscillator
P: Pupal stage
PBST: Phosphate-buffered saline + Triton X
Pcdh: Clustered protocadherin
PCR: Polymerase chain reaction
Psn: Presinilin
PTP: Protein tyrosine phosphatase
R: Retinula cell
Rel: Relish
Rh: Rhodopsin
RNAi: RNA interference
Robo: Roundabout
sAPPL: Secreted APPL
SEM: Standard error of the mean
Sema1a: Semaphorin 1a
Spn: Spinophilin
SSH: Slingshot
TESK: TES kinase
UAS: Upstream activation sequence
Vang: Van Gogh
VDRC: Vienna *Drosophila* resource center
VNC: Ventral nerve cord
Vnd: Ventral nervous system defective
 μm : micrometer

APPENDICES

APPENDIX 2 | LIST OF FIGURES

FIG. 1. DRAWINGS OF VARIOUS NEURONAL STRUCTURES BY RAMÓN Y CAJAL.	3
FIG. 1.1.3. CELL ADHESION MOLECULES INDUCE ATTRACTIVE AND REPULSIVE NEURONAL INTERACTIONS.	6
FIG. 1.2.1. STRUCTURE OF THE ADULT FLY VISUAL SYSTEM.	10
FIG. 1.2.2. DEVELOPMENT OF THE FLY VISUAL SYSTEM.	12
FIG. 1.3.1. THE <i>EX VIVO</i> BRAIN CULTURE IMAGING CHAMBER.	14
FIG. 3.2.1.1-1. <i>LAR</i> AND <i>LIPRIN-α</i> ARE NOT REQUIRED FOR <i>R7</i> TARGETING.	31
FIG. 3.2.1.1-2. <i>LAR</i> <i>R7</i> S RETRACTION PATTERN IS OVERLAPPING WITH BUT NOT IDENTICAL TO <i>LIPRIN-α</i> <i>R7</i> S.	32
FIG. 3.2.1.2. <i>TRIO</i> OVEREXPRESSION RESCUES THE EARLY RETRACTIONS OF <i>LAR</i> <i>R7</i>	34
FIG. 3.2.1.3. <i>LAR</i> <i>R7</i> S RETRACT TO THE LAYER WHERE <i>R8</i> TERMINALS ARE.	36
FIG. 3.2.1.4. LOSS OF <i>LAR</i> AND <i>LIPRIN-α</i> IN <i>R7</i> S CAUSE SYNAPTIC DEFECT.	38
FIG. 3.2.1.5. <i>LAR</i> AND <i>LIPRIN-α</i> DO NOT AFFECT SYNAPSE FORMATION IN DORSAL RIM <i>R7</i> S AND SYNAPTIC TRANSMISSION IN PHOTORECEPTORS.	40
FIG. 3.2.2.1-1. LOSS OF <i>DIA</i> CAUSES EYE DEFORMATION.	42
FIG. 3.2.2.1-2. MICROTUBULES ARE RECRUITED TO BULBOUS TIPS.	43
FIG. 3.2.2.2-1. <i>LIPRIN-α</i> PRECEDES MICROTUBULES TO BULBOUS TIPS.	45
FIG. 3.2.2.2-2. MICROTUBULES ARE NOT STABILIZED IN BULBOUS TIPS OF <i>LAR</i> AND <i>LIPRIN-α</i> <i>R7</i> S.	47
FIG. 3.2.3.1. <i>DCIN</i> AFFECTS <i>R7</i> FILOPODIAL DYNAMICS.	49
FIG. 3.2.3.2. <i>DCIN</i> KNOCK-DOWN ENHANCES SYNAPSE FORMATION IN PHOTORECEPTORS.	51
FIG. 3.3.6. A MODEL SUGGESTING THE FUNCTION OF <i>LAR</i> AND <i>LIPRIN-α</i> IN <i>R7</i> BULBOUS TIP STABILIZATION.	54
FIG. 4.2.1-1. CONFIRMING THE <i>PTP69D^{D1689}</i> ALLELE.	58
FIG. 4.2.1-2. <i>PTP69D</i> LOSS CAUSE <i>R7</i> RETRACTION AND A FILOPODIA FORMATION DEFECT.	59
FIG. 4.2.2. <i>PTP69D</i> IS NOT REQUIRED FOR SYNAPSE FORMATION IN PHOTORECEPTORS.	61
FIG. 5.2.1. <i>NRX</i> IS NOT REQUIRED FOR <i>R7</i> TARGETING.	65
FIG. 5.2.2. LOSS OF <i>NRX</i> LEADS TO AN INCREASE IN SYNAPTIC TRANSMISSION.	67
FIG. 5.2.3. <i>NRX</i> <i>R7</i> S FORM CONTACTS WITH ABERRANT SYNAPTIC PARTNERS.	68
FIG. 5.2.4. <i>NRX</i> <i>R7</i> S FORM NUMEROUS UNSTABLE BULBOUS TIPS.	69
FIG. 6.2.1.1-1. <i>R7</i> S TERMINATE IN <i>M3</i> IN <i>APPL^D</i> FLIES.	72

APPENDICES

FIG. 6.2.1.1-2. <i>APPL^D</i> R7S INITIALLY TARGET CORRECTLY BEFORE THEY RETRACT.....	73
FIG. 6.2.1.2. <i>APPL^D</i> R7S DO NOT FORM STABLE BULBOUS TIPS AND HAVE A SYNAPTIC DEFECT.....	75
FIG. 6.2.1.3. SENSITIZING THE <i>APPL^D</i> MUTANT WITH GENETIC HETEROZYGOUS BACKGROUNDS DOES NOT ENHANCE THE R7 RETRACTION PHENOTYPE.	76
FIG. 6.2.1.4. EXPRESSION OF FULL-LENGTH APPL DOES NOT RESCUE R7 RETRACTION IN <i>APPL^D</i> FLIES.	78
FIG. 6.2.1.5. LOSS OF <i>APPL</i> DOES NOT CAUSE R7 RETRACTION.	79
FIG. 6.2.2.1-1. APPL IS EXPRESSED IN THE NERVOUS SYSTEM OF DEVELOPING AND ADULT FLIES.....	81
FIG. 6.2.2.1-2. APPL IS A NEURON-SPECIFIC PROTEIN	83
FIG. 6.2.2.2-1. LOCALIZATION OF THE APPL PROTEOLYTIC FRAGMENTS IN DEVELOPING AND ADULT PHOTORECEPTORS.....	85
FIG. 6.2.2.2-2. sAPPL COVERS BRAIN CORTICES WHEN APPL-DT IS EXPRESSED IN DIFFERENT NEURONAL TISSUES.....	87
FIG. 6.2.2.2-3. sAPPL GRADUALLY MIGRATES AWAY FROM PHOTORECEPTORS IN THE OPTIC LOBE TOWARDS THE CENTRAL BRAIN.	88
FIG. 6.2.2.2-4. sAPPL IS RELEASED FROM NEURONS AND PICKED UP BY GLIA.....	89
FIG. 6.2.2.3-1. APPL OVEREXPRESSION IN PHOTORECEPTORS AND LOSS OF FUNCTION AFFECTS ENDOLYSOSOMAL TRAFFICKING IN INNER CHIASM GLIA.....	90
FIG. 6.2.2.3-2. APPL OVEREXPRESSION IN PHOTORECEPTORS AND LOSS OF FUNCTION AFFECT ENDOLYSOSOMAL TRAFFICKING IN PHOTORECEPTORS AND MEDULLA NEURONS.....	92
FIG. 6.2.2.4. SECRETED APPL FROM NEURONS ACCUMULATES IN NEPHROCYTES.....	95

APPENDIX 3 | LIST OF GENOTYPES

Fig. #	Genotype
3.2.1.1-1	GMRflp; $\frac{\text{FRT40A, Tub} - \text{Gal80}}{\text{FRT40A, ry}}$; $\frac{\text{GMRmyrtdTom, GMR} - \text{Gal4, UAS} - \text{CD4tdGFP}}{+}$
	GMRflp; $\frac{\text{FRT40A, Tub} - \text{Gal80}}{\text{FRT40A, lar}^{2127}}$; $\frac{\text{GMRmyrtdTom, GMR} - \text{Gal4, UAS} - \text{CD4tdGFP}}{+}$
	GMRflp; $\frac{\text{FRT40A, Tub} - \text{Gal80}}{\text{FRT40A, liprin} - \alpha^E}$; $\frac{\text{GMRmyrtdTom, GMR} - \text{Gal4, UAS} - \text{CD4tdGFP}}{+}$
3.2.1.1-2	ey3.5flp; $\frac{\text{FRT40A, cl, w}^+}{\text{FRT40A, ry}}$
	ey3.5flp; $\frac{\text{FRT40A, cl, w}^+}{\text{FRT40A, lar}^{2127}}$
	ey3.5flp; $\frac{\text{FRT40A, cl, w}^+}{\text{FRT40A, liprin} - \alpha^E}$
	GMRflp; $\frac{\text{FRT40A, Tub} - \text{Gal80}}{\text{FRT40A, ry}}$; $\frac{\text{GMRmyrtdTom, GMR} - \text{Gal4, UAS} - \text{CD4tdGFP}}{+}$
	GMRflp; $\frac{\text{FRT40A, Tub} - \text{Gal80}}{\text{FRT40A, lar}^{2127}}$; $\frac{\text{GMRmyrtdTom, GMR} - \text{Gal4, UAS} - \text{CD4tdGFP}}{+}$
	GMRflp; $\frac{\text{FRT40A, Tub} - \text{Gal80}}{\text{FRT40A, liprin} - \alpha^E}$; $\frac{\text{GMRmyrtdTom, GMR} - \text{Gal4, UAS} - \text{CD4tdGFP}}{+}$
3.2.1.2	GMRflp; $\frac{\text{FRT40A, Tub} - \text{Gal80}}{\text{FRT40A, ry}}$; $\frac{\text{GMRmyrtdTom, GMR} - \text{Gal4, UAS} - \text{CD4tdGFP}}{+}$
	GMRflp; $\frac{\text{FRT40A, Tub} - \text{Gal80}}{\text{FRT40A, lar}^{2127}}$; $\frac{\text{GMRmyrtdTom, GMR} - \text{Gal4, UAS} - \text{CD4tdGFP}}{\text{UAS} - \text{Trio}}$
3.2.1.3	GMRflp; $\frac{\text{FRT40A, Tub} - \text{Gal80}}{\text{FRT40A, lar}^{2127}}$; $\frac{\text{GMRmyrtdTom, GMR} - \text{Gal4, UAS} - \text{CD4tdGFP}}{+}$
	GMRflp; $\frac{\text{FRT40A, Tub} - \text{Gal80}}{\text{FRT40A, lar}^{2127}}$; $\frac{\text{GMRmyrtdTom, GMR} - \text{Gal4, UAS} - \text{CD4tdGFP}}{\text{IGMR} - \text{GFP} - \text{Hth}}$
3.2.1.4	GMRflp; $\frac{\text{FRT40A, Tub} - \text{Gal80}}{\text{FRT40A, ry}}$; $\frac{\text{GMR} - \text{Gal4, UAS} - \text{CD4tdTom}}{\text{UAS} - \text{BrpD3} - \text{GFP}}$
	GMRflp; $\frac{\text{FRT40A, Tub} - \text{Gal80}}{\text{FRT40A, lar}^{2127}}$; $\frac{\text{GMR} - \text{Gal4, UAS} - \text{CD4tdTom}}{\text{UAS} - \text{BrpD3} - \text{GFP}}$
	GMRflp; $\frac{\text{FRT40A, Tub} - \text{Gal80}}{\text{FRT40A, liprin} - \alpha^E}$; $\frac{\text{GMR} - \text{Gal4, UAS} - \text{CD4tdTom}}{\text{UAS} - \text{BrpD3} - \text{GFP}}$
	GMRflp; $\frac{\text{FRT40A, Tub} - \text{Gal80}}{\text{FRT40A, lar}^{2127}}$; $\frac{\text{GMR} - \text{Gal4, UAS} - \text{CD4tdTom}}{\text{UAS} - \text{Trio, UAS} - \text{BrpD3} - \text{GFP}}$
3.2.1.5	GMRflp; $\frac{\text{FRT40A, Tub} - \text{Gal80}}{\text{FRT40A, ry}}$; $\frac{\text{GMR} - \text{Gal4, UAS} - \text{CD4tdTom}}{\text{UAS} - \text{BrpD3} - \text{GFP}}$
	GMRflp; $\frac{\text{FRT40A, Tub} - \text{Gal80}}{\text{FRT40A, lar}^{2127}}$; $\frac{\text{GMR} - \text{Gal4, UAS} - \text{CD4tdTom}}{\text{UAS} - \text{BrpD3} - \text{GFP}}$

	$\text{GMRflp}; \frac{\text{FRT40A, Tub} - \text{Gal80}}{\text{FRT40A, liprin} - \alpha^E}; \frac{\text{GMR} - \text{Gal4, UAS} - \text{CD4tdTom}}{\text{UAS} - \text{BrpD3} - \text{GFP}}$ $\text{ey3.5flp}; \frac{\text{FRT40A, cl, w}^+}{\text{FRT40A, ry}}$ $\text{ey3.5flp}; \frac{\text{FRT40A, cl, w}^+}{\text{FRT40A, lar}^{2127}}$ $\text{ey3.5flp}; \frac{\text{FRT40A, cl, w}^+}{\text{FRT40A, liprin} - \alpha^E}$ $\text{ey3.5flp}; \frac{\text{FRT82B, cl, w}^+}{\text{FRT82B, syd} - 1^{w46}}$
3.2.2.1-1	$\text{ey3.5flp}; \frac{\text{FRT40A, cl, w}^+}{\text{FRT40A, ry}}$ $\text{ey3.5flp}; \frac{\text{FRT40A, cl, w}^+}{\text{FRT40A, dia}^5}$
3.2.2.1-2	$\text{GMRflp}; \frac{\text{FRT40A, Tub} - \text{Gal80}}{\text{FRT40A, ry}}; \frac{\text{GMR} - \text{Gal4, UAS} - \text{CD4tdTom}}{\text{UAS} - \text{GFP} - \text{Tub}}$
3.2.2.2-1	$\text{hsflp}; \frac{\text{GMR} > \text{Stop} > \text{Gal4}}{\text{UAS} - \text{Liprin} - \alpha - \text{GFP}}; \frac{\text{UAS} - \text{Eb1} - \text{mCherry}}{+}$
3.2.2.2-2	$\text{GMRflp}; \frac{\text{FRT40A, Tub} - \text{Gal80}}{\text{FRT40A, lar}^{2127}}; \frac{\text{GMR} - \text{Gal4, UAS} - \text{CD4tdTom}}{\text{UAS} - \text{GFP} - \text{Tub}}$ $\text{GMRflp}; \frac{\text{FRT40A, Tub} - \text{Gal80}}{\text{FRT40A, liprin} - \alpha^E}; \frac{\text{GMR} - \text{Gal4, UAS} - \text{CD4tdTom}}{\text{UAS} - \text{GFP} - \text{Tub}}$
3.2.3.1	$\text{hsflp}; \frac{\text{GMR} > \text{Stop} > \text{Gal4}}{\text{UAS} - \text{scRNAi}}; \frac{\text{GMRmyrtdTom, UAS} - \text{CD4tdGFP}}{+}$ $\text{hsflp}; \frac{\text{GMR} > \text{Stop} > \text{Gal4}}{\text{UAS} - \text{dcin RNAi}}; \frac{\text{GMRmyrtdTom, UAS} - \text{CD4tdGFP}}{+}$
3.2.3.2	$\text{hsflp}; \frac{\text{GMR} > \text{Stop} > \text{Gal4}}{\text{UAS} - \text{scRNAi}}; \frac{\text{UAS} - \text{CD4tdTom, UAS} - \text{BrpD3} - \text{GFP}}{+}$ $\text{hsflp}; \frac{\text{GMR} > \text{Stop} > \text{Gal4}}{\text{UAS} - \text{dcin RNAi}}; \frac{\text{UAS} - \text{CD4tdTom, UAS} - \text{BrpD3} - \text{GFP}}{+}$ $; \frac{\text{UAS} - \text{scRNAi}}{+}; \frac{\text{GMR} - \text{Gal4}}{+}$ $; \frac{\text{UAS} - \text{dcin RNAi}}{+}; \frac{\text{GMR} - \text{Gal4}}{+}$
4.2.1-1	$;; \frac{\text{FRT80B, ptp69d}^{D1689}}{\text{Tm6B}}$
4.2.1-2	$\text{ey3.5flp}; \frac{\text{FRT80B, RpS17}^4, w^+}{\text{FRT80B, ry}}$ $\text{ey3.5flp}; \frac{\text{FRT80B, RpS17}^4, w^+}{\text{FRT80B, ptp69d}^{D1689}}$

APPENDICES

	$\frac{\text{UAS} - \text{scRNAi}}{+}; \frac{\text{GMR} - \text{Gal4}}{+}$ $; \frac{\text{UAS} - \text{ptp69d RNAi}}{+}; \frac{\text{GMR} - \text{Gal4}}{+}$ $;; \frac{\text{GMR} - \text{Gal4}}{\text{UAS} - \text{ptp69d RNAi}}$ $\text{GMRflp}; \frac{\text{GMR} - \text{Gal4}, \text{UAS} - \text{CD4tdGFP}}{\text{GMRmyrtdTom}}; \frac{\text{FRT80B, Tub} - \text{Gal8}}{\text{FRT80B, ptp69d}^{D1689}}$
4.2.2	$\text{GMRflp}; \frac{\text{GMR} - \text{Gal4}, \text{UAS} - \text{CD4tdGFP}}{\text{UAS} - \text{BrpD3} - \text{mKate2}}; \frac{\text{FRT80B, Tub} - \text{Gal8}}{\text{FRT80B, ry}}$ $\text{GMRflp}; \frac{\text{GMR} - \text{Gal4}, \text{UAS} - \text{CD4tdGFP}}{\text{UAS} - \text{BrpD3} - \text{mKate2}}; \frac{\text{FRT80B, Tub} - \text{Gal80}}{\text{FRT80B, ptp69d}^{D1689}}$ $\text{ey3.5flp}; \frac{\text{FRT80B, RpS17}^4, w^+}{\text{FRT80B, ry}}$ $\text{ey3.5flp}; \frac{\text{FRT80B, RpS17}^4, w^+}{\text{FRT80B, ptp69d}^{D1689}}$ $; \frac{\text{UAS} - \text{scRNAi}}{+}; \frac{\text{GMR} - \text{Gal4}}{+}$ $; \frac{\text{UAS} - \text{ptp69d RNAi}}{+}; \frac{\text{GMR} - \text{Gal4}}{+}$ $;; \frac{\text{GMR} - \text{Gal4}}{\text{UAS} - \text{ptp69d RNAi}}$
5.2.1	yw $;; \frac{\text{FRT82B, nrx}^{241}}{\text{Tm6B}}$ $;; \frac{\text{Df(3R)5Ca}}{+}$ $;; \frac{\text{Df(3R)5Ca}}{\text{FRT82B, nrx}^{241}}$ $\text{ey3.5flp}; \frac{\text{FRT82B, cl, w}^+}{\text{FRT82B, ry}}$ $\text{ey3.5flp}; \frac{\text{FRT82B, cl, w}^+}{\text{FRT82B, nrx}^{241}}$
5.2.2	$\text{ey3.5flp}; \frac{\text{FRT82B, cl, w}^+}{\text{FRT82B, ry}}$ $\text{ey3.5flp}; \frac{\text{FRT82B, cl, w}^+}{\text{FRT82B, nrx}^{241}}$
5.2.3	$\frac{\text{UAS} - \text{myrGFP, QUAS} - \text{mtdTomato(3xHA)}}{\text{GMRflp}}; \frac{\text{trans} - \text{Tango}}{\text{Rh4} - \text{Gal4}}; \frac{\text{FRT82B, Tub} - \text{Gal80}}{\text{FRT82B, y}^+}$ $\frac{\text{UAS} - \text{myrGFP, QUAS} - \text{mtdTomato(3xHA)}}{\text{GMRflp}}; \frac{\text{trans} - \text{Tango}}{\text{Rh4} - \text{Gal4}}; \frac{\text{FRT82B, Tub} - \text{Gal80}}{\text{FRT82B, nrx}^{241}}$

5.2.4	$\text{GMRflp}; \frac{\text{GMR} - \text{Gal4, UAS} - \text{CD4tdGFP}}{\text{GMRmyrtdTom}}; \frac{\text{FRT82B, Tub} - \text{Gal8}}{\text{FRT82B, } y^+}$ $\text{GMRflp}; \frac{\text{GMR} - \text{Gal4, UAS} - \text{CD4tdGFP}}{\text{GMRmyrtdTom}}; \frac{\text{FRT82B, Tub} - \text{Gal8}}{\text{FRT82B, } nrx^{241}}$
6.2.4.1-1	cs $\frac{\text{appl}^d, \text{hsflp}}{+}$ $\text{appl}^d, \text{hsflp}$
6.2.4.1-2	$\text{appl}^d, \text{hsflp}; \frac{\text{GMR} > \text{stop} > \text{Gal4}}{+}; \frac{\text{GMRmyrtdTom, UAS} - \text{CD4tdGFP}}{+}$
6.2.1.2	$\text{hsflp}; \frac{\text{GMR} > \text{stop} > \text{Gal4}}{+}; \frac{\text{GMRmyrtdTom, UAS} - \text{CD4tdGFP}}{+}$ $\text{appl}^d, \text{hsflp}; \frac{\text{GMR} > \text{stop} > \text{Gal4}}{+}; \frac{\text{GMRmyrtdTom, UAS} - \text{CD4tdGFP}}{+}$ $\text{hsflp}; \frac{\text{GMR} > \text{stop} > \text{Gal4}}{+}; \frac{\text{UAS} - \text{CD4tdTom, UAS} - \text{BrpD3} - \text{GFP}}{+}$ $\text{appl}^d, \text{hsflp}; \frac{\text{GMR} > \text{stop} > \text{Gal4}}{+}; \frac{\text{UAS} - \text{CD4tdTom, UAS} - \text{BrpD3} - \text{GFP}}{+}$
6.2.1.3	cs $\frac{\text{appl}^d, \text{hsflp}}{+}$ $\text{appl}^d, \text{hsflp}$ $\frac{\text{appl}^d, \text{hsflp}}{+}; \frac{\text{FRT40A, } lar^{2127}}{+}$ $\frac{\text{appl}^d, \text{hsflp}}{+}; \frac{\text{FRT80B, } ptp69d^{D1689}}{+}$ $\frac{\text{appl}^d, \text{hsflp}}{+}; \frac{\text{FRT40A, } cadn^{405}}{+}$ $\frac{\text{appl}^d, \text{hsflp}}{+}; \frac{\text{FRT80B, } gogo^{H1675}}{+}$ $\frac{\text{appl}^d, \text{hsflp}}{+}; \frac{\text{FRT2A, } caps^{c28fs}}{+}$ $\frac{\text{appl}^d, \text{hsflp}}{+}; \frac{\text{FRT42D, } fmi^{e59}}{+}$ $\frac{\text{appl}^d, \text{hsflp}}{+}; \frac{\text{FRT82B, } syd - 1^{w46}}{+}$ $\frac{\text{appl}^d, \text{hsflp}}{+}; \frac{\text{FRT40A, } liprin - \alpha^E}{+}$ $\frac{\text{appl}^d, \text{hsflp}}{+}; \frac{\text{FRT42D, } brp^{c04298}}{+}$ $\frac{\text{appl}^d, \text{hsflp}}{+}; \frac{\text{FRT2A, } trio^3}{+}$

APPENDICES

	$\frac{appl^d, hsflp}{+}; \frac{FRT40A, rab5^2}{+}$
	$\frac{appl^d, hsflp}{+}; ; \frac{FRT82B, rab7^{KO}}{+}$
	$appl^d, hsflp; \frac{FRT40A, lar^{2127}}{+}$
	$appl^d, hsflp; ; \frac{FRT80B, ptp69d^{D1689}}{+}$
	$appl^d, hsflp; \frac{FRT40A, cadn^{405}}{+}$
	$appl^d, hsflp; ; \frac{FRT80B, gogo^{H1675}}{+}$
	$appl^d, hsflp; ; \frac{FRT2A, caps^{c28fs}}{+}$
	$appl^d, hsflp; \frac{FRT42D, fmi^{e59}}{+}$
	$appl^d, hsflp; ; \frac{FRT82B, syd - 1^{w46}}{+}$
	$appl^d, hsflp; \frac{FRT40A, liprin - \alpha^E}{+}$
	$appl^d, hsflp; \frac{FRT42D, brp^{c04298}}{+}$
	$appl^d, hsflp; ; \frac{FRT2A, trio^3}{+}$
	$appl^d, hsflp; \frac{FRT40A, rab5^2}{+}$
	$appl^d, hsflp; ; \frac{FRT82B, rab7^{KO}}{+}$
	$appl^d, hsflp; \frac{FRTG13, fra^3}{+}$
	$appl^d, hsflp; \frac{vang^1}{+}$
	$appl^d, hsflp; ; \frac{psn^9}{+}$
	$appl^d, hsflp; ; \frac{rel^{E20}}{+}$
	$appl^d, hsflp; ; \frac{abl^2}{+}$
	$appl^d, hsflp; ; \frac{dab^1}{+}$
	$appl^d, hsflp; ; \frac{red^1, e^*, nrt^2}{+}$
6.2.1.4	$appl^d, hsflp$

	$appl^d, hsflp; \frac{GMR - Gal4}{+}$
	$appl^d, hsflp; \frac{GMR - Gal4}{UAS - APPL}$
	$appl^d, hsflp; \frac{Elav - Gal4}{+}$
	$appl^d, hsflp; \frac{Elav - Gal4}{UAS - APPL}$
	$appl^d, hsflp; \frac{UAS - APPL}{+}; \frac{Elav - Gal4}{+}$
	$appl^d, hsflp; \frac{FRT42D, GMR - Gal80}{+}; \frac{Elav - Gal4}{+}$
	$appl^d, hsflp; \frac{FRT42D, GMR - Gal80}{UAS - APPL}; \frac{Elav - Gal4}{+}$
	$appl^d, hsflp;; \frac{9B08 - Gal4}{+}$
	$appl^d, hsflp; \frac{UAS - APPL}{+}; \frac{9B08 - Gal4}{+}$
	$appl^d, hsflp; \frac{GMR - Gal4}{+}; \frac{9B08 - Gal4}{+}$
	$appl^d, hsflp; \frac{GMR - Gal4}{UAS - APPL}; \frac{9B08 - Gal4}{+}$
	$appl^d, hsflp;; \frac{Repo - Gal4}{+}$
	$appl^d, hsflp; \frac{UAS - APPL}{+}; \frac{Repo - Gal4}{+}$
	$appl^d, hsflp; \frac{GMR - Gal4}{+}; \frac{Repo - Gal4}{+}$
	$appl^d, hsflp; \frac{GMR - Gal4}{UAS - APPL}; \frac{Repo - Gal4}{+}$
6.2.1.5	$\frac{APPL - TG4}{+}$ $APPL - TG4$ $appl^d, hsflp$ <i>cs</i> $appl^{dc21}$
6.2.2.1	$\frac{APPL - TG4}{+}; \frac{UAS - CD4tdGFP}{+}; \frac{Repo - lexA, lexAop - CD4tdTom}{+}$
6.2.2.2-1	$\frac{UAS - mCherry - APPL - GFP}{+}; \frac{GMR - Gal4}{+}$
6.2.2.2-2	$\frac{UAS - mCherry - APPL - GFP}{+}; \frac{GMR - Gal4}{+}$ $\frac{UAS - mCherry - APPL - GFP}{+}; \frac{Elav - Gal4}{+}$

APPENDICES

	$\frac{\text{UAS} - \text{mCherry} - \text{APPL} - \text{GFP}}{+}; \frac{\text{Rh3} - \text{Gal4}}{+}$ $\frac{\text{UAS} - \text{mCherry} - \text{APPL} - \text{GFP}}{\text{UAS} - \text{kuz RNAi}}; \frac{\text{GMR} - \text{Gal4}}{\text{UAS} - \text{bace RNAi}}$
6.2.2.2-3	$\frac{\text{UAS} - \text{mCherry} - \text{APPL} - \text{GFP}}{+}; \frac{\text{GMR} - \text{Gal4}}{+}$
6.2.2.2-4	$\frac{\text{UAS} - \text{mCherry} - \text{APPL} - \text{GFP}}{\text{lexAop} - \text{CD4tdGFP}}; \frac{\text{GMR} - \text{Gal4}}{\text{Repo} - \text{lexA}}$
6.2.2.3	$cs; \frac{\text{GMR} - \text{Gal4}}{+}$ $appl^d, \text{hsflp}; \frac{\text{GMR} - \text{Gal4}}{+}$ $\frac{\text{UAS} - \text{APPL}}{+}; \frac{\text{GMR} - \text{Gal4}}{+}$
6.2.2.4	$\frac{\text{UAS} - \text{mCherry} - \text{APPL} - \text{GFP}}{+}; \frac{\text{GMR} - \text{Gal4}}{+}$ $\frac{\text{APPL} - \text{TG4}}{+}; \frac{\text{UAS} - \text{mCherry} - \text{APPL} - \text{GFP}}{+}$ $\frac{\text{UAS} - \text{mCherry} - \text{APPL} - \text{GFP}}{+}; \frac{\text{Repo} - \text{Gal4}}{+}$ $\text{Hand} - \text{GFP}; \frac{\text{UAS} - \text{mCherry} - \text{APPL} - \text{GFP}}{+}; \frac{\text{GMR} - \text{Gal4}}{+}$

APPENDIX 4 | PUBLICATIONS

Özel MN*, Kulkarni*, **Hasan A***, Schallau J, Moldenhauer M, Daumann IM, Wolfenberg H, Dercksen VJ, Kiral FR, Weiser M, Prohaska S, von Kleist M[§], Hiesinger PR[§]. Serial synapse formation through filopodial competition for synaptic seeding factors. *Developmental Cell* 2019, 10.1016/j.devcel.2019.06.014.

Gizem Sancer, Emil Kind, Haritz Plazaola-Sasieta, Jana Balke, Tuyen Pham, **Amr Hasan**, Lucas O. Münch, Maximilien Courgeon, Thomas F. Mathejczyk, and Mathias F. Wernet. Modality-Specific Circuits for Skylight Orientation in the Fly Visual System. *Current Biology* Volume 29, Issue 17, 2019. <https://doi.org/10.1016/j.cub.2019.07.020>

Irini A. Kessissoglou, Dominique Langui, **Amr Hasan**, Maral Maral, Suchetana Bias Dutta, P. Robin Hiesinger and Bassem A. Hassan. The Drosophila Amyloid Precursor Protein homologue mediates neuronal survival and neuro-glial interactions. *In preparation*

APPENDICES

APPENDIX 5 | CURRICULUM VITAE

Education and training

Nov 2015 – Present: **PhD Candidate** in The Neurogenetics Laboratory – Freie Universität Berlin, Berlin (Germany)

Mar 2015 – Oct 2015: **Researcher** in the Laboratory of Molecular Oncology and Angiogenesis - Vesalius Research Centre, Leuven (Belgium)

Feb 2014 – Sep 2014: **Master's thesis** in the Neuronal wiring lab - Vesalius Research Centre, Leuven (Belgium)

Sep 2012 – Sep 2014: **Master's degree in Biochemistry and Biotechnology** from the Faculty of Sciences, Ghent University, Ghent (Belgium)

Sep 2005 – Jun 2010: **Bachelor's degree in Pharmacy and Pharmaceutical sciences** from the Faculty of Pharmacy, Cairo University, Cairo (Egypt)

Teaching experience

April-May 2019: Supervised the practical part of Neurodevelopment and neurodegeneration II master course – Freie Universität Berlin

Awards

Mar 2015 – Oct 2015: KU-Leuven scholarship

Sep 2012 – Sep 2014: Erasmus Mundus Widening Egyptian and Lebanese COoperation and Mobility with Europe (EM-WELCOME)

Work experience

Nov 15 – Aug 19: Research Assistent – Freie Universität Berlin (Berlin, Germany)

Sep 11 – Sep 12: Personalized search engine evaluator - Leapforce Inc.

Jul 11 – Sep 11: English language instructor - Berlitz Corporation, Giza (Egypt)

Nov 10 – Jun 11: Community pharmacist - Tarek pharmacy, Giza (Egypt)

Additional information

Language skills

Arabic		Native proficiency
English		Bilingual proficiency
German		Limited working proficiency

Dutch		Elementary proficiency
Turkish		Elementary proficiency

Community service

Co-founded El Bedaya mn Hena (Arabic for: It all starts here) NGO that aimed at offering proper education to the underprivileged children in poor neighborhoods of Cairo, Egypt

Extra-curricular activities

2009, organized the 20th Cairo International Model United Nations' Development Program, the American University in Cairo, Cairo, Egypt.

2008, edited and published 'Vanguard', the Cairo International Model United Nations' magazine, the American University in Cairo, Cairo, Egypt.

2008, organized the 19th Cairo International Model United Nations' Awareness Program, the American University in Cairo, Cairo, Egypt.

July 2007, organized and attended the 14th iEARN (International Education And Resource Network) annual international conference, Cairo, Egypt.

July 2004, attended the 11th iEARN annual international conference, Kosice, Slovakia.